

# **The Budget of Tungsten in Altered Oceanic Crust**

Inaugural-Dissertation  
zur Erlangung des Doktorgrades  
der Mathematisch-Naturwissenschaftlichen Fakultät  
der Universität zu Köln

vorgelegt von  
Ramon Reifenröther  
aus Fensdorf

Köln, 2020

Gutachter: Prof. Dr. Carsten Munker  
Prof. Dr. Reiner Kleinschrodt

Tag der mündlichen Prüfung: 27.05.2020

Poor man wanna be rich  
Rich man wanna be king  
And a king ain't satisfied  
'Til he rules everything  
I wanna go out tonight  
I wanna find out what I got

Springsteen, Bruce "Badlands", *Darkness on the Edge of Town* (1978). Columbia Records. LP

# Contents

Contents.....	I
Abstract .....	1
Kurzzusammenfassung.....	3
1. Introduction .....	5
1.1 Aim of this study and chapter overview .....	6
1.2 Tungsten (W) and its basic geochemical properties.....	8
1.3 Formation of the Earth, its differentiation and the influence on global W distribution...	9
1.4 Structure and formation of the oceanic crust.....	12
1.5 Alteration of oceanic crust and its significance for global elemental distribution.....	14
1.6 Global cycle of W .....	19
1.7 Stable W isotope composition of Earth's main reservoirs .....	22
2. Evidence for tungsten mobility during oceanic crust alteration .....	24
2.1 Introduction .....	25
2.2 Geological and geochemical overview of site 1256.....	27
2.3 Analytical Techniques.....	30
2.4 Results .....	35
2.4.1 Downhole variation of trace element concentrations and ratios .....	35
2.4.2 Evaluation of different digestion protocols and U-series patterns .....	39
2.5 Discussion .....	42
2.5.1 Influence of partial melting processes on immobile HFSE and U-Th abundances.	42
2.5.2 Origin of W-enrichment in different units of altered oceanic crust .....	48
2.5.3 Tungsten enrichment relative to U and Th enrichments .....	50
2.5.4 Comparison with ODP hole 504B.....	51
2.5.5 Tungsten enrichment in the AOC compared to arc settings.....	53
2.6 Conclusions .....	55
3. Extreme W enrichment during alteration of peridotites from the lower oceanic crust, IODP Leg 209.....	57
3.1 Introduction .....	58
3.2 Geological Overview of IODP Leg 209.....	60
3.2.1 Lithology and alteration styles at the drilled sites.....	60
3.2.2 Alteration effects common to all drilling sites .....	64
3.3 Analytical Protocols .....	65
3.4 Results .....	68
3.4.1 HFSE variations in Leg 209 drill holes.....	68
3.5 Discussion.....	70
3.5.1 Combined W-HFSE and U-Th systematics .....	70

3.5.2	Tungsten behaviour during different alteration styles and melt impregnation ....	73
3.5.3	Comparison with altered upper oceanic crust at hole 1256D.....	84
3.5.4	Implications for the understanding of W enrichment in Arc Magmas.....	86
3.6	Conclusions .....	88
4.	The stable W isotope composition of altered oceanic crust .....	90
4.1	Introduction .....	91
4.2	Geological Overview.....	95
4.2.1	Lithology and alteration styles at the investigated drilling sites .....	95
4.2.2	Lithology and elemental W systematics at hole 1256D .....	95
4.2.3	Lithology and elemental W systematics at Leg 209 drill holes .....	98
4.3	Analytical Protocol.....	101
4.4	Results .....	105
4.4.1	Stable W isotope patterns at different drilling sites .....	105
4.5	Discussion.....	106
4.5.1	The source of W in altered oceanic crust .....	106
4.5.2	The effect of different alteration styles on the stable W isotope composition .....	110
4.5.3	Implications on the source of seawater stable W isotope signature .....	115
4.5.4	Implications for the understanding of the behaviour of W in subduction zones...	116
4.6	Conclusions .....	118
	Bibliography .....	120
	Acknowledgements .....	135
	Erklärung .....	136

# Abstract

The key task of modern geochemistry and petrology is to understand the present and past development of the solid Earth and to deduce the mechanisms of its formation. Since it is only possible to study fresh rocks within the first 10 km of the Earth (all other exhumed rocks from greater depth were subject to metamorphism or alteration), geochemists learned how abundances and ratios of specific elements provide information of Earth's crust-mantle-dynamics, subduction zone dynamics or core-mantle processes.

Tungsten is one of these key elements in modern geochemistry since it is both a moderately siderophile as well as a highly incompatible element. In consequence, during early differentiation of the Earth, ca. 90% of Earth's W was sequestered into the core, leaving the Earth's mantle strongly depleted (ca. 12 ppb, König et al., 2011; Palme and O'Neill, 2014). Since uranium, thorium and tantalum are similarly magma-incompatible but did not behave siderophile in early Earth's history, combined W-Th-U-Ta systematics are a very powerful tool to mass balance W in various reservoirs on Earth. Because of their similar incompatibility, ratios of W-Th-U-Ta have long been regarded as constant in most silicate reservoirs. In contrast to this view, it was demonstrated that W is highly mobile in late magmatic hydrous environments and can be concentrated in hydrothermal systems up to ore grade. Furthermore, W enrichments relative to U, Th and Ta in many arc lavas have been found and were attributed to fluid-controlled enrichment in the sub-arc mantle wedge. During sub-arc enrichment, ratios of W/Th, W/U and W/Ta are elevated to various extents, depending on the type of subduction component involved. These findings require a closer assessment of the W behaviour in altered oceanic crust (AOC), which is a major source of subduction components in sub-arc mantle environments. Since W data from the oceanic crust are mainly available from fresh MORB glasses, little is known, whether seafloor alteration of the oceanic crust could trigger W redistribution in oceanic crust on its way to the subduction factory. Furthermore, AOC covers more than 60 % of the Earth's surface, and thus the knowledge of W redistribution in the oceanic crust during alteration is of pivotal importance to understand the global geochemical cycle of W. Altered oceanic crust is known to be a geochemical sink for some elements (Alkali metals, Mg, S, U) and source for others, e.g., Ca, Si, and Sr. Serpentinization of peridotitic oceanic crust is known as major sink for B and K, Rb, Cs, Na. Other elements like Lu, Hf, Zr, Th, and Ta remain largely unaffected by alteration. The combination of mobile and immobile elements makes the combined study of W, U, and Th a powerful tool to investigate the behaviour of W in altered oceanic crust.

In this thesis, results of precise isotope dilution measurements of Lu-Hf-Zr-Nb-U-Th-Ta-W are presented for oceanic crust with variable extent and type of alteration. Besides W, Ta, U

and Th the precise measurement of Lu, Hf, Zr, Nb allows to further characterize the initial magmatic diversity of the magma source regions. One of the key findings in this thesis is the demonstration of selective W enrichment during alteration of oceanic crust. This behaviour of W in marine environments was unknown before and could only be constrained by elemental ratios in arc systems. Furthermore, the thesis demonstrates that there is a systematic enrichment of W relative to the similarly incompatible Th, U, and Ta during hydrothermal alteration, pointing towards a progressive enrichment of W in the upper altered oceanic crust, with enrichment factors being as high as 13 relative to fresh MORB and 200 relative to fresh peridotites. It could be demonstrated as well that elevated W/Th is best suited to study selective W mobility in altered oceanic crust. Moreover, the isotopic state of altered oceanic crust (expressed as  $\delta^{186/184}\text{W}$ ) was unknown before. The results show how especially low-T oxidative weathering and high-T talc formation result in a lighter stable W isotope composition whereas initial serpentinization is not reflected in the isotopic state of oceanic crust. These findings indicate that progressive alteration of peridotitic oceanic crust releases isotopically heavy fluids, resembling the heavy counterpart of the light alteration mineral assemblage, that may represent a net source for isotopically heavy seawater W. Moreover, the heavy stable W isotope signatures from arc magmas potentially originates from fractionation during low-T dehydration of subducting slabs or release of isotopically heavy interstitial fluids from subduction slabs. The lighter stable W isotope composition of magmas more distant from the subduction zone thus may resemble the dehydration of an alteration mineral assemblage, light in stable W isotopes.

The combined study of W/Th and  $\delta^{186/184}\text{W}$  thus provides a powerful tool to distinguish between various alteration styles, the input of oceanic crust in subduction zones and the origin of W in seawater.

# Kurzzusammenfassung

Die Hauptaufgabe moderner Geochemie und Petrologie ist das Verständnis vergangener und heutiger Entwicklungen der festen Erde, sowie das Untersuchen der Mechanismen der Erdentstehung. Da es nur möglich ist, frische Gesteine der obersten 10 km der Erdkruste zu untersuchen (alle Gesteine tieferen Ursprungs sind stark alteriert oder metamorph überprägt), haben Geochemiker Methoden entwickelt mittels der Vorkommen und Verhältnisse spezifischer Elemente Rückschlüsse auf Kruste-Mantel Dynamik, Subduktionszonendynamik und Kern-Mantel Prozesse zu ziehen.

Wolfram ist eines dieser Schlüsselemente in der modernen Geochemie da es sowohl moderat siderophil als auch hoch inkompatibel ist. Auf Grund dieser Eigenschaften sind ca. 90 % des irdischen Wolframs während der Differentiation der Erde in den Kern migriert. Somit ist der Erdmantel stark verarmt (ca. 12 ppb, König et al., 2011; Palme and O'Neill, 2014). Da Uran, Thorium und Tantal ähnlich magmeninkompatibel wie W sind, aber nicht siderophil während der Kernbildung waren, hat sich die kombinierte W-Th-U-Ta Systematik zu einem bedeutenden Hilfsmittel entwickelt um Massenbilanzen für W in den verschiedenen geochemischen Reservoiren zu berechnen. Auf Grund ihrer ähnlichen Magmeninkompatibilität wurden die Elementverhältnisse von W-Th-U-Ta in den meisten silikatischen Umgebungen lange Zeit als konstant angesehen. Demgegenüber wurde eine hohe W-Mobilität in spätmagmatischen, wasserreichen Umgebungen festgestellt, wodurch es zu Anreicherungen bis hin zu Vererzung in hydrothermalen Systemen kommen kann. Darüber hinaus wurden W-Anreicherungen relativ zu U, Th und Ta in zahlreichen Inselbogenvulkaniten gefunden. Diese werden in Verbindung zu fluidkontrollierten Anreicherungen im Mantelkeil unterhalb des Vulkanbogens gebracht. Während dieser fluidkontrollierten Anreicherung variieren die erhöhten W/Th, W/U und W/Ta mit den Unterschieden im subduzierten Ausgangsmaterial. Diese Erkenntnisse heben die Notwendigkeit einer genaueren Betrachtung des Verhaltens von W in der alterierten ozeanischen Kruste hervor. Sie stellt ein Hauptquelle des subduzierten Materials im Mantelkeil dar. Bisher sind nur wenige W-Daten der ozeanischen Kruste von Gläsern der mittelozeanischen Rücken verfügbar. Somit ist nur wenig bekannt, ob Meerwasseralteration der ozeanischen Kruste bereits zu Umlagerungen von W auf dem Weg zur Subduktionszone führen kann. Alterierte ozeanische Kruste bedeckt mehr als 60 % der Erdoberfläche, somit ist die Kenntnis von W-Umlagerungen während ihrer Alteration von großer Bedeutung für das Verständnis des weltweiten geochemischen Zyklus von W. Alterierte ozeanische Kruste ist bekannt als geochemische Senke für einige Elemente (Alkalimetalle, Mg, S, U) und als Quelle für andere wie beispielsweise Ca, Si und Sr. Insbesondere die Serpentinisierung peridotitischer ozeanischer Kruste ist eine Senke für Li, B und K, Rb, Cs and Na. Andere Elementgehalte wie beispielsweise von Lu, Hf, Zr, Th und Ta werden dagegen



kaum von Alteration beeinflusst. Die Kombination aus mobilen und immobilen Elementen macht die Systematik aus W, U und Th zu einem wichtigen Hilfsmittel, um das Verhalten von Wolfram in alterierter ozeanischer Kruste zu untersuchen.

In dieser Arbeit werden Ergebnisse hochpräziser Isotopenverdünnungsmessungen von Lu-Hf-Zr-Nb-U-Th-Ta-W an unterschiedlich stark alterierter ozeanischer Kruste vorgestellt. Neben W, Ta, U und Th erlauben präzise Messungen von Lu, Hf, Zr, und Nb eine weitere Charakterisierung der initialen Magmendiversität der Proben und ihrer Ursprungsregion. Eines der Hauptergebnisse dieser Arbeit ist der Nachweis selektiver W-Anreicherungen in alterierter ozeanischer Kruste. Auf dieses Verhalten von W in marinen Umgebungen konnte bisher nur aus Ergebnissen von Studien an Inselbogenmagmen geschlossen werden. Darüber hinaus konnte nachgewiesen werden, dass W während hydrothermaler Alteration relativ zu den ähnlich inkompatiblen Th, U und Ta systematisch angereichert wird. Die resultierenden Anreicherungsfaktoren reichen dabei von 13 relativ zu frischem MORB bis hin zu 200 gegenüber unalterierten Peridotiten. Es konnte des Weiteren gezeigt werden, dass ein erhöhtes W/Th-Verhältnis am besten geeignet ist W-Anreicherungen zu identifizieren. Die Isotopie der ozeanischen Kruste (ausgedrückt als  $\delta^{186/184}\text{W}$ ) war im Vorfeld unbekannt. Diese konnte in der Arbeit bestimmt werden und ihr Einfluss auf die Zusammensetzung von Meerwasser umrissen werden. So konnte gezeigt werden, wie insbesondere niedrig-T, oxidierende Verwitterung und hoch-T Talkbildung zu einer leichten stabilen W-Isotopie führen. Demgegenüber werden stabile W-Isotope nicht während initialer Serpentinisierung fraktioniert. Diese Ergebnisse zeigen wie voranschreitende Alteration peridotitischer Ozeankruste zum Ausfluss von schweren Fluiden (das schwere Gegengewicht zur isotopisch leichten Alterationsfazies) ins Meerwasser führen. Diese Fluide stellen womöglich eine Quelle der schweren W Isotopie des Meerwassers dar. Darüber hinaus stammt die schwere Isotopie von Inselbogenmagmen vermutlich von Isotopenfraktionierung während der Dehydrierung der subduzierten ozeanischen Kruste oder isotopisch schweren Alterationsfluiden, welche bei der Dehydrierung aus der ozeanischen Platte ausgepresst werden. Die leichtere W-Isotopie von Magmen welche weiter entfernt von der Subduktionszone ausfließen, repräsentieren in diesem Modell die Dehydration der isotopisch leichten Alterationsfazies.

Das Studium von W/Th und  $\delta^{186/184}\text{W}$  stellt daher ein umfassendes Werkzeug dar, anhand dessen verschiedene Alterationstypen, sowie der Ursprung des Meerwasser-Wolframs und der Einfluss der subduzierten ozeanischen Kruste auf die Zusammensetzung von Inselbogenmagmen untersucht werden kann.

# **1.Introduction**

## 1.1 Aim of this study and chapter overview

The aim of this study is to describe the behaviour of W during oceanic crust alteration and to study its implications on the global geochemical cycle of W. A first introduction (**chapter 1**) describes the recent knowledge of the formation of the Earth and its crust, the geochemical behaviour of W and the stable W isotope systematics. It is followed by the description of the W behaviour in oceanic crust formed at super-fast spreading rates in **chapter 2**. In this chapter alteration effects on the W budget are studied at IODP hole 1256D, which was the first hole to sample a complete, intact section of oceanic crust down to the gabbros (Wilson et al., 2003). Drill hole 1256D was deepened into the Cocos plate, which was formed 15 Ma ago at very high spreading rates ( $> 220 \text{ mm a}^{-1}$ ) at the east-pacific rise (EPR). Because of the inverse relationship between spreading rate and the depth to axial low-velocity zones all major elements of the oceanic crust are accessible for drilling and could be sampled (Wilson et al., 2003). The chapter is focussed on the mafic basement of 1256D, where fluids from different provenance (downwelling evolved seawater vs. upwelling hydrothermal fluids) intersect. Alteration intensity is limited to recrystallization of  $< 35 \%$ . Nevertheless, significant W enrichment relative to U, Th, Ta could be identified in all encountered portions (total range of  $W/Th = 0.18 - 3.3$ ). Most extreme enrichment was identified at zones of extensive hydrothermal alteration and peak-T conditions at the interface of the sheeted dike section and gabbroic intrusions ( $W/Th = 0.75 - 3.3$ ). In the latter, W concentrations resemble fluid circulation cells defined by Sr-isotope data (Harris et al., 2015). Tungsten depletion is absent, but as the extent of W enrichment is decreasing from its highpoint at lower sheeted dike section towards the lowest drilled portions, the origin of W addition might be in the hydrothermal root zone below the drilled gabbro intrusions.

Whereas chapter 2 is focussed on basaltic super-fast spreading upper oceanic crust, the altered oceanic crust studied in **chapter 3** is composed of strongly serpentinized mantle-peridotites, exhumed in a super-slow, magma starved spreading environment. The crust formed at the Mid-Atlantic Ridge, near the 15°20' fracture zone and was drilled during ODP Leg 209 (Kelemen et al., 2004). The oceanic basement in this region consists of highly serpentinized abyssal peridotites ( $> 95 \%$  recrystallisation) and associated gabbroic intrusives. The drilled dunites and harzburgites are amongst the most depleted ever encountered in oceanic crust. Major alteration styles covered in the sample suite are hydrothermal alteration, rock/fluid-dominated serpentinization, talc alteration, and low-T oxidative seawater alteration. Selective W enrichment is by orders of magnitude higher than at site 1256. Moreover, the enrichment of W over U, Th and Ta is not restricted to a specific alteration style but is a ubiquitous feature common to all alteration facies at Leg 209. Specific characteristics of the studied alteration styles cover strong W enrichment during early serpentinization (sampled in hole 1268A, 1270 and 1271,  $W/Th = 0.27 - 208$ ), W leaching by silica metasomatism (hole

1268A, W/Th 40 – 0.2, decreasing with proceeding Si-metasomatism) and W enrichment during late-stage oxidative seawater alteration (hole 1270D and 1272A, W/Th = 0.12 - 11). Thus, serpentinized peridotitic oceanic crust most likely constitutes an important geochemical reservoir in the global geochemical cycle of W. Altered portions of the lower oceanic crust may therefore contribute significantly to the enrichment of W found in arc lavas, and to the recycling of W into the Earth's mantle.

In chapter 2 and 3, zones of W enrichment in altered oceanic crust have been identified and described. Nevertheless, the origin of the excess W remains largely enigmatic. Potential W sources include a) seawater W that is retained during alteration or serpentinization, b) hydrothermal fluids venting on-ridge or c) local redistribution during various alteration processes. Since processes invoking these reservoirs are active at different temperatures, and temperature is a major controlling factor in stable isotope fractionation (Bigeleisen and Mayer, 1947; Schauble, 2004) the stable W isotope method was employed to samples from different types of altered oceanic crust to trace the sources and the geochemical cycling of W along mid-ocean ridge systems in **chapter 4**. Moderately altered basaltic oceanic crust from hole 1256D shows  $\delta^{186/184}\text{W}$  between +0.046 ‰ and +0.116 ‰, close to the modern mantle value of  $+0.085 \pm 0.019$  ‰, indicating only limited isotope fractionation. Melt-impregnated, mainly serpentinized samples from Leg 209 are strongly enriched in W but show mantle-like  $\delta^{186/184}\text{W}$  values between +0.055 ‰ and +0.125 ‰. In contrast, W-enriched serpentinites that were subsequently Si-metasomatized have very low  $\delta^{186/184}\text{W}$  values between -0.117 ‰ and -0.040 ‰. Most low-T oxidative weathered peridotites have isotopically light compositions ( $\delta^{186/184}\text{W}$  between -0.071 ‰ and -0.005 ‰). Tungsten in seawater (+0.545 ‰, Kurzweil et al., 2020) and in sediments (+0.085 – +0.300 ‰) is isotopically extremely heavy, representing an unlikely source of secondary W enrichment in altered oceanic crust. Thus, igneous rocks located at the root zone of hydrothermal alteration systems close to the magma chamber beneath the actual spreading centre most likely represent the predominant source of secondary W enrichments. Additional sources of localized enrichment might be abundant mafic dikelets found at Leg 209. Tungsten leaching and its secondary enrichment have not led to stable isotope fractionation as these are high-T processes, where fractionations are probably very small. Significant W isotope fractionation occurred during late-stage alteration processes such as talc formation during Si-metasomatism or low-T oxidative seawater weathering, thereby preferentially mobilizing isotopically heavy W by fluids.

## 1.2 Tungsten (W) and its basic geochemical properties

The name „tungsten“ for W originates from the Swedish word for its most important ore mineral scheelite ( $\text{CaWO}_4$ ) (“tungsten, n.,” OED - 2019). In this context, “tung-“ means heavy and “-sten” stone. Even though tungsten has been known as a chemical element from the early 18<sup>th</sup> century onwards, its industrial applications were limited until the dawn of the 20<sup>th</sup> century when it was used as glowing filament in light bulbs and as steel additive to harden it for its application in heavy artillery and body armour.

In Earth’s crust W ranks 56<sup>th</sup> of the most common elements, with  $1\,000\text{ ng}\cdot\text{g}^{-1}$  in the Earth’s crust, and  $12\text{ ng}\cdot\text{g}^{-1}$  in the Earth’s mantle (König et al., 2011; Rudnick and Gao, 2003). As metallic transition element, it has an atomic number of 74 and belongs to the 6<sup>th</sup> period in the periodic table of elements. The relative average atomic mass of tungsten is  $183.85 \pm 0.03$  amu. Tungsten’s most important isotopes are  $^{180}\text{W}$  (0.13 % natural abundance),  $^{182}\text{W}$  (26.3 %),  $^{183}\text{W}$  (14.3 %),  $^{184}\text{W}$  (30.67 %), and  $^{186}\text{W}$  (28.6 %, abundances from Lassner and Schubert, 1999). As highly refractory element during solar system formation, W condensed with other refractory elements to alloys which can be found in chondritic meteorites today. Main oxidation states of W on Earth are  $\text{W}^{4+}$  and  $\text{W}^{6+}$  with the latter being the most significant in recent magmatic settings (Fonseca et al., 2014; Kurzweil et al., 2019). The combined systematics of the similarly incompatible W, U, Th, and Ta is a well-known and widely used tool in geochemistry to trace subduction zone dynamics, early Earth processes like core formation and early solar system formation. Nevertheless, the knowledge of W behaviour during seafloor alteration is still limited even though altered oceanic crust forms the majority of the Earth’s surface (> 60 %, Wilson et al., 2006). Furthermore, altered oceanic crust is a major element carrier for crust-mantle exchange and its subduction exerts strong control on the composition of ocean island basalts (OIBs) and the composition of arc magmas.

In the presented work I will thus elaborate how tungsten, the “hard stone”, acts during seawater alteration of oceanic crust formed in different environments and spreading rates and how this affects the W global geochemical cycle.

### 1.3 Formation of the Earth, its differentiation, and the influence on global W distribution

While the universe itself is 13.7 billion years (Ga) old (Bennett et al., 2003), the solar system formed 4.6 Ga ago by condensation, contraction, and collapse of an interstellar cloud. Most of the collapsing matter is He and H generated during primordial nucleosynthesis. Star generations preceding the Sun enriched the interstellar cloud with heavier elements such as Si, Mg, Al, Hf, and W. The collapse resulted ultimately in the formation of a protosun, where the converging gas rises in density and temperature, enabling the start of fusion processes. The movement of masses towards the centre of gravity adds torsional momentum to the system resulting in a rotating accretionary disk. Turbulent and magnetic drag by further ongoing gravitational compaction transfer this momentum further outwards and allow the core to reach temperatures that ignite fusion processes. Resulting radiation heats the gas in the accretionary disk and pushes most of it into far space. Portions of dust that neither collapsed into the protosun, nor were pushed out of its gravitational influence build up the planets, asteroids, meteorites, and comets.

Remaining protoplanetary dust was initially amalgamated by non-gravitational accumulation to planetesimals with 1 – 10 km diameter within the first ca. 10 ka of solar system existence. Growing influence of gravitation and resulting tidal forces led to the formation of protoplanets with up to 4 000 km in diameter. All these processes reduced the number of (proto-)planetary bodies in the solar system. After the first 1 Ma, only 22 protoplanets were left in the space between Mercury and Mars (Weidenschilling et al., 1997). The collisions and mergers of these protoplanets in a period of 10 – 100 Ma after solar system formation led to the terrestrial planets as we know them today. The Moon is probably a legacy of such a giant impact between the planetary body *Theia* and the protoearth. For a correct dating of this event, the decay of  $^{182}\text{Hf}$  to  $^{182}\text{W}$  was used and it could be demonstrated that the Moon was most likely formed at ca. 4.51 Ga or 50 Ma after solar system formation (Thiemens et al., 2019) when the Earth's core was already formed (Kleine et al., 2002).

Early Earth was subject to large-scale mixing, convection, (local) homogenisation and equilibration. These happened at temperatures above the magma solidus. In early Earth, thermal energy was provided by conversion of potential gravitational energy during accumulation, by decay of  $^{26}\text{Al}$  and  $^{60}\text{Fe}$ , and by conversion of kinetic energy of large impactors on the protoearth. Heated by the named processes, large magma oceans with depths up to 1500 km were formed. These magmas contained immiscible melt droplets, comprising mainly Fe and Ni which, due to their high density, descended fast towards the bottom of the magma ocean and formed layers of liquid metal. Large seas of molten metal developed to metal diapirs that broke through the solid lower mantle and descended to the centre of gravity, ultimately

forming a solid metal core in the inner Earth. Lighter minerals crystallized and formed an early crust upon the magma oceans. During that phase of Earth's history, overall geochemical conditions were reducing. In this environment W occurred as metal acting highly siderophile, and was sequestered almost completely into the metallic core, leaving the mantle and proto-crust strongly W-depleted (ca. 12 ppb, Palme and Rammensee, 1981, König et al., 2011, Palme and O'Neill, 2014).

Continental crust has an average thickness of roughly 40 km, its cores are composed of Archaean Tonalite-Trondhjemitic-granodioritic (TTG) rocks. TTG formed in the Archaean when the mantle temperature was ~ 300 K above today's level and fragments of oceanic crust were not (completely) subducted but thrust over each other, giving rise to partial melting and fractionation of granitic melts from a basaltic magma. The lower density of the so formed continental cores ( $2.7 \text{ g cm}^{-3}$ ) compared to mantle and oceanic crust ( $2.95 \text{ g cm}^{-3}$ ) prevented them from being subducted. Its magma incompatibility led to enrichment of W in continental crust with concentrations of ca. 1000 ppb (König et al., 2011). Over the course of Earth's history, these cratons grew through mergers with smaller plates. Erosion over billions of years left behind only few remains of archaic crust.

Much younger than the continental crust is the oceanic crust. It is continuously formed at mid ocean ridges (MOR) and steadily recycled at convergent plate boundaries, like the Andes (Fig. 1.1). During its lifespan, oceanic crust is subject to continuous alteration which affects the elemental distribution in the crust (e.g. Hart and Staudigel, 1982; Staudigel et al., 1996). The formation and alteration of oceanic crust will be further discussed in chapters 1.4 and 1.5. A sketch in Figure 1.2 illustrates processes at an active spreading centre. At collisional continental margins, altered oceanic crust is subducted. Dehydration of the downgoing slab allows magma generation in the mantle wedge between subducted slab and continental crust. Dehydration fluids transport significant amounts of the trace element record of subducted slab. Elevated W/Th, W/U and W/Ta representing selective W enrichment have been identified in arc settings (König et al., 2008) and were attributed to dehydration fluids carrying significant amounts of W from subducted crust. The geologically quick cycle of oceanic crust formation, alteration and recycling is responsible for a maximum age of ~ 200 Ma of the oldest preserved oceanic crust (Fig. 1.1). Due to the inaccessibility of in-situ oceanic crust, the behaviour of trace elements such as W in this setting is not yet completely understood.

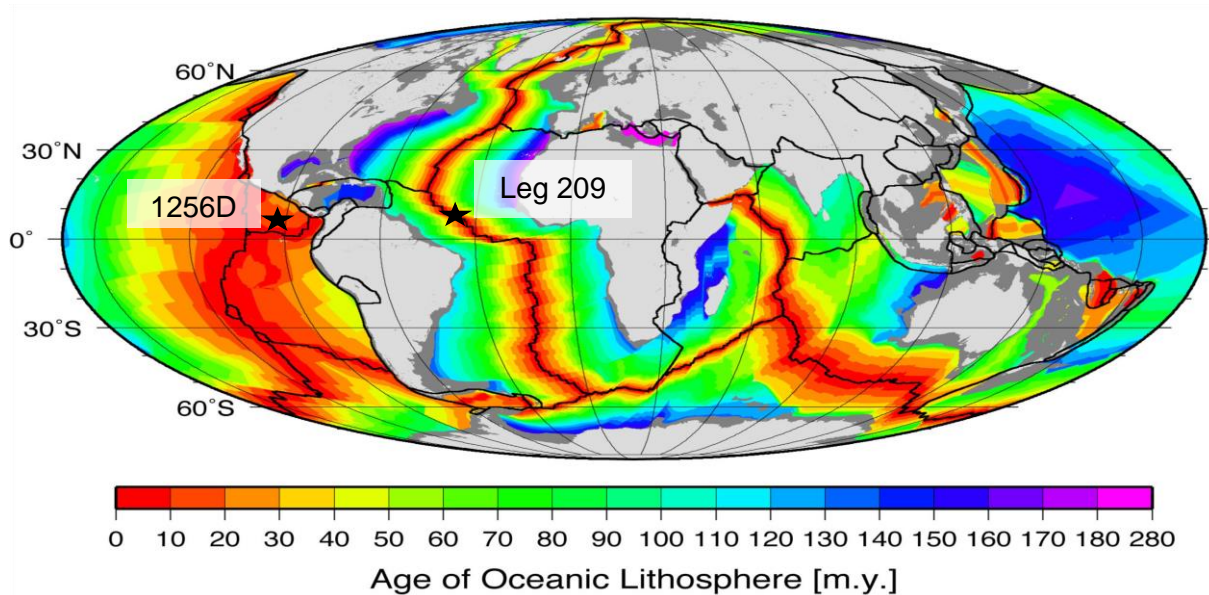


Figure 1.1: Age distribution of oceanic crust. Coloured parts of the map reflect oceanic crust which composes more than 60 % of the Earth's surface. Studied sites in this thesis are marked with stars (modified after Müller et al., 2008).

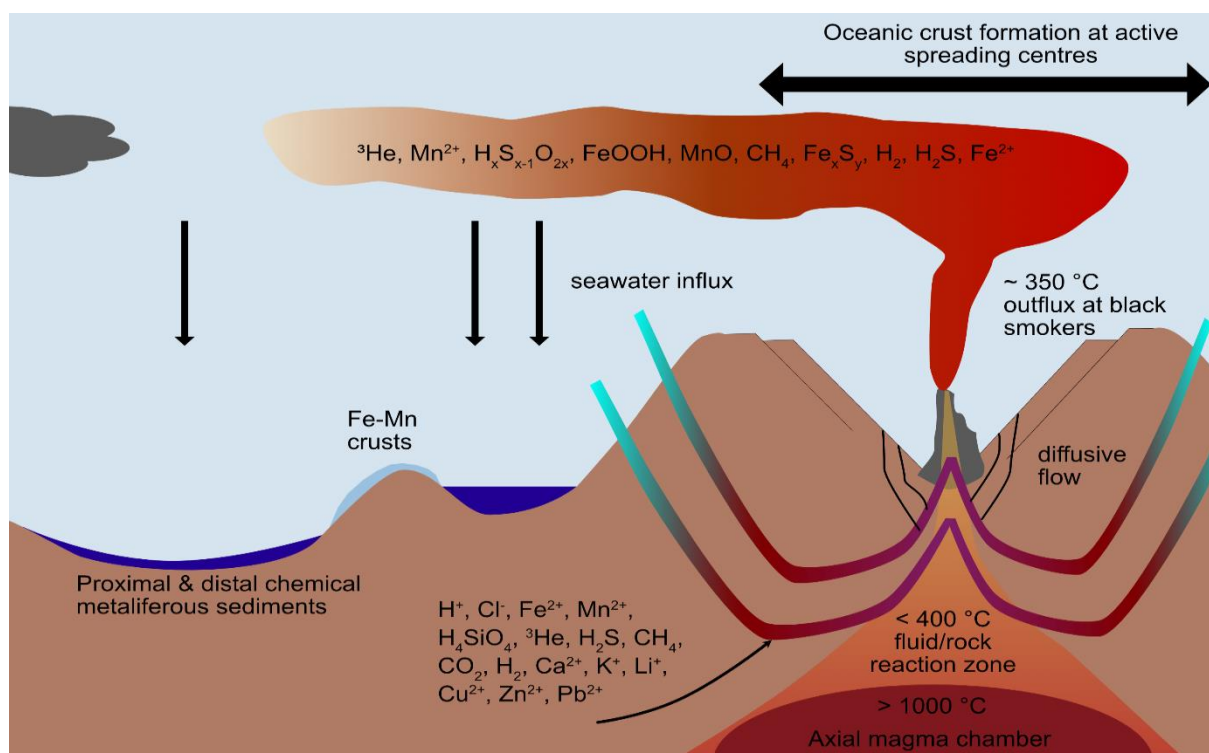


Figure 1.2: Sketch of typical elemental redistribution at active spreading centres. Downward percolating seawater is heated when approaching the magma chamber. The heated fluid leaches numerous elements as e.g. Fe, Mn, Pb from the basalts and transports its upwards where it emanates at black smokers or through diffusive flow along the spreading centre. The resulting submarine cloud is rich in base and precious metals, by reaction with seawater-anions they precipitate as chemical sediments in the surrounding of the spreading ridge. (modified after: <https://oceanexplorer.noaa.gov/explorations/02fire/background/hirez/chemistry-hires.jpg>)



## 1.4 Structure and formation of the oceanic crust

As the main chapters of the presented thesis will frequently draw back on the structure of the oceanic crust with its characteristic properties, this section will provide the reader with the main information to locate manifestations of W mobilization in altered oceanic crust (AOC). Formed at active plate boundaries at average depths of 4 500 mbsf (meters below seafloor), the oceanic crust is much thinner than its continental counterpart (10 – 12 km vs. > 30 km). The driving force of sea-floor spreading is the pull of downgoing slabs at oceanic-continental plate boundaries such as the Andes (Carlson et al., 1983). The resulting formation of oceanic crust at MOR is one of the major mechanisms of heat loss from the Earth's interior.

By seismic studies, three layers of oceanic crust have been identified. Layer 1 is the uppermost and characterized by low velocities ( $< 3.4 \text{ km s}^{-1}$ ) and consists of unconsolidated terrigenous and pelagic sediments. Sedimentation rate and thus the extent of Layer 1 is highly variable and depends on the availability of sedimentary influx, local deep-sea currents, their variations, as well as the distance from spreading centres. In general, the sedimentary cover thickens away from active plate boundaries and has a global average thickness of ca. 400 m. Seismic Layer 2 comprises consolidated sediments, inflated flows and parts of the sheet and massive flows that are produced by effusive volcanism at spreading centres. It is characterized by seismic velocities ranging between  $3.4 \text{ km s}^{-1}$  and  $6.2 \text{ km s}^{-1}$ . Where Layer 2A is present at spreading centres, its initially porous nature enables hydrothermal circulation. An effect of this circulation is the precipitation of minerals in pores and vugs. Over time, Layer 2A develops to Layer 2B with higher seismic velocity and lower porosity. In the absence of Layer 2A, 2B constitutes the basement of Layer 1. Layer 2C is characterized by high seismic velocities of  $5.8 - 6.2 \text{ km s}^{-1}$  and lower porosity. It is composed of intrusive, (ultra-)mafic rocks like the sheeted dike complex but can also include the lower parts of sheet and massive flows. Layer 3 is characterized by further increasing seismic velocities ( $> 6.7 \text{ km s}^{-1}$ ). It is associated with the deepest portion of the sheeted dike complex, comprising local intrusions of gabbros and with the onset of the plutonic section, completely constructed of gabbroic rocks. A typical section of oceanic crust with its rheology can be found in Fig. 1.3A & B. Samples presented in this thesis cover all three layers.

Spreading rates at MOR have strong influence on the morphology and the rock types composing the oceanic crust. The two endmembers are slow-spreading ridges with rates of  $< 11 \text{ mm a}^{-1}$ , e.g., at Gakkel ridge in the Arctic Ocean (Michael et al., 2003) and the fast-spreading ridges East Pacific Rise with rates as high as  $220 \text{ mm a}^{-1}$  (Wilson et al., 2006). On fast-spreading ridges an axial high with up to 400 m in height and up to 2 km in width forms mainly in response to buoyancy of the hot magma supply (Carbotte and Macdonald, 1994). In contrast, at typical slow-spreading ridges, a rift valley with a depth of 500 – 2500 m depth and

30 – 50 km width is developed. Within the valley, sometimes a small central high is built by limited volcanic activity (Macdonald, 1982, Fig. 1.2). Like rheology, the spreading rate influences the geochemistry of freshly produced oceanic crust. Magma chambers below slow-spreading ridges are characterized by accumulation of calcic plagioclase, phenocryst-magma reactions, and pyroxene. Magma chambers below fast-spreading ridges are characterized by low-pressure basalt fractionation to Fe-rich composition with little to no plagioclase accumulation and crystal-magma interaction (Flower, 1981; Kearey et al., 2009). Fast-spreading crust is mainly composed of basaltic intrusive and effusive rocks whereas slow-spreading crusts are typical ultramafic mantle rocks, exhumed by tectonic forces. In chapter 2, W distribution in crust formed at super-fast spreading rates will be discussed. The shallow structure of slow-spreading ridges is characterized by brittle deformation of upper, due to starving magma supply, cold crust with pervasive extension by normal faulting (Smith and Cann, 1993). Moreover, the extensional tectonics result in the exhumation of mantle rocks effects of alteration within are discussed in chapter 3.

Usually, several episodes of volcanic and tectonic extension are exposed at MOR. Extensional tectonics lead to a thin mafic crust and regions with frequent exposure of peridotites – rocks that solidified at depths of 2 – 3 km. Crust at fast-spreading ridges is characterized by effusive magmatism resulting in relatively smooth surfaces, a thicker mafic crust covering the gabbroic section with about 2 km height (Kearey et al., 2009).

## 1.5 Alteration of oceanic crust and its significance for global elemental distribution

Its origin in zones with high fluid circulation and the subsequent long exposure to abrasive influences lead to extensive alteration of nearly all portions of oceanic crust over time (Fig. 1.2 and Fig. 1.3). The formation of oceanic crust and its subduction produces and consumes large quantities of heat and crust volume. Approximately  $16 \text{ km}^3$  ( $\sim 7 * 10^{13} \text{ kg} \cdot \text{a}^{-1}$ ) of oceanic crust is produced and consumed at active and passive continental margins each year. Hydrothermal water fluxes include about  $3.5 * 10^{12} \text{ kg} \cdot \text{a}^{-1}$  of black smoker fluxes and  $6.4 * 10^{14} \text{ kg} \cdot \text{a}^{-1}$  from low-temperature off-axis venting (Elderfield and Schultz, 1996). Alteration-related fluids mix with large volumes of seawater and modify its chemical composition in geologically short times of 0.1 -10 Ma (Kadko, 1993). Alteration mainly depends on the rate of seafloor-spreading which limits the flow rate of hot, metal-rich hydrothermal fluids at spreading centres and determines the rock type that constitutes oceanic crust and is exposed to seawater. Additionally, sedimentation, which potentially seals igneous and plutonic portions of oceanic crust from seawater influence, plays a major role on alteration intensities. Alteration of oceanic crust is strongly related to fluid flow through veins and vugs. Thus, completely altered samples can be found in close vicinity to nearly unaltered specimen. Prominent results of hydrothermal fluid circulation are black and white smoker deposits, which are extremely enriched in anhydrite and numerous base and precious metals (Fig. 1.2).

Hydrous alteration by relatively low-temperature (low-T) fluids hydrates (ultra-)mafic crust. The involved processes are summarized under the term “serpentinization”. Serpentinization comprises a series of hydration reactions that occur when ultramafic rocks are exposed to aqueous fluids at  $T < 350^\circ - 400^\circ\text{C}$  along the spreading centre. It is dominated by progressive alteration of olivine to lizardite and chrysotile ( $\pm$  brucite  $\pm$  talc  $\pm$  magnetite; e.g., Bach et al., 2004; Moody, 1976). Other prominent serpentinization reactions include the formation of chrysotile and brucite by the hydration of forsterite and the formation of chrysotile by the hydration of forsterite and talc (Caruso and Chernosky, 1979; Johannes, 1968; O’Hanley et al., 1989). The extent of hydration and serpentinization is largely based on the crust’s mineral budget, e.g., with olivine being more readily hydrated than plagioclase. The uppermost oceanic crust is much more porous and permeable than its underlying sections (see above). Consequently, great volumes of fluid can circulate through it, leading to a sequence of alteration effects such as the formation of celadonic alteration halos in young ( $< 2.5 \text{ Ma}$ ) lava, formation of reddish iron oxyhydroxide-rich alteration halos by cold seawater solutions ( $> 2.7 \text{ Ma}$ ), growth of saponite and pyrite by the flow of more evolved seawater solutions, and precipitation of late carbonate filling fractures (Alt, 2004). Young, dark celadonic alteration halos are enriched in Fe, K, Rb, Cs, B and  $\text{H}_2\text{O}$  relative to unaltered basalt (Fig. 1.2). Only 1 –

2 % of the volcanic section is affected by this alteration type. Retaining the celadonitic halos, continued hydrothermal reactions during off-axis fluid circulation forms alteration halos in which olivine is replaced and pores are filled by amorphous Fe-oxyhydroxides, Fe-oxides ± saponite ± celadonite (Alt, 2004). Saponite formed during oxidative alteration is characterized by Mg-rich chemical composition (Andrews, 1980). Bulk-rock chemical changes include enrichment of Fe, H<sub>2</sub>O, K, U, Li, Rb, Cs, B, increased Fe<sup>3+</sup>, <sup>87</sup>Sr/<sup>86</sup>Sr, δ<sup>11</sup>B, δ<sup>7</sup>Li, δ<sup>18</sup>O and losses of S and Ca, as well as decreased δ<sup>34</sup>S. Restrictedly, Mg is lost from single rock portions but is gained by the whole rock through redistribution and rearrangement resulting in the formation of vein-filling smectite (Alt, 2004 and sources therein).

Throughout its downward percolation, seawater evolves to more reacted compositions, diminishing oxidation effects with time. Additionally, burying of oceanic crust with sediments and/or starving heat supply may lead to a more restricted seawater circulation developing reducing conditions (Alt, 2004). Characteristic alteration minerals in this advanced stage of alteration are Fe-rich saponites. In general, 20 % of the original mineral assembly is recrystallized at this stage, again varying strongly on a limited depth scale (Alt, 2004). The overall net chemical change of the whole rock is limited due to the finite exchange with other reservoirs. The volume of olivine while altering to saponite may increase by > 100 % mainly by hydration reactions resulting in further sealing of the oceanic crust (Alt, 2004 and sources therein). More alkaline conditions cause the transition of Fe-oxyhydroxides to carbonates and zeolites, which marks the last alteration stage in the basaltic section. Formation of carbonates and zeolites is triggered by the extraction of OH<sup>-</sup> by Mg or Fe from the solution and the consequently increasing pH of the fluid (Alt, 2004 and sources therein).

Interferences of downwelling heated seawater with upwelling hydrothermal fluids are manifested in intense alteration and mineralization in the so-called mixing zone (Alt et al., 2010). This mixing or *transition zone* is characterized by the lithologic transition from volcanic sheet and massive flows to the igneous sheeted dike complex (Wilson et al., 2006). Proceeding downwards into the hydrothermal alteration regime, magmatic fluids are the most important alteration agents. The ever-increasing temperature is reflected in the alteration mineral assemblage. Saponite (< 100 °C) changes to chlorite-smectite (100 – 200 °C) and to chlorite (> 200 °C); actinolite (> 300 °C) and ultimately hornblende (> 450 °C) are typical alteration phases. Temperatures > 230 °C give rise to greenschist facies mineral assemblages (Fig. 1.3). The highest alteration intensities are to be found at the base of the sheeted dikes and in the plutonic section where greenschist- to actinolite-grade metamorphic assemblages are formed at temperatures exceeding 450 °C. Locally, even higher temperatures caused by the intrusion of gabbroic melts or fluids developed therefrom, lead to local contact metamorphism and play an important role on the whole-rock trace element budget. Vertical movement of the axial

magma chamber and the conductive boundary layer right above give rise to several cycles of pro- and retrograde metamorphism, dehydration and hydrous partial melting in the root zone of hydrothermal fluid circulation (France et al., 2010). The root zone of the hydrothermal fluids is within the lowest parts of the sheeted dike complex and the uppermost plutonic section. The influence of hydrous alteration decreases significantly beneath this root zone, where solidified portions of the axial melt lens have only limited porosity (Alt et al., 2004; Alt et al., 2010). Nevertheless, intrusion of mafic dikelets in already serpentinized crust may result in local fluid generation and provide further heat and incompatible trace elements to the alteration mineral assemblage.

During lateral movement away from the spreading centre, lithospheric cooling prevents seawater from deep penetration of lower crustal sections resulting in (a) retrograde metamorphism under relatively static, isochemical conditions in former hydrothermally altered sections and (b) seafloor weathering of low-T altered samples on top of the oceanic crust. A typical sequence of alteration types and their effects can be seen in Figure 1.3. To sum up, the alteration and weathering of the aging crust results in significant redistribution of Fe, K, Rb, Cs, B, Mg,  $^{18}\text{O}$ ,  $^{87}\text{Sr}$ , U,  $\text{H}_2\text{O}$ ,  $\text{SO}_4^{2-}$  and C as well as in the enrichment of numerous base and precious metals in the volcanic section (Alt and Teagle, 1999; Hart and Staudigel, 1982). The alteration effects described above may offset each other and elements are significantly redistributed throughout different layers of oceanic crust. Moreover, repeated cycles of pro- and retrograde metamorphism caused, e.g., by melt intrusion or migration of the axial melt lens may lead to an extremely complex alteration history.

The lifespan of oceanic crust compared to continental crust is relatively limited. Today's oldest crust is ca. 200 Ma old (Fig. 1.1). Oceanic crust will be subducted in collisional settings which may be characterized as oceanic-oceanic plate collision (e.g. Tonga trench) or oceanic-continental plate collision (e.g. Andes). As the slab sinks through the mantle, heat is transferred from the surrounding asthenosphere to oceanic crust resulting in dehydration processes in the upper basalts of the subducted slab. Sediments covering oceanic crust also dehydrate and may melt due to their low melting temperatures. The solidus of rocks is lowered in the presence of hydrous fluids which largely facilitates melting in subduction zone regimes. The release of metamorphic fluids from the slab is occurring in several tens of thousands of years. If sufficient (5 – 15 %) partial melting occurs, the melt aggregates and begins to rise toward the base of the crust (Pearce and Peate, 1995). As the magma moves into the crust it differentiates and may mix with either new, crust-derived melts or older melts. In continental arc settings, the generation of crust-derived melts is common because the solidus of continental crust in presence of hydrous fluids may be low enough to result in partial melting. Melts that move through a thick layer of continental crust may become enriched in incompatible elements

before reaching the surface. These magmas also may lose some of their water content and begin to crystallize, with or without cooling. The emplacement of plutons and volcanic rock within or on top of the crust represents the final stage of magma transport (Kearey et al., 2009). Ultimately, the magmas derived from subducted oceanic crust will largely contribute with their specific trace element geochemistry to the chemical composition of the volcanism at arc settings. Moreover, large ore provinces form in response to magma emplacement (e.g. Yongbao et al., 2014). Not the whole oceanic crust is molten by subduction zone processes. Significant portions will be subducted into the Earth's lower mantle where they consolidate to form layers and contribute largely to the chemical composition of OIBs, besides MORB the second important mantle upwelling process on the Earth (Sun et al., 2011).

In summary, the composition of altered oceanic crust has huge implications on the trace element budget of the whole Earth as it a) covers more than 60% of the Earth's surface, b) is subject to intense reworking and alteration by seawater, and c) is subducted and related fluids carry elemental signatures to the melting region of arc magmatism as well as remaining oceanic crust potentially consolidates in lower mantle where it acts as source region for mantle plume generation. The binary characteristics of W and its behaviour during oceanic crust alteration thus potentially provide a good tool to examine various geochemical problems related to crust-mantle processes.

**(A)** Petrographic and metamorphic sketch of typical oceanic crust at fast spreading ridges **(B)** Fluid circulation within young oceanic crust

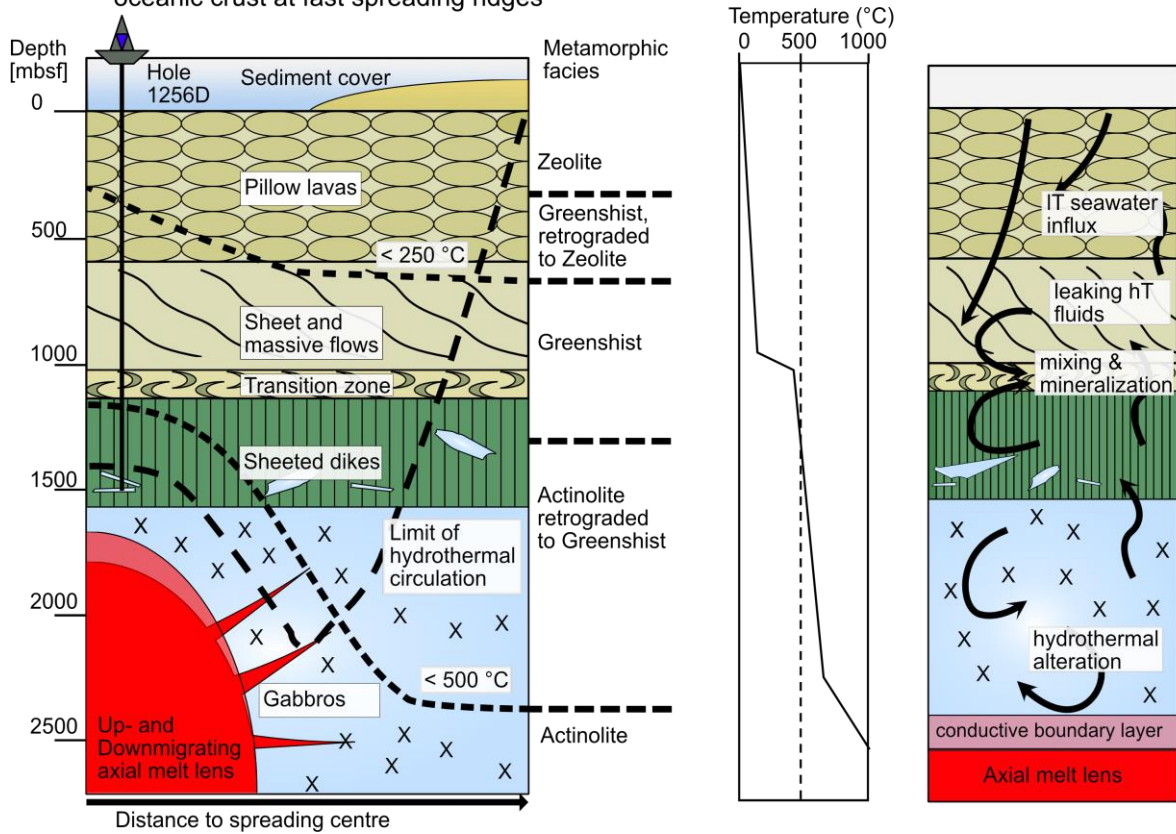


Figure 1.3: The lithologic situation at hole 1256D (A). By moving horizontally away from spreading centre, T supply form axial melt lens and the penetration depth of downward percolating seawater decreases resulting in retrograde metamorphism (A, modified after Elthon, 1981). Temperature and fluid supply in young hydrothermal systems allows the development of circulation cells within distinct portions of oceanic crust and extensive alteration in the mixing zone (B, modified after Alt et al., 2010).

The lithology encountered at slow-spreading ridges, such as the MAR at Leg 209, differs greatly from lithologies at superfast-spreading ridges (C). The structures are dominated by tectonic processes like faulting and thrusting rather than effusive magma production. Prograde alteration is largely facilitated by limited gabbroic dike intrusions and heated seawater recharge. Retrograde alteration is focussed along fluid pathways of high-T hydrothermal fluid outflow.

## 1.6 Global cycle of W

After defining the setting in which W mobility is studied in this work, the recent knowledge of the geochemical W cycle will be summarized in the following section. The distribution of W in the silicate Earth is defined by binary processes. Tungsten is moderately siderophile (“iron loving”) under reducing conditions such as early core-mantle differentiation of the Earth and extremely incompatible during silicate Earth differentiation (Palme and Rammensee, 1981). At the oxidizing conditions during continental crust formation, W is predominantly in its hexavalent  $W^{6+}$  state and acts as lithophile element. The more reduced  $W^{4+}$  has been identified in lunar samples but is not common in recent geochemical reservoirs (Fonseca et al., 2014). Moreover, as W is highly incompatible in magmas, it is enriched in the evolved granitic melts that play a major role in continental crust formation. This process ultimately resulted in a depleted mantle between a W-enriched core and crust (König et al., 2011; Lassner and Schubert, 1999; Palme and Rammensee, 1981).

Tungsten shares its incompatibility with thorium, uranium, and tantalum. As similarly incompatible elements are not fractionated from each other during silicate melting, W/Th, W/U and W/Ta can be regarded as constant in most geochemical reservoirs and have been used to trace the influence of various geochemical processes on W distribution (e.g., Arevalo and McDonough, 2008; König et al., 2011; Newsom et al., 1996; Noll et al., 1996, Fig. 1.4). Canonical values for W/U in the modern mantle are  $0.65 \pm 0.45$  (Arevalo and McDonough, 2008). W/Th and W/Ta in modern mantle are 0.09 – 0.14 and 0.28 (König et al., 2011). As outlined above, continental crust is enriched in W relative to the mantle, resulting in W/Ta of ~ 1.4 and 1000 ppb W (König et al., 2011). The named elemental ratios have been used to constrain the bulk abundance of W in the silicate Earth, e.g., by Palme and O'Neill, 2003, Rudnick and Gao, 2003 and König et al., 2011. Another application of W systematics are the dating of core and moon formation, e.g., by Thiemens et al., 2019.

Selective W enrichment over similar incompatible Th, U and Ta has been identified in arc settings (König et al., 2008) and was attributed to dehydration fluids, carrying significant amounts of W from subducted crust, particularly, if fluids from the subducted slab control the elemental budget in the sub-arc mantle. Independently of oxygen fugacity and salinity, W strongly partitions into aqueous fluids, (Bali et al., 2012). Tungsten enrichment in the sub-arc mantle wedge is most pronounced in arcs where subducted sediments with high W concentrations are involved (e.g., Indonesia, Kermadec, Cyprus) and less striking in arcs where negligible amounts of pelagic sediments are involved (e.g., W-Pacific arcs, König et al., 2011). During fluid enrichment, ratios of W/Th, W/U and W/Ta are elevated to various extents, depending on the type of subduction component involved (König et al., 2008, 2011; Bali et al., 2012). Recently, arc lavas have also been identified as sites of variable W stable isotope



signatures (Kurzweil et al., 2019, Mazza et al., 2020). These studies demonstrated that the range in  $\delta^{186/184}\text{W}$  values of arc lavas is significantly larger compared to MORBs and OIBs (e.g., Kurzweil et al., 2019, Mazza et al., 2020). In arc lava suites, where the W budget is controlled by melts from subducted mafic crust,  $\delta^{186/184}\text{W}$  values are close to the upper mantle value or slightly elevated (e.g., Papua New Guinea, New Britain, +0.079 to +0.133 ‰; Kurzweil et al., 2019). In arc suites, where the W budget is controlled by subducted pelagic sediments (e.g., Sunda, Cyprus),  $\delta^{186/184}\text{W}$  values are significantly higher (Kurzweil et al., 2019). Consistently, most sediments transported towards subduction zones show heavy stable W isotope compositions (+0.085 – 0.302 ‰, Kurzweil et al., 2019). This larger variability is attributed to variations in the stable W isotope compositions of different subduction components, retention of light W in residual phases like rutile or to stable W isotope fractionation processes during subduction (Kurzweil et al., 2019, Mazza et al., 2020). The isotopic state of the altered oceanic crust itself is yet unconstrained and thus, its influence on the isotopic state of arc magmas remains unclear. A sketch of the global geochemical cycle of W and the recently known stable W isotope composition is given in Fig. 1.4.

The fluid immobility of Th and Ta as well as the mobility of U is well documented (e.g., Niu, 2004) but of W, which was long considered to be immobile little is known about how it behaves during alteration processes. Since arc lavas are greatly influenced by fluids originating from dehydration of the subducted oceanic crust, it is of great importance to study whether W may be enriched by alteration in the oceanic crust itself and if elevated W/Th, W/U and W/Ta in arc lavas may potentially be (partially) inherited from altered oceanic crust. The examination of in-situ drilled portions of oceanic crust is necessary since the only places where oceanic crust is available to field work on dry land are ophiolites. As they were thrust on land at arc settings, they were subject to enormous tectonic forces resulting in extensive faulting giving rise to much higher porosity and permeability than typical in-situ oceanic crust. Consequently, extrapolations of results from alteration studies on ophiolites on altered oceanic crust is potentially misleading.

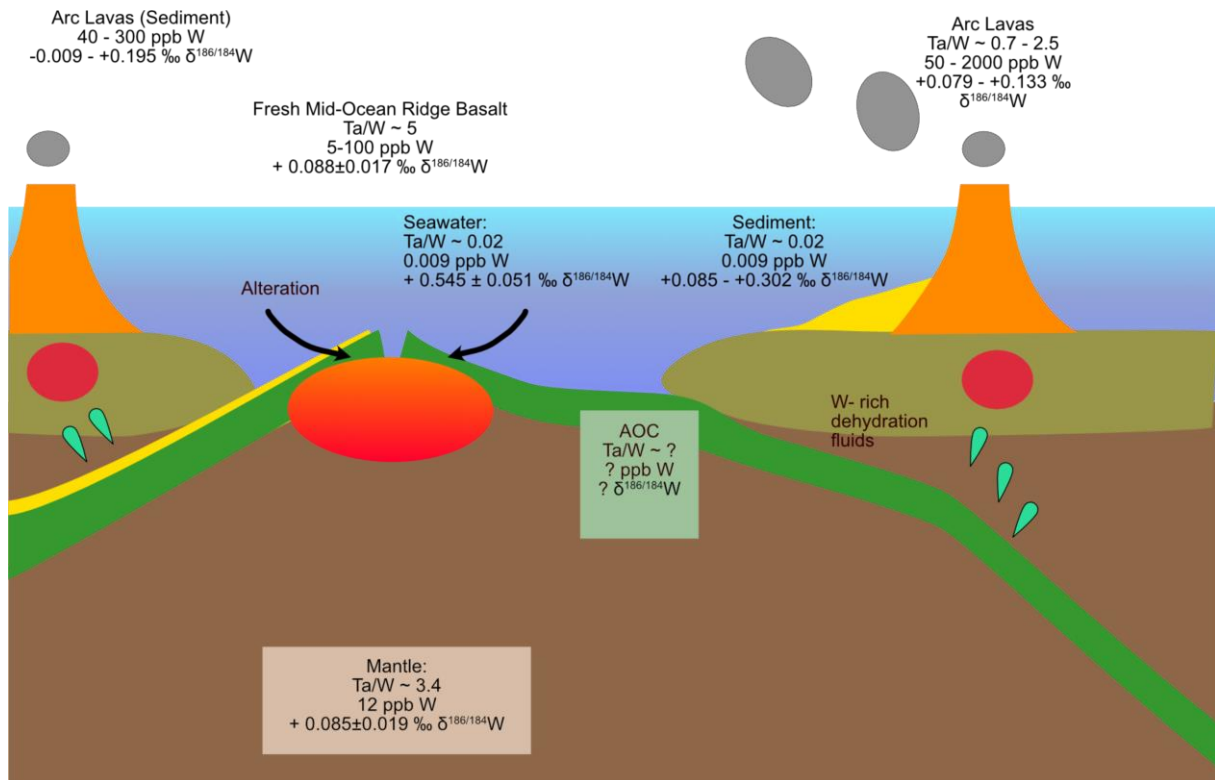


Figure 1.4: Sketch of the global geochemical cycle of W. Selective enrichment or depletion of W relative to similar incompatible but rather immobile Ta is expressed as Ta/W. Ta/W below canonical 3.4 indicate selective W enrichment. Data from König et al., 2011 and Kurzweil et al., 2019.

## 1.7 Stable W isotope composition of Earth's main reservoirs

Isotopic studies on W mainly were mainly focused on the short-lived  $^{182}\text{Hf} - ^{182}\text{W}$  system to date the Earth's core and the Moon formation. While  $^{182}\text{W}$ , in this context the daughter isotope, partitions into the core, the parent  $^{182}\text{Hf}$  is lithophile and remains in the silicate portion of the early Earth. This fractionation occurred in the live span of  $^{182}\text{Hf}$  (half-life  $t_{1/2} = 9 \text{ Ma}$ ), leaving a radiogenic  $^{182}\text{W}$  excess in the silicate Earth which can be used to date core formation (Harper and Jacobsen, 1996).

Recently, stable W isotopes moved into focus of research as well. Here and in following chapters, stable W isotope composition are expressed as permille deviation of sample material relative to NIST SRM 3163 reference material ( $\delta^{186/184}\text{W}$ , eq. 1).

$$(1) \delta^{186/184}\text{W} = \left( \frac{\left( \frac{^{186}\text{W}}{^{184}\text{W}} \right)_{\text{Sample}}}{\left( \frac{^{186}\text{W}}{^{184}\text{W}} \right)_{\text{NIST SRM 3163}}} - 1 \right) * 1000$$

The extent of equilibrium isotope fractionation is dependent on temperature and relative mass differences between isotopes as well as the stiffness of the bonding environments (Bigeleisen and Mayer, 1947; Schauble, 2004; Urey, 1947). In aqueous solutions at pH 7 tetrahedrally coordinated  $(\text{WO}_4)^{2-}$  is the most common W form (Cruywagen, 1999). The protonated forms  $\text{HWO}_4^-$  and  $\text{H}_2\text{WO}_4$  are octahedrally coordinated and more common in acidic, low-pH environments (Cruywagen, 1999). As shown for various stable isotope systems, higher coordinated forms are preferred by lighter isotopes (Schauble, 2004). In the absence of redox change, significant isotopic fractionation is mainly driven by changes in coordination chemistry (Kashiwabara et al., 2013). The adsorption of W on abundant, submarine Fe-Mn oxide concretions is associated with an increase in coordination number from +4 in dissolved species to +6 in adsorbed species. As lighter isotopes prefer stiffer bonds, preferentially lighter W isotopes are fixated (Kashiwabara et al., 2013). Whereas the stable W isotope composition in altered oceanic crust is largely unconstrained, various igneous reservoirs have recently been characterized (Fig. 1.4). The stable W isotope compositions of MORBs and OIBs show a very narrow range proposing a stable W isotope composition of the mantle of  $\delta^{186/184}\text{W} = +0.085 \pm 0.017 \text{ ‰}$  (Kurzweil et al., 2019). The invariance of the value from different sources suggests that partial melting has no resolvable influence on the stable W isotopy (Kurzweil et al., 2019). Sediments from Eastern Mediterranean Sea and Sunda Arc are characterized by high  $\delta^{186/184}\text{W}$  ( $\delta^{186/184}\text{W} = +0.085 - 0.302 \text{ ‰}$ , Kurzweil et al., 2019). In contrast to the homogenous mantle composition, arc lavas show regional variability, from mantle-like  $\delta^{186/184}\text{W}$  towards both lower

and higher  $\delta^{186/184}\text{W}$  ( $\delta^{186/184}\text{W}$  between -0.009 and +0.195 ‰) which is attributed to the local variance of the subducted material (Kurzweil et al., 2019, Mazza et al. 2020). Seawater is now known to have a heavy stable W isotope composition of  $\delta^{186/184}\text{W} = +0.545 \pm 0.051$  ‰ (Kurzweil et al., 2020). The precise determination of the stable W isotope state of the altered oceanic crust helps to further constrain the origin of elevated W/Th, W/U and W/Ta in arc magmas and to understand the geochemical cycle of W.

## **2.Evidence for tungsten mobility during oceanic crust alteration**

## 2.1 Introduction

Tungsten is one of the key elements in modern geochemistry since it is both a moderately siderophile as well as a highly incompatible element. During early differentiation of the Earth, W has been strongly depleted in the Earth's mantle (ca. 12 ppb, König et al., 2011, Palme & O'Neill, 2014) and ca. 90% of the Earth's W was sequestered into the core (Palme and O'Neill, 2014). During crust-mantle differentiation, W was enriched in the Earth's continental crust, by a factor of 100 relative to the primitive mantle concentration (Rudnick and Gao, 2013). Additionally, due to its high charge/size ratio W has long been regarded as geochemically immobile in a hydrothermal regime (Noll et al., 1996), but more recent observations (König et al., 2011, 2008) substantially changed this view.

Combined W-Th-U-Ta systematics are a very powerful tool to mass balance W in various reservoirs on Earth and can also contribute to constraining the  $^{182}\text{Hf}$ - $^{182}\text{W}$  age of core formation (e.g. Kleine et al., 2002; König et al., 2008; Noll et al., 1996). Due to their similar incompatibility, ratios of W-Th-U-Ta have long been regarded as constant in most silicate reservoirs and were taken to mass balance the global W distribution (Palme and Rammensee 1981, Newsom et al., 1996, Palme and O'Neill, 2014; Rudnick and Gao, 2013). In contrast to this view, previous studies have shown that W is highly mobile in late magmatic hydrous environments and can be concentrated in hydrothermal systems up to ore grade (e.g. Arnórsson and Óskarsson, 2007, Yongbao et al., 2014). Furthermore, W enrichments relative to U, Th and Ta in many arc lavas have been found and were attributed to fluid-controlled enrichment in the sub-arc mantle wedge (König et al., 2008). Depending on the type of subduction component involved during fluid enrichment, ratios of W/Th, W/U and W/Ta are elevated to various extents (Bali et al., 2012; König et al., 2011, 2008).

These findings require a closer assessment of the W behaviour in altered oceanic crust (AOC), which is a major source of subduction components in sub-arc mantle environments. Since W data for the oceanic crust are mainly available from fresh MORB glasses (Arevalo and McDonough, 2008, König et al., 2011 and references therein), very little is known, as to whether seafloor alteration of the oceanic crust could trigger a systematic W redistribution in oceanic crust on its way to the subduction factory. Furthermore, AOC covers more than 60 % of the Earth's surface (Wilson et al., 2006) and thus the knowledge of W redistribution in the oceanic crust during alteration is of pivotal importance for understanding the global geochemical cycle of W.

For some elements, altered oceanic crust acts as geochemical sink (e.g., alkaline metals, Mg, S, O, U; Albarede and Michard, 1986), for others as source (e.g., Ca, Si, Sr; Albarede and Michard, 1986; Bach et al., 2003; Hart and Staudigel, 1982). The concentrations of the highly incompatible element U are typically elevated in uppermost volcanic zone and

within transition zones separating effusive from intrusive portions of oceanic crust (Bach et al., 2004). While proceeding downcore, the mineral phase controlling the U budget changes from abundant Fe-oxyhydroxides in the upper portions to carbonate veins at deeper crustal levels (Bach et al., 2003). Contrasting to U, Th concentrations are stable during alteration of oceanic basalts, similar to other immobile elements like Zr, Nb, Hf or Ta and the rare earth element group (Staudigel, 2013).

In contrast to U and Th, information on the mobility of W in the AOC is so far limited. The aim of this chapter is to examine the influence of seafloor alteration on the budget of W in oceanic crust formed under super-high spreading rates and to clarify the effects of possible W redistribution in AOC on the elevated W contents in many arc rocks. To achieve this, a complete section of altered upper oceanic crust and portions of the uppermost section of the lower oceanic crust at the ODP/IODP Hole 1256D (Cocos Plate/East Pacific) is studied in this chapter. The crust is regarded as a fossil remnant of fast-spreading mid-oceanic crust (Wilson et al., 2006) This borehole was drilled during the ODP Leg 206 and IODP Expeditions 309, 312 and 335. Hole 1256D represents the first in-situ and intact section of upper oceanic crust down to the dike-gabbro boundary (Wilson et al., 2006). This sample suite therefore permits to study the dependence of W mobility on defined alteration styles. With a high number of samples, it is also possible to investigate putative small- and medium-scaled heterogeneities in alteration patterns of the examined host rocks.

## 2.2 Geological and geochemical overview of site 1256

The studied oceanic crust at site 1256 was formed at ~ 15 Ma during an interval of superfast spreading with spreading rates as high as 220 mm/a along the East Pacific Rise (EPR) and is presently located at 6°44.1 N, 91°56.1 E (Fig. 2.1) (Wilson et al., 2003). The uppermost volcanic basement of the crust formed off axis and is composed of a > 75m thick ponded lava flow followed downhole by inflated sheet and massive flows, sheeted dikes and the uppermost gabbroic intrusions. The extrusive and intrusive sections are separated by a 57 m long transition zone (TZ). This transition is characterized by intrusive contacts and sulphide-mineralized hyaloclastite breccias. Basalts underlying the transition zone compose the sheeted dike complex (SDC) for the following 350 m (Wilson et al., 2006). The SDC formed on-ridge and is cut by subvertical dikes with brecciated and mineralized chilled margins, testifying intense hydrothermal activity (Alt et al., 2010). The following downhole transition from the intrusive section to the plutonic complex is characterized by pervasive granoblastic overprint of the lower dike section, resulting in the formation of granoblastic dikes (GB) (Alt et al., 2010). The plutonic section itself is defined by two gabbroic bodies crosscutting the granoblastic dikes, starting at a depth of 1407 mbsf. The two 52 m and 24 m thick massive gabbros are separated by an 24 m, highly recrystallized metabasaltic upper dike screen (UDS) with granoblastic texture (Dziony et al., 2008; Teagle et al., 2012). Within both gabbroic bodies, stoped clasts from the granoblastic dikes were found (Koepke et al., 2008; Wilson et al., 2003).

The recovered extrusive section is pervasively altered (typical ~ 10 %, general range 2 – 20 %) by low temperature fluids (< 150 °C). Its dominating alteration style is the replacement of olivine by saponite. Basaltic glasses at flow margins range in condition from fresh to saponite-trace phillipsite alteration (Alt et al., 2010). The conversion from low temperature to hydrothermal alteration ( $\geq 200$  °C) is preserved in the mineral record at depths ranging from 649 to 749 mbsf and thus ca. 250 m above the lithologic transition from the extrusive to the intrusive section. Late magmatic hydrothermal effects such as the formation of Nahedenbergite reaction rims on primary augite are preserved as well (Laverne et al., 2006). Alteration in the transition zone and the sheeted dike complex is characterized by a sub-greenschist to greenschist facies mineral assemblage, mainly comprising chlorite and actinolite formed at temperatures from 200 – 400 °C. The transition zone itself is defined by high degrees of recrystallization and the presence of a chlorite-smectite dominated mineralogy. Although it exhibits similar alteration features, the transition zone in hole 1256D is not as pronounced as in Hole 540B in terms of thickness and alteration overprint (Alt et al., 1996; Wilson et al., 2003). The alteration intensity in the intrusive section is highly variable (typical ~ 30 – 50 %, general range 1 – 80 %), although it is pervasive. Heated and trace element enriched seawater is the main driving force for on-ridge hydrothermal alteration, as recorded in elevated  $^{87}\text{Sr}/^{86}\text{Sr}$  (Harris et al., 2015). In response to an overall increasing heat supply, the



alteration grade increases and actinolite becomes more common than chlorite below depths of 1300 mbsf. The formation of hornblende below 1350 mbsf indicates peak temperatures exceeding 400 °C (Alt et al., 2010; Koepke et al., 2008).

After initial cooling and hydrothermal alteration of the dikes, the emplacement of two gabbro bodies as well as an upwelling of the conductive boundary layer above the axial melt lens led to formation of granoblastic textures in the lower dike section (~ 60 m) right above the gabbros. Within the gabbros, assimilation features such as micro-granoblastic xenoliths, plagioclase, two-pyroxene patches, oxides and locally amphiboles highlight assimilation of the sheeted dike rocks by the mafic intrusions. At peak conditions of granoblastic overprint, hydrous partial melting, preserved as single crosscutting dikes, also occurred (Koepke et al., 2011). Fluid circulation at this state was highly focused along the dike margins and tectonic faulting. Dike margins provided preferential channels for recharge and discharge fluid flow in response to localized changes in permeability during dike intrusion (Harris et al., 2015). The gabbroic bodies themselves were subject to intense later-stage hydrothermal alteration (Harris et al., 2015; Koepke et al., 2011). Petrographic evidence like the close association of subophitic and granular domains in the upper gabbro most likely indicate an origin from frozen melt. For the upper gabbro cumulates are only a minor component (Koepke et al., 2011). The origin of the lower gabbro is not yet fully understood (France et al., 2009).

High spreading and sedimentation rates at site 1256 led to limited seawater recharge after 5 Ma (Tominaga et al., 2009) resulting in only moderate, yet pervasive alteration of the fresh crust. Geochemical studies carried out on pool powders unveiled for most of the samples typical N-MORB-like REE patterns. Samples from lower sheeted dike section show LREE enriched patterns, whereas the deepest studied rock (234 – 1, Table 2.1) is characterized by a fractionated composition, implying that late-stage magmatism, as represented by the late dike and lava pond that formed the uppermost basement at Site 1256, is characterized by evolved magma with low Mg# (38.9 vs. 50 - 65 in lava section, Neo et al., 2009). Further reported exceptions from the general N-MORB REE patterns are samples 189–1, (0-13 cm) and 189–1, (71-89 cm), overlying the granoblastic dikes. Both are enriched in LREE which testifies for extensive alteration by hydrothermal fluids (Allen and Seyfried, 2005; Michard et al., 1983; Yongliang and Yusheng, 1991).

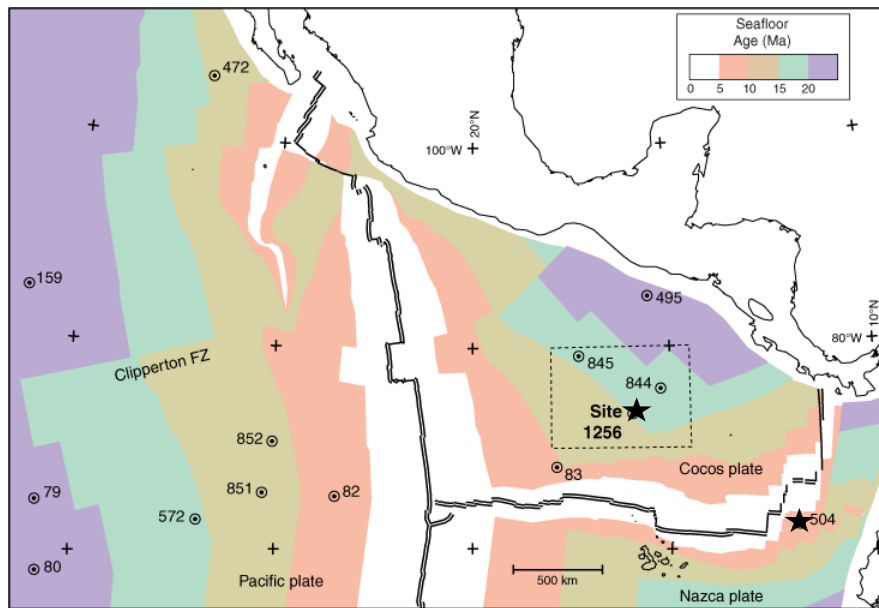


Figure 2.1: Location of IODP hole 1256D and other IODP/ODP sites on the Cocos Plate (modified after *Wilson et al., 2006*).

## 2.3 Analytical Techniques

Sample selection was guided by the petrographic description of the Shipboard Party (Wilson et al., 2006) and covers different lithologies and alteration styles. Care was taken to sample all major alteration styles at high depth resolution. Special emphasis was placed on the lower portions of the volcanic section and the sheeted dike complex, as in this section fluids of both seawater and magmatic origin with different chemical compositions and temperatures interacted with the host lithologies (Alt et al., 2010). For a total number of 43 samples, high precision concentrations of Lu, Zr, Nb, Hf, Ta, W, U and Th were determined by isotope dilution (Table 2.1). Whereas W, Ta, U and Th were selected because of their similar melt incompatibility but different mobility in aqueous regimes, the precise measurement of Lu, Hf, Zr, Nb allows to further characterize the initial magmatic diversity of the samples and their source regions. Classically, Zr, Nb, Lu, Hf are regarded as immobile in oceanic crust alteration whereas, e.g., U is known for its mobility (Hart and Staudigel, 1982; Staudigel, 2013). Thirteen of the samples were freshly cut and ground using an agate disc mill, additional 30 sample powders are splits from the shared sample inventory (“pool samples”) provided by the shipboard party. The depth resolution achieved reaches from ~ 50 m in the geologically rather uniform sheet & massive flows down to ca. 1.30 m in the more heterogeneous plutonic section. To assure complete digestion of refractory phases like zircon that are reported to increase with depth (Neo et al., 2009), most samples exceeding a depth of 1200 mbsf were digested in a two-step scheme described below. For elemental analyses, 100 - 200 mg of the powdered samples were weighed in and spiked with mixed HFSE ( $^{176}\text{Lu}$ ,  $^{94}\text{Zr}$ ,  $^{180}\text{Hf}$ ,  $^{180}\text{Ta}$ ,  $^{183}\text{W}$ ) and  $^{233/236}\text{U}$ - $^{229}\text{Th}$  tracers in Savillex® vials. The sample-spike mixture was tabletop-digested for 12 h in a 1:1 mixture of concentrated  $\text{HNO}_3$  - HF at 120°C. After evaporation to dryness, the samples were re-dissolved in 6 ml of a 2:3 mixture of concentrated  $\text{HNO}_3$  – HF and placed inside Parr® bombs for 36 h at 180°C. Subsequently, 1 ml  $\text{HClO}_4$  was added to the solution to remove fluorides during dry down.

Samples originating from depths greater than 1200 mbsf are reported to comprise accessory phases like rutile or zircon (Neo et al., 2009). Since the latter is known to contain significant amounts of U and Th, incomplete digestion can lead to lower U-Th contents and misleading interpretations. Hence, these samples underwent a modified digestion scheme, where the above described first tabletop-digestion is followed by evaporation to dryness and the dissolution of the sample-spike material in 6 ml of a 1:3 mixture of concentrated  $\text{HNO}_3$  – HF. The closed beakers were then placed for additional 36 h in Parr® bombs. After evaporation of the acid mixture, the samples were again dissolved in 6 ml of pure HF and bombed for additional 72 h. After the addition of 1 ml  $\text{HClO}_4$ , the sample solutions were again evaporated to dryness.

All digested samples were treated with 3 ml of concentrated HNO<sub>3</sub> - trace HF (< 0.05N), evaporated and fully dissolved in 6 ml 6N HCl - trace HF for 12 h to achieve sample/spike equilibrium. From these equilibrated sample solutions, a 1 ml (ca. 17 %) aliquot for W chemistry was taken, following a modified method as described in (Kleine et al., 2004). The remaining sample solution underwent a three-stage ion exchange separation as described in, e.g., Münker et al. (2001), Weyer et al. (2002) and Thiemens et al. (2019). The U-Th cut was collected in 2 M HF at stage 2 of this protocol and U was separated from Th on Tru-Spec ion resin (Luo et al., 1997).

All measurements were carried out using a THERMO Neptune MC-ICP-MS at the University of Cologne (Münker et al., 2001; Weyer et al., 2002). External reproducibility was assessed by repeated measurements of 100 mg splits BHVO-2 standard (Table 2.2). The average 2 s.d. of all measured BHVO-2 splits is below 2 % for Zr, Ta, W, Th, U, Lu, Hf, Zr/Hf, Lu/Hf, U/Th. For most elements blanks for the two different digestion schemes are similar, with a slight tendency to higher values in the double-bomb charges (Zr: c 600 pg/1600 pg, Nb: 12.5 pg/ 6 pg, Lu: 204 pg/160 pg, Hf: 120 pg/54 pg, U: 20 pg/54 pg, Th: 10 pg/34 pg, W: 28 pg/ 47 pg and Ta: 22 pg/20 pg, where the first number is always after 36 h bomb-digestion, the second after 108h two step bomb digestion).

Table 2.1: High precision HFSE and U-Th data for samples of hole 1256D, S&MF = Sheet and Massive Flows, TZ = Transition Zone, SDC = Sheeted Dike Complex, GD = Granoblastic Dikes. UG = Upper Gabbro, UDS = Upper Dike Screen, LG = Lower Gabbro, LDS = Lower Dikes Screen; c.f. chemistry failed

Core	Interval (cm)	Depth (mbsf)	Subdivison	Digestion Method	Zr (ppm)	Nb (ppm)	Ta (ppm)	W (ppm)	Th (ppm)	U (ppm)	Lu (ppm)	Hf (ppm)
087 - 1	22 - 35	831.10	S&MF	36h PB	64.38	1.73	0.123	0.0375	0.138	0.0473	0.492	1.998
102 - 1	17 - 29	926.86	S&MF	36h PB	67.50	2.05	0.131	0.0503	0.147	0.0520	0.507	2.048
110 - 1	26 - 32	927.86	S&MF	36h PB	71.77	2.67	0.168	0.0407	0.180	0.0552	0.510	2.111
114 - 1	127 - 142	989.87	S&MF	36h PB	64.98	3.22	0.173	0.0425	0.205	0.0725	0.427	1.779
122 - 1	67 - 79	1027.55	TZ	36h PB	56.00	1.56	0.119	0.101	0.140	1.48	0.377	1.903
129 - 1	34 - 51	1062.26	SDC	36h PB	87.28	2.89	0.182	0.0492	0.162	0.0520	0.556	2.528
134 - 2	40 - 52	1086.54	SDC	36h PB	90.30	3.02	0.182	0.0404	0.202	0.0658	0.563	2.585
142 - 2	40 - 55	1087.54	SDC	36h PB	88.90	2.86	0.172	0.0330	0.186	0.0627	0.465	2.357
144 - 2	39 - 56	1125.34	SDC	108h PB	59.79	2.61	0.160	0.0552	0.185	0.0567	0.436	1.780
146 - 1	30 - 54	1142.50	SDC	36h PB	53.28	2.78	0.167	0.0519	0.194	0.0586	0.384	1.579
155 - 2	60 - 80	1186.47	SDC	36h PB	75.36	3.06	0.178	0.0565	0.201	0.0639	0.540	2.272
159 - 1	98 - 110	1204.63	SDC	36h PB	79.48	3.05	0.172	0.0802	0.195	0.0625	c.f.	c.f.
162 - 2	40 - 54	1215.60	SDC	36h PB	56.16	1.95	0.123	0.0335	0.136	0.0425	0.439	1.669
165 - 2	71 - 91	1230.17	SDC	36h PB	82.37	2.94	0.180	0.0540	0.213	0.0664	0.590	2.490
166 - 3	49 - 65	1235.75	SDC	36h PB	88.73	3.05	0.193	0.0572	c.f.	c.f.	0.624	2.639
168 - 1	58 - 72	1243.18	SDC	36h PB	83.66	3.19	0.199	0.0679	0.224	0.0732	0.553	2.449
168 - 4	78 - 90	1247.03	SDC	36h PB	83.90	3.29	0.200	0.0645	0.222	0.0700	0.540	2.462
169 - 2	/	1248.75	SDC	36h PB	61.04	2.79	0.209	0.0667	0.248	0.0756	0.438	1.828
170 - 2	130 - 144	1254.31	SDC	36h PB	47.62	1.43	0.0886	0.0315	0.101	0.0326	0.379	1.486
170 - 3	22 - 40	1254.68	SDC	36h PB	48.79	1.52	0.0888	0.0272	0.105	0.0334	0.388	1.512
187 - 2	35 - 39	1325.88	SDC	36h PB	67.53	2.76	0.191	0.335	0.233	0.0809	0.521	2.025
188 - 1	6 - 9	1330.00	SDC	108h PB	87.03	3.37	0.213	0.210	0.280	0.0870	0.599	2.584
196 - 1	54 - 57	1363.86	GD	36h PB	87.42	3.76	0.237	0.0949	0.124	0.0310	0.632	2.064
206 - 1	4 - 7	1386.98	GD	108h PB	66.36	2.46	0.155	0.108	0.190	0.0693	0.491	2.002
212 - 1	9 - 11	1404.14	GD	36h PB	68.92	3.58	0.219	0.0659	0.239	0.0766	0.548	2.083
213 - 1	5 - 7	1405.14	GD	36h PB	81.19	3.97	0.247	0.0658	0.228	0.0794	0.661	2.557
214 - 2	119 - 129	1413.55	UG	108h PB	56.24	2.20	0.134	0.0479	0.131	0.0434	0.406	1.694
215 - 2	90 - 94	1416.30	UG	36h PB	33.40	1.82	0.104	0.0677	0.126	0.0408	0.332	1.053
216 - 1	35 - 40	1416.30	UG	36h PB	30.47	1.64	0.103	0.0499	0.0960	0.0322	0.337	0.9931
219 - 1	25 - 32	1430.26	UG	108h PB	44.03	1.70	0.113	0.0551	0.107	0.0350	0.333	1.329
220 - 1	92 - 100	1435.92	UG	36h PB	44.37	1.89	0.116	0.0437	0.129	0.0402	0.386	1.354
222 - 1	74 - 86	1446.37	UG	108h PB	61.89	1.98	0.132	0.0729	0.185	0.0606	0.344	1.721
223 - 3	12 - 24	1452.40	UG	108h PB	31.94	1.13	0.0714	0.0384	0.0785	0.0227	0.265	1.004
227 - 1	113 - 126	1469.00	UDS	108h PB	78.89	2.80	0.172	0.0439	0.211	0.0650	0.515	1.843
230 - 1	72 - 83	1483.72	LG	36h PB	39.88	1.87	0.100	0.0470	0.108	0.0324	0.407	1.409
230 - 1	87 - 90	1484.00	LG	108h PB	71.03	2.77	0.169	0.0371	0.196	0.0678	0.467	2.101
230 - 2	49 - 61	1484.99	LG	108h PB	48.86	1.39	0.0883	0.0319	0.131	0.0353	0.396	1.268
231 - 1	90 - 100	1488.80	LG	108h PB	49.57	1.70	0.108	0.0309	0.125	0.0361	0.422	1.526
231 - 1	74 - 86	1489.80	LG	36h PB	63.27	2.74	0.173	0.0557	0.286	0.0620	0.462	1.887
231 - 3	80 - 98	1490.80	LG	108h PB	37.07	1.49	0.0975	0.0412	0.0942	0.0315	0.337	1.186
232 - 1	66 - 81	1491.80	LG	108h PB	45.39	1.38	0.0855	0.0325	0.0943	0.0321	0.392	1.334
232 - 2	35 - 50	1494.33	LG	108h PB	54.05	2.02	0.125	0.0295	0.131	0.0406	0.441	1.626
234 - 1	10 - 13	1502.00	LDS	108h PB	131.3	4.80	0.291	0.0778	0.361	0.125	0.830	3.915

Table 2.2: High precision HFSE and U-Th data illustrating the effects of a two-step bombing process on measured elemental concentrations for three 1256D samples and the BHVO-2 reference material. Sample 155 – 2 contains no significant amounts of residual Zircon. In contrast, 223 – 3 contains little and 231 – 1 significant amounts of residual zircon. n.m. = not measured, c.f. = chemistry failed

Core	Digestion Method	Zr (ppm)	Nb (ppm)	Ta (ppm)	W (ppm)	Th (ppm)	U (ppm)	Lu (ppm)	Hf (ppm)
155 – 2 (60 – 80)	36h PB	75.51	2.90	0.180	0.0558	0.216	0.0657	0.542	2.258
155 – 2 (60 – 80)	36h PB	74.32	2.84	0.177	0.0456	0.202	0.0629	0.538	1.943
155 – 2 (60 – 80)	36h PB	74.65	2.83	0.177	0.0474	0.199	0.0632	0.536	2.253
155 – 2 (60 – 80)	36h PB	76.30	2.87	0.178	0.0680	0.202	0.0648	0.538	2.272
155 – 2 (60 – 80)	108h PB	77.26	3.06	0.180	0.0547	0.200	0.0627	0.545	2.289
155 – 2 (60 – 80)	Alkali Fusion*	86.10	3.12	0.200	n.m.	0.210	0.0700	0.490	2.210
223 – 3 (12 – 24)	36h PB	26.77	1.13	0.0704	0.0398	0.0755	0.0214	0.266	0.8838
223 – 3 (12 – 24)	108h PB	31.49	1.09	0.0703	0.0399	0.0795	0.0227	c.f.	c.f.
223 – 3 (12 – 24)	108h PB	32.56	1.16	0.0735	0.0368	0.0795	0.0237	0.264	1.004
223 – 3 (12 – 24)	Alkali Fusion*	35.80	1.27	0.0800	n.m.	0.0900	0.0260	0.270	0.9800
231 – 1 (90 – 100)	36h PB	33.89	1.27	0.0700	0.0280	0.0880	0.0265	0.358	1.155
231 – 1 (90 – 100)	36h PB	27.55	1.06	0.0850	0.0280	0.0800	0.0234	0.358	1.050
231 – 1 (90 – 100)	108h PB	49.47	1.69	0.107	0.0310	0.124	0.0361	c.f.	c.f.
231 – 1 (90 – 100)	108h PB	49.83	1.72	0.108	0.0300	0.127	0.0362	0.422	1.526
231 – 1 (90 – 100)	Alkali Fusion*	52.10	1.79	0.120	n.m.	0.130	0.0370	0.420	1.480
BHVO – 2	36h PB	165.3	18.3	1.09	0.213	1.19	0.410	0.274	4.453
BHVO – 2	36h PB	166.0	18.1	1.08	0.211	1.13	0.388	0.276	4.451
BHVO – 2	108h PB	166.6	18.5	1.09	0.213	1.18	0.414	-	-
BHVO – 2	108h PB	165.0	17.9	1.09	0.213	1.19	0.398	0.275	4.452
BHVO – 2	Tabletop*	171.6	18.3	1.15	0.220	1.18	0.430	0.273	4.387

Table 2.3: U-Th isotope data, all data given as activity ratios

Sample	Interval (cm)	Subdivision	$^{238}\text{U}/^{232}\text{Th}$ (A)	$^{230}\text{Th}/^{232}\text{Th}$ (A)	$^{230}\text{Th}/^{238}\text{U}$ (A)
087 - 1	22 – 35	S&MF	1.05	1.11	1.06
102 - 1	17 – 29	S&MF	1.10	1.09	0.988
114 - 1	127 – 144	S&MF	1.09	1.10	1.01
122 - 1	67 – 79	TZ	31.4	31.7	1.01
134 - 2	40 – 52	SDC	1.00	0.984	0.985
142 - 2	40 – 55	SDC	1.03	1.06	1.02
144 - 2	39 – 55	SDC	0.948	1.01	1.07
146 - 1	30 – 54	SDC	0.927	0.943	1.02
155 - 2	60 – 80	SDC	0.964	1.04	1.08
162 - 2	40 – 54	SDC	0.961	0.956	1.00
165 - 2	71 – 91	SDC	0.947	1.00	1.05
168 - 1	58 – 72	SDC	1.00	0.971	0.976
168 - 4	78 – 90	SDC	0.964	0.953	0.988
169 - 2	/	SDC	0.918	0.943	1.03
170 - 2	130 – 144	SDC	0.987	1.00	1.02
170 - 3	22 – 40	SDC	0.976	0.984	1.01
187 - 2	35 – 39	SDC	1.06	1.03	0.971
188 - 1	6 – 9	SDC	0.954	0.964	1.01
206 - 1	54 – 57	GD	1.12	1.14	1.02
213 - 1	5 – 7	GD	1.06	1.03	0.968
214 - 2	119 – 129	UG	1.05	1.03	0.980
219 - 1	25 – 32	UG	1.05	1.10	1.05
223 - 3	12 – 24	UG	0.940	1.04	1.10
227 - 1	113 – 126	UDS	0.910	0.958	1.05
230 - 1 (AC)	72 – 83	LG	0.897	0.882	0.984
230 - 1	87 – 90	LG	1.04	1.13	1.08
230 - 2	49 – 61	LG	0.657	0.955	1.45
231 - 1	90 – 100	LG	0.899	0.947	1.05
231 - 1 (AC)	74 – 86	LG	0.661	0.952	1.44
232 - 2	39 – 50	LG	0.958	1.02	1.07
234 - 1	10 - 13	LDS	1.03	1.08	1.05

## 2.4 Results

### 2.4.1 Downhole variation of trace element concentrations and ratios

The concentration of W in the AOC at hole 1256D varies between 27 ppb and 330 ppb (Table 2.1) with a median value of 50 ppb. This matches the known concentration range of 5 – 700 ppb for fresh MORB reported by Arevalo et al. (2008) and König, et al. (2011) but is significantly higher than the respective medians of 25 and 28 ppb in these two datasets (Fig. 2.2A, B). Compared to the primitive mantle value (12 ppb, König et al., 2011), W is enriched in all analysed portions of AOC. Downhole variation diagrams underline that the concentrations of W are significantly elevated in the contact zones between different lithologies such as the transition zone between the lava section and the sheeted dikes (sample 122–1), the transition zone between upper and lower crust, which is represented by the granoblastic dikes (samples 187–2 and 188–1), or the contact zone separating the granoblastic dikes from the upper gabbro (sample 206–1; Fig. 2.2B). The W concentrations in the volcanic section (< 1024 mbsf) and in the upper dike section (1062.3 – 1330 mbsf) are less variable, whereas the W concentrations in both gabbroic units are highest at their upper and lower margins (Fig. 2.2B).

The concentrations of Lu, Hf, Zr, Nb, U, Th, and Ta are in the same range as previously published for Hole 1256D (e.g. Höfig et al., 2014; Neo et al., 2009; Yamazaki et al., 2009), confirming that the 1256D crust shows typical N-MORB element concentration patterns. As it is the case for W, the concentrations for Lu, Hf, Zr, Nb and Ta are typically less variable in the sheet and massive flows and the sheeted dike complex (Fig. 2.2C). As described for W, concentrations of all other measured trace elements in both gabbroic bodies are elevated at the gabbro margins (Fig. 2.2D). A prominent enrichment of U over Th, resulting in U/Th as high as 10, can be seen in the transition zone between the lava and sheeted dike sections at 1027 mbsf. Apart from this zone, U/Th are typically ca. 0.32, indistinguishable from the canonical value of 0.316 for fresh MORB (Gale et al., 2013). Ratios of W/Hf (0.019 – 0.165), W/Th (0.27 – 3.3), W/U (0.07 – 1.7), and W/Ta (0.24 – 1.75) in Hole 1256D are elevated relative to typical ratios in fresh MORBs ( $Hf/W = 0.002 - 0.025$ ,  $W/Ta = \sim 0.18$ ,  $W/Th_{\text{canonical}} = 0.15$ ,  $W/U_{\text{canonical}} = 0.46$ ) and even locally relative to arc lavas ( $W/Th_{\text{Arc}} = 0.01 - 1$ ,  $W/U_{\text{Arc}} = 0.01 - 3$ ,  $W/Ta_{\text{Arc}} = 0.08 - 0.25$ ,  $W/Hf_{\text{Arc}} = 0.03 - 0.4$ , Arc data from König et al., 2008 and 2011) values throughout the whole depth range.

The effusive sheet and massive flows as well as the intrusive upper dike section have relatively uniform Hf/W (50 – 100), W/Th (0.18 – 0.40), W/U (0.59 – 0.97), and W/Ta (0.20 – 0.41). Ratios of W with similar incompatible Th, Ta, and U (Fig. 2.3A) are highest in the granoblastic dikes approaching the contact to gabbroic intrusions ( $W/Th = 0.75 - 3.30$ ,  $W/U = 2.42 - 4.14$ ,  $W/Ta = 0.4 - 1.75$ ). From the highest W/Th, W/U, and W/Ta at the interface of sheeted dike complex and granoblastic dikes, the ratios are continuously decreasing to W/Th



= 0.22,  $W/U = 0.62$  and  $W/Ta = 0.27$  in the greatest encountered depths of 1490 – 1502 mbsf. A closer assessment of the two gabbroic bodies (Fig. 2.3B) shows that despite this overall decrease there are local variations with more elevated  $W/U$ ,  $W/Th$ , and  $W/Ta$  at the gabbro margins and lower ratios in the centre of the gabbro bodies.

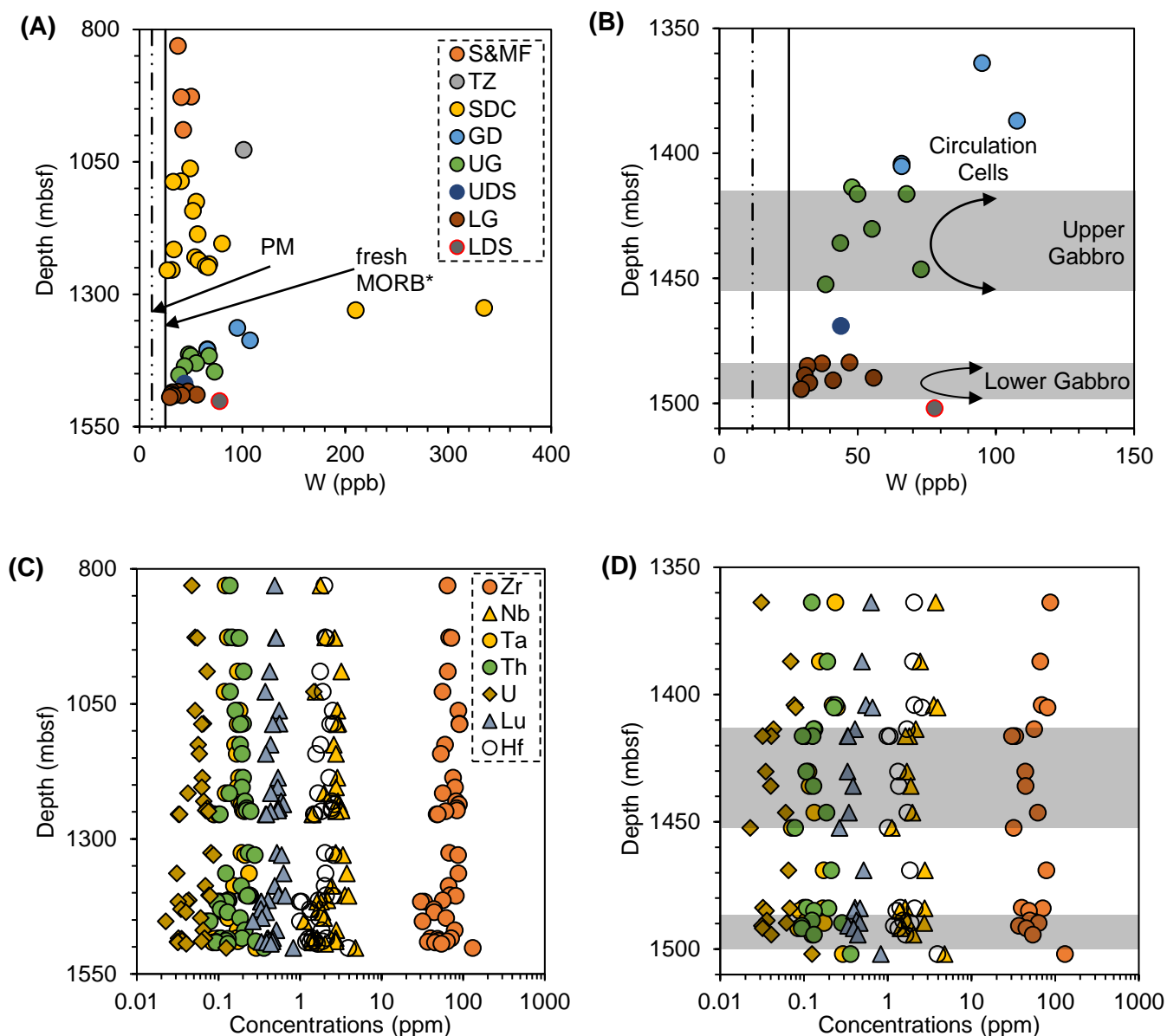


Figure 2.2: Plots of W and other HFSE concentrations versus depth, illustrating the absolute W enrichment over fresh MORB (median value of published data by Arevalo et al., 2008) and König et al. (2011) and primitive mantle values (PM, König et al. 2011) over the whole drilled depth range. Plots B and D show the lower section of the drillhole in greater detail. Most HFSE concentration are invariant throughout the lava and sheeted dike sections (C) and only show local enrichments at the gabbro margins (D). Conversely, extreme W enrichments can be found at the transition zone (TZ) and at the margin of the sheeted dike section (SDC), close to the upper gabbro (UG) and at the margin of the gabbros themselves (A, B). These zones correspond to the circulation cells proposed by Harris et al. 2015. Despite the local peaks at the gabbro margins, there is an overall decrease of W concentrations with depth from ca. 1400 mbsf (B).

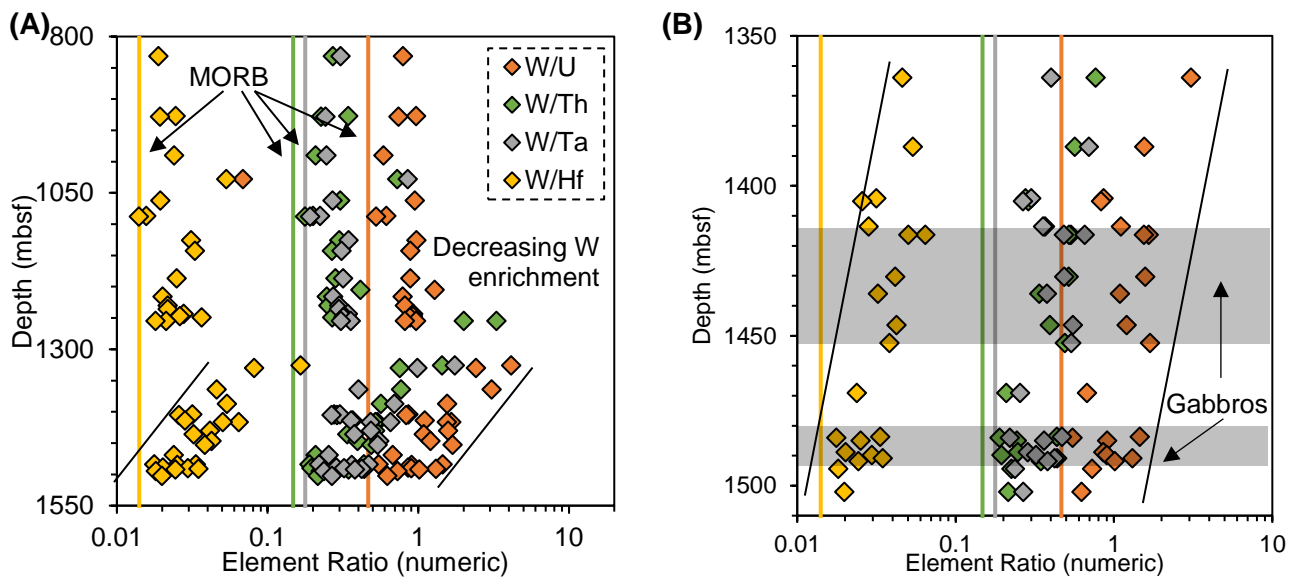


Figure 2.3: Plots of elemental ratios of W vs. other HFSE and U-Th, demonstrating the selective enrichment of W over the more immobile U, Th, Ta, and Hf in most alteration facies (A). Plot B shows the lower section of the borehole. Canonical ratios as inferred from medians of fresh MORB are shown as coloured straight lines. A notable exception is W/U at 1027.55 mbsf in the transition zone with large U enrichment and correspondingly lowered W/U. A closer look at the gabbroic section (B) confirms the overall decreasing W enrichment with local peaks along the gabbro margins. MORB values are taken from *König et al., 2008*.

## 2.4.2 Evaluation of different digestion protocols and U-series patterns

Previous studies on hole 1256D samples reported the presence of accessory acid resistant mineral phases in samples from deeper drill-hole sections, which caused problems using conventional acid digestion methods for trace elements (Neo et al., 2009, Höfig et al., 2014). The differences in Zr contents between samples digested with tabletop protocols and alkali fusion as published by Neo et al. (2009) led to the conclusion that zircon is the most likely accessory mineral that causes this bias. To overcome this problem, replicates of samples were digested with both the above described single- and double-bombing digestion protocols. Results obtained by the different protocols are listed in Table 2.2. It is striking that measured Zr and Nb contents in some samples were almost twice as high after the second bombing step (e.g., sample 231–1, Table 2.2). Additionally, residual zircon was found to be present in distinct samples originating from depths as high as ca. 1100 mbsf (e.g., sample 144–2) which is roughly 200 m higher than previously published (Neo, et al. 2009).

The effects of a second bombing step are further illustrated in Table 2.2 and Figure 2.4. In Table 2.2, concentrations of Zr, Nb, Ta, W, Th, U, Lu, and Hf are displayed for each single and double bombing step. One sample (231–1) has a particularly high Zr deficit of ca. 45 % ( $Zr_{def}$ , difference of Zr concentration after one bombing step from Zr concentration after the second bombing, one contains little (223–3, ca. 17 %), while one sample (155–2, ca. 0 - 4 %) and as expected BHVO–2 do not contain significant amounts of residual zircon, if any. In this context, it is important to note that the Zr deficits after one bombing step do not correlate with the absolute Zr contents, which can be seen, for instance, by the comparison between sample 155–2 and 231–1. Whereas sample 155–2 contains ca. 50 % more Zr and Nb than sample 231–1, sample 231–1 has a higher apparent amount of residual zircon that is only digested after additional bombing in concentrated HF. Importantly, repeated measurements of the BHVO–2 reference material going through both digestion paths demonstrate that there is no shift in concentrations or elemental ratios when the samples are bombed for a longer period.

By comparing the Zr deficit between single- and double-bombed samples with relative deficits of other HFSE, it becomes evident, that the deficits of most HFSE also increase with the Zr deficits, once the deficits in Zr are larger than ca. 25 %  $Zr_{Def}$  (Fig. 2.4). Only W concentrations appear to be unaffected up to 45 %  $Zr_{Def}$ . The individual HFSE and U-Th deficits are significantly correlated with Zr deficits ( $R^2_{Lu} = 0.48$ ,  $R^2_{Hf} = 0.46$ ,  $R^2_U = 0.73$ ,  $R^2_{Th} = 0.51$ ). These observations mirror the different D values for individual HFSE in zircon (Fujimaki, 1986; Kirkland et al., 2015; Thomas et al., 2002). While W is only to a minor amount incorporated in zircon, particularly Hf, Lu, U, and Th are more affected (Fig. 2.4). Collectively, the large efforts in improving the digestion protocols are required to fully benefit from the low uncertainties of the isotope dilution method, where only completely digested samples permit to resolve small

variations of W, U, Th, and Ta. When comparing the measured concentrations of the double bombed samples in this thesis with previously published data (e.g., by Neo et al. 2009, Höfig et al., 2014) it becomes evident that the concentrations for different samples agree to within a range of  $\pm 5-10\%$ . Neo et al. (2009) trace element data are reported with higher analytical uncertainties (typically  $\pm 10\%$ ).

Uranium series measurements can provide further proof of efficient sample digestion, as the 15 Ma old samples should all plot on the equiline of secular equilibrium (Fig. 2.5, Table 2.3), provided they were not disturbed by ca. <350 kyrs old off-axis seawater alteration. In  $^{230}\text{Th}/^{232}\text{Th}$  vs.  $^{238}\text{U}/^{232}\text{Th}$  isochron space, most samples indeed plot on the equiline (Fig. 2.5), and significant modification of the U budget by alteration over the last ca. 350 kyrs can therefore be excluded for them. Importantly, all samples are lower in both  $^{230}\text{Th}/^{232}\text{Th}$  and  $^{238}\text{U}/^{232}\text{Th}$  than samples measured previously further to the north along the EPR (Turner et al., 2011). In contrast to most samples from Hole 1256D, three of the samples (122–1, 230–2, 231 – 1 AC) show significant Th excess of  $\sim 20\%$ . As disturbance by zircon can be ruled out, available explanations are the influence of more recent intensive alteration (122 – 1) which is also reflected in significantly elevated U/Th of  $> 10$ , or the intrusion of younger magma batches from a different source region (230–2, 231–1 AC) as these samples both originate from the gabbro unit and are characterized by sub-canonical U/Th.

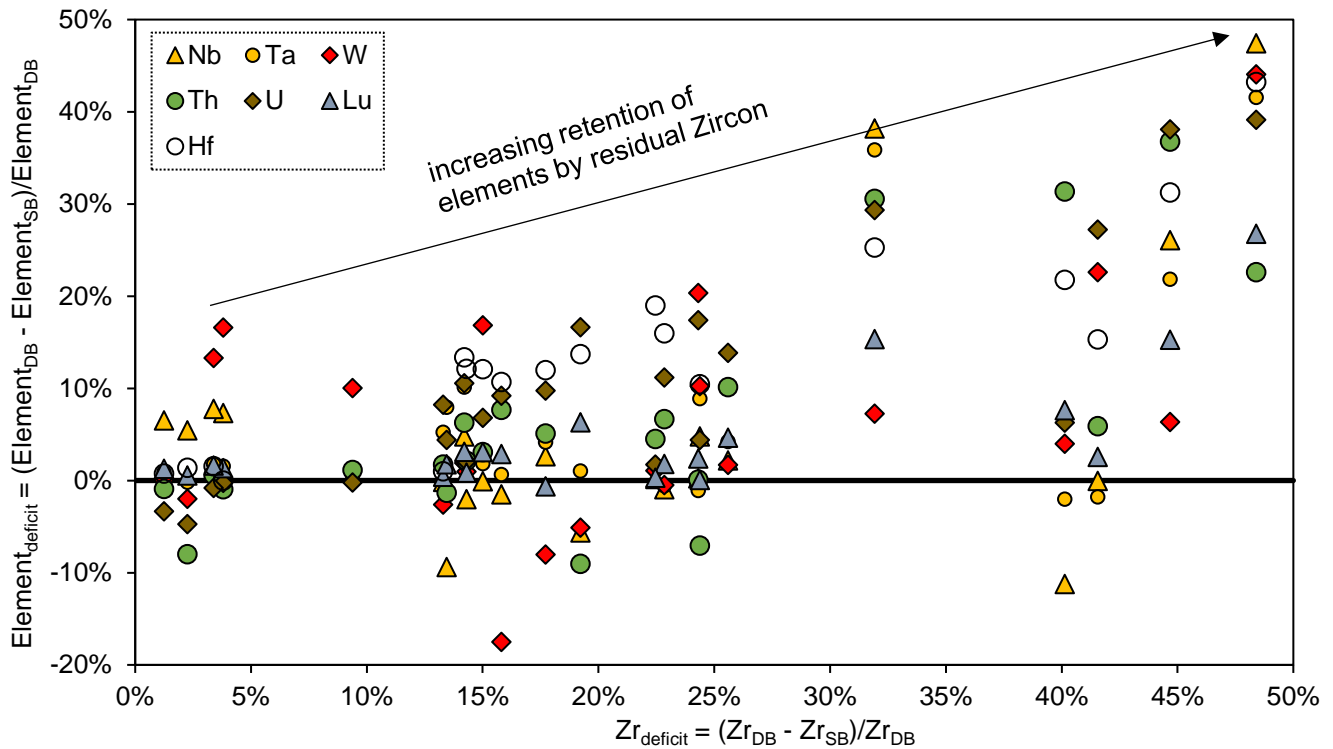


Figure 2.4: Influence of incomplete zircon digestion on the measured abundances of HFSE and U-Th. The X-Axis shows the deficit of measured Zr concentrations relative to the concentration measured in double bombed digestions. The Y-Axis denotes the deficit for all other HFSE. Each group of vertically aligned sample points represents a single-bombed digestion and a given Zr deficit. It can be seen, that with increasing Zr deficit (i.e., more acid-resistant zircon) other HFSEs and Th, U, Lu show increasing deficits.

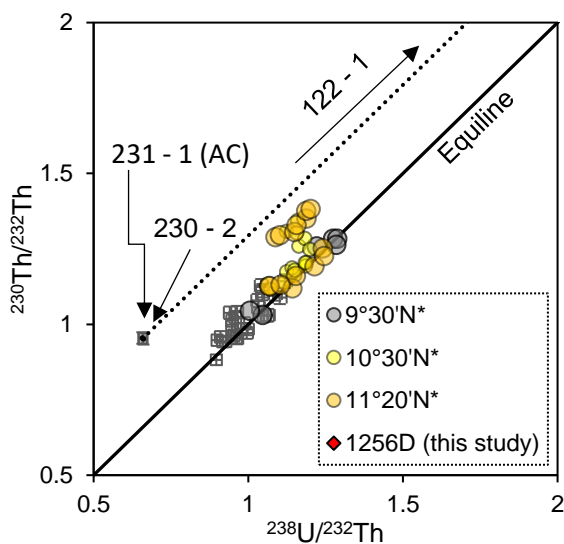


Figure 2.5: Samples from Leg 1256D and other localities from East-Pacific Rise plotted in  $^{230}\text{Th}$ - $^{238}\text{U}$  equiline space. Most samples plot on the equiline (A), remarkable exceptions are 122 – 1 from the transition zone not shown) and samples 230 – 2, and 231 – 1 AC from the upper gabbro section. As sample 122 – 1 contains much more U than Th ( $^{238}\text{U}/^{232}\text{Th} = 31.45$ ,  $^{230}\text{Th}/^{232}\text{U} = 31.73$ ,  $\text{U}/\text{Th} = 10.56$ ) the deviation may be caused by extensive U enrichment during late stage alteration. One group of samples originating from  $10^{\circ}30'$  and  $11^{\circ}20'$  N displays excess in  $^{230}\text{Th}$  which is attributed to off-axis lava formation and injection by Turner et al., 2011. \* Turner et al., 2011

## 2.5 Discussion

### 2.5.1 Influence of partial melting processes on immobile HFSE and U-Th abundances

To reconstruct the fluid mobility of W by comparison with other HFSE and U-Th element abundances it is crucial to evaluate possible other magmatic processes that may affect relative HFSE and U-Th abundances. One typical example is the preservation of variable mantle source depletion in MORBs like the negative correlation between Zr/Hf and Lu/Hf. The latter was previously reported for Hole 1256D (Neo, et al. 2009, Höfig, 2014) and is also confirmed by the high precision data of this thesis (Fig. 2.6A). Exceptions for decoupling of the two ratios are to be found in samples originating from the vicinity of the gabbroic intrusions (with high Zr/Hf of ca. 42), possibly caused by formation of mineral cumulates with high trace element concentrations as reported for, e.g. Oman Ophiolite (France et al., 2009; Koepke et al., 2011, 2008). Petrographic evidence for such processes is rare in hole 1256D gabbros (Koepke et al., 2011). In contrast, trace element data published by Neo et al., 2009 reveal slightly depleted REE pattern and elevated Rb, Ba, K and Sr abundances, typical for cumulate gabbros (Seifert et al., 1996) at the intrusive contact of the upper gabbro. It is thus suspected that elevated Zr/Hf in these gabbros originate from the formation of gabbro cumulates.

In Nb/Ta versus Zr/Hf space the data obtained in this chapter and by Höfig et al. (2014) broadly overlap for most of the samples, also overlapping the fresh MORB field as defined by Münker et al. (2003) (Fig. 2.6B). Some previously published samples exhibit a much larger scatter in Nb/Ta than the dataset presented here. Many samples with lower Nb/Ta originate from depths exceeding 1200 mbsf, where residual zircon plays an increasingly important role. In Fig. 2.4 it is demonstrated how even concentrations of HFSE like Nb may be affected by incomplete digestion of zircon. As in the study of Höfig et al. (2014) the powdered samples were only bombed once, residual zircon may not have completely dissolved and the measured Nb concentrations were likely too low, resulting in erratically lower Nb/Ta ratios. In the here outlined dataset, Nb/Ta data is confined to a much narrower range and a co-variation of Nb/Ta and Zr/Hf as expected for different degrees of source depletion cannot be seen (Fig. 2.6B). Likewise, the 1256D samples show no overall co-variation in Nb/Ta vs. Zr/Nb space (Fig. 2.6C). Only samples from the sheet & massive flow and the transition zone define a tentative co-variation ( $R^2 = 0.87$ ) indicating some variation in source depletion. The trend is much steeper than observed in fresh global MORBs (Weyer et al., 2003) and may potentially mirror local source variations. Collectively, the overall Nb/Ta, Zr/Nb and Zr/Hf variations of the 1256D samples in comparison to the global fresh MORB array indicate that source depletion along the ridge segment sampled by hole 1256D is rather limited.

It was shown experimentally that during melting of depleted mantle, clinopyroxene and garnet control the fractionation of Th, U, Nb, Ta, Zr, Hf and Lu. In clinopyroxene Ta, U, Th, and

W are highly incompatible ( $D_{\text{cpx}} < 0.1$ , Hill et al., 2000; McDade et al., 2003) and Zr-Hf are moderately incompatible ( $D_{\text{cpx}} \sim 0.5$ , McDade et al., 2003). Consequently, W, U, Th, Ta may be significantly fractionated from Zr and Hf during partial melting of clinopyroxene-bearing mantle. The highly incompatible W, U, Th, Ta have slightly different  $D_{\text{cpx}}$  as well.  $D_{\text{cpx}}$  for Ta (0.035) is higher, than  $D_{\text{cpx}}$  for U (0.018) and  $D_{\text{cpx}}$  for Th (0.021), and W is the most incompatible element in clinopyroxene ( $D_{\text{W}} < 0.005$ ;  $D$  values from Hill et al., 2000 & McDade et al., 2003). Thus, with larger degree of source depletion, W/Ta, W/Th, W/U will be continuously lowered whereas due to their overall extreme incompatibility different degrees of partial melting will have negligible effects on these element ratios. This experimental constraint is underlined by relatively small variations of W/Ta, W/U, W/Th and the much larger variations in W/Hf and W/Zr in natural fresh MORB samples (König et al., 2011). The variable concentrations of W with W/U, W/Th, W/Ta, and W/Hf in the 1256D samples are shown in a log-log diagram in Figure 2.7A. If a variable source depletion trend would dominate the elemental ratios, decreasing W concentrations would correlate with decreasing W/Th, W/U, W/Ta, below the canonical ratios. The three element ratios would be largely insensitive to variable degrees of melting, unlike ratios of W/Hf or Zr/Nb (see above). In marked contrast, measured W/Th, W/U, and W/Ta show a positive correlation with the W contents ranging towards higher values than the canonical ratios, implying that the W content is not controlled by melting properties (Fig. 2.7A).

The combined evaluation of Ta/W ratios and Ta contents reveals that the absolute Ta concentrations in 1256D samples overlap those of unaltered MORB and also those of arc basalts. The Ta/W are significantly lower in 1256D samples ranging to values as low as in arc lavas (Fig. 2.7B). A covariation of W/Hf with Hf contents as could be expected from clinopyroxene-controlled melting also cannot be seen (Fig. 2.7C). A plot of Ta/W versus Hf/W shows that fresh MORBs follow a steep melt-depletion trend whereas the AOC samples at hole 1256D (Fig. 2.7B) follow a shallower trend controlled by selective W enrichment. When comparing Ta/W with Th/W (Fig. 2.7D), the samples form a straight trend, again consistent with a selective enrichment of W over both Ta and Th. Importantly, U ( $R^2 = 0.66$ ), Th ( $R^2 = 0.60$ ), and Ta ( $R^2 = 0.75$ ) concentrations show a significant correlation with the contents of the immobile elements Zr and Hf (Fig. 2.8A), indicative for a magmatic control of these element abundances and little alteration. In contrast, there is no correlation of W with Zr and Hf contents ( $R^2_{\text{Zr-W}} = 0.046$ ).

With respect to fractional crystallisation, another typical proxy is MgO content, which show negative correlations with U ( $R^2 = 0.10$ ), Th ( $R^2 = 0.54$ ), and Ta ( $R^2 = 0.59$ ). The correlations are in general weaker than for Zr which may reflect the modification of MgO contents during multiple stages of alteration represented, for instance, by the formation of Mg-Smectite in the upper oceanic crust (e.g., Bach et al., 2003). Interestingly, W contents are weakly correlated



with MgO contents ( $R^2_{\text{MgO-W}} = 0.47$ ), also suggesting an alteration control of W contents during seafloor alteration (Fig. 2.8B). In summary, the 1256D data indicate that, with respect to highly incompatible elements, the abundances of U-Th-Ta exhibit magmatic patterns and are largely controlled by variable degrees of source depletion, whereas the budget of W is strongly decoupled and appears to be strongly overprinted by alteration.

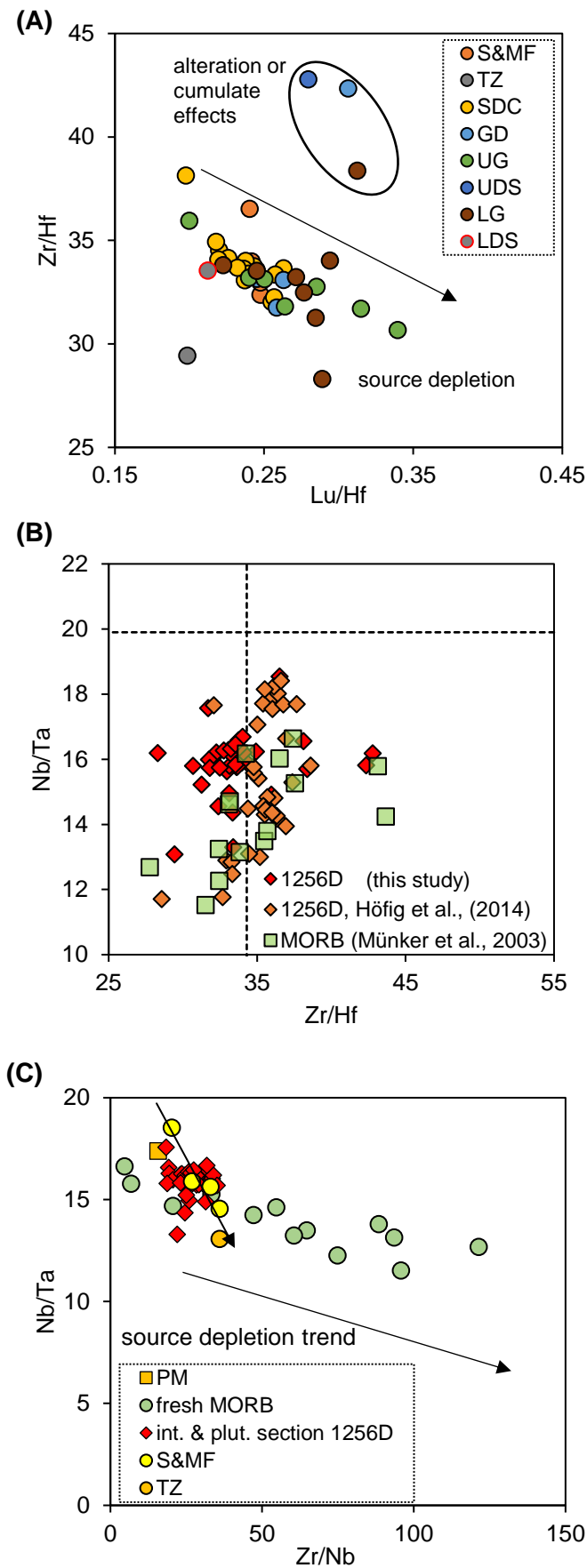


Figure 2.6: Immobile trace element patterns of hole 1256D samples, illustrating the effects of mantle source depletion on HFSE systematics

Most samples display a negative co-variation in Zr/Hf vs. Lu/Hf space, indicating variable degrees of source depletion (A). Notable exceptions are some samples from the transition zone (TZ), granoblastic dikes (GD), upper dike screen (UDS), and the lower gabbro (LG), where compositions are likely affected by either extensive alteration or cumulate effects. In Nb/Ta vs. Zr/Hf space (B), most samples plot close to or within the field define by fresh MORBs. In Nb/Ta – Zr/Nb space (C), a co-variation as could expected form pronounced partial melting cannot be observed. Notably, effusive sheet and massive flow samples and transition zone preserved a melt-fractionation trend ( $R^2 = 0.87$ ) that is steeper than that defined by fresh MORB.

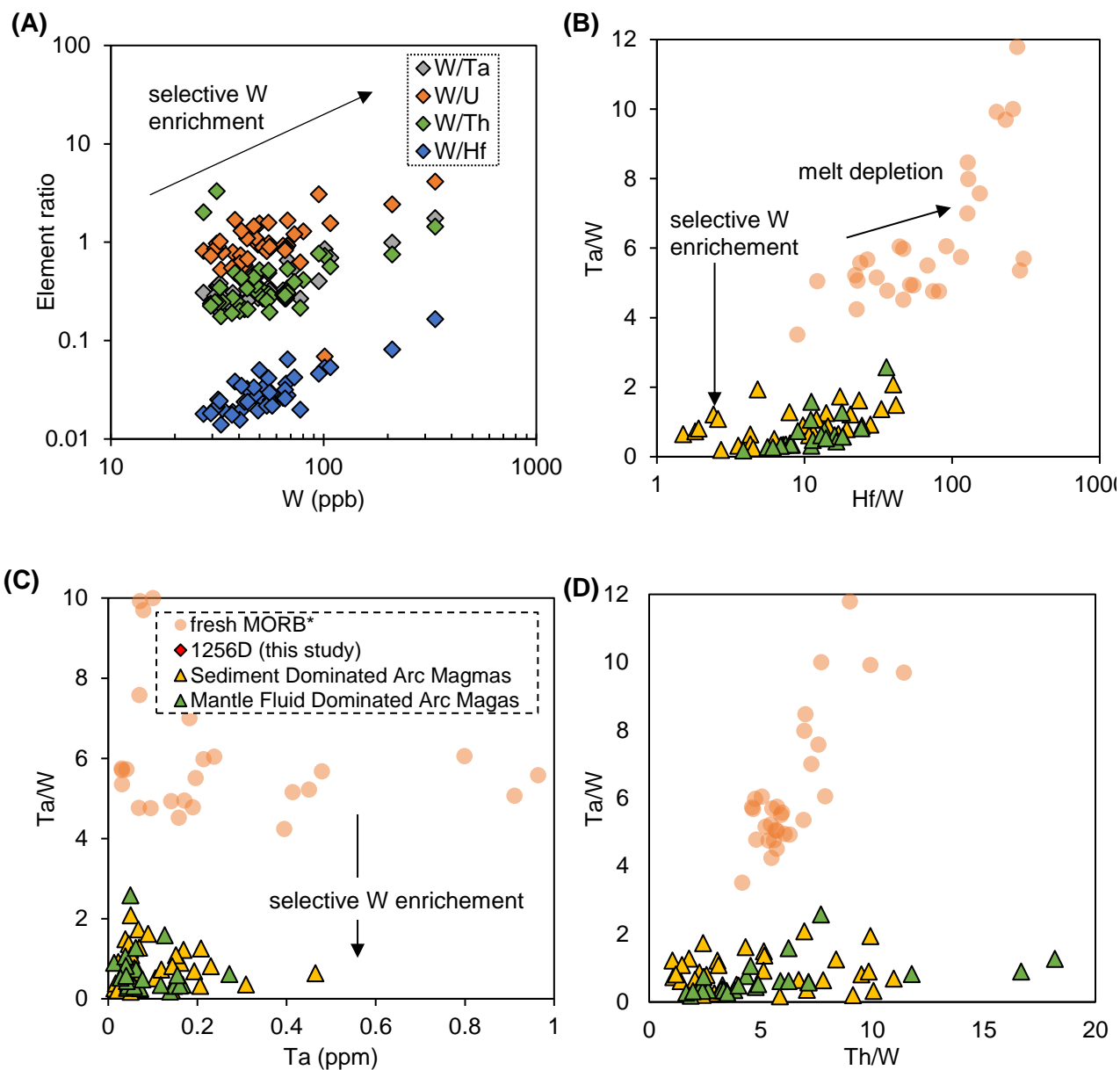


Figure 2.7: Compositional variations of W relative to other HFSE. Ratios of W/Th, W/U, W/Th, and W/Hf increase with W concentrations (A), indicating selective W enrichment. In Ta/W vs. Ta space (B), AOC samples from hole 1256D fill the gap between fresh MORB samples and different arc systems (B). Ta/W versus Hf/W relationships (C) indicate that the W enrichment is not caused by clinopyroxene-controlled melting. Rather, the data points fill the gap between fresh MORB (orange) with Ta/W > 4 and arc lavas with Ta/W < 2. The selective W enrichment is very pronounced relative to Ta and Th (D) that show little variation. (\* = König et al., 2011)

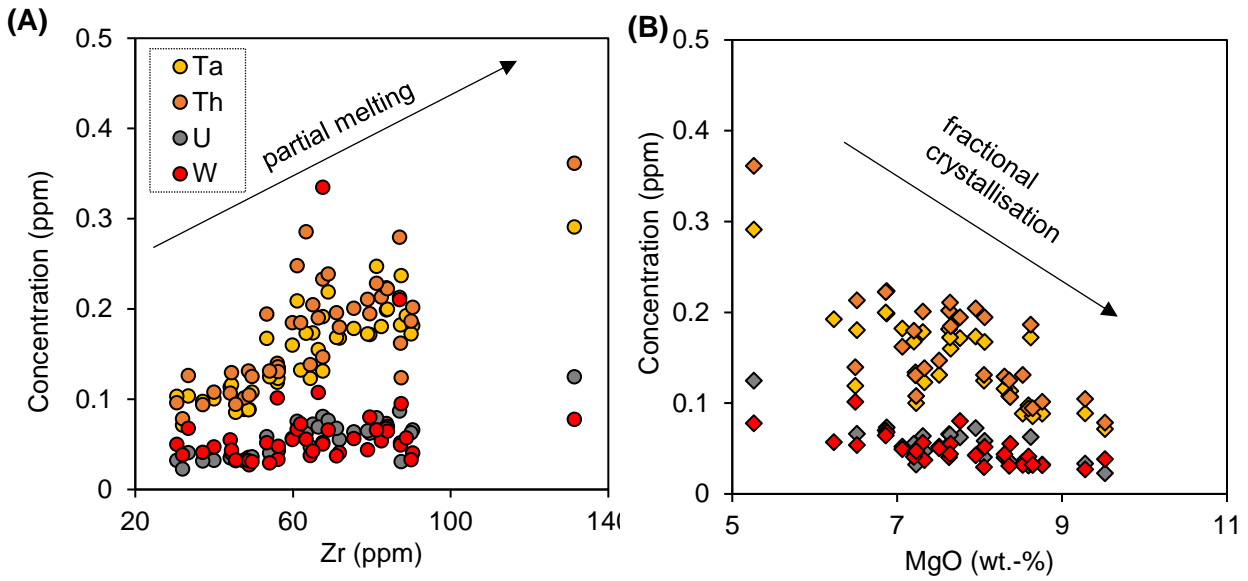


Figure 2.8: Co-variation diagrams of some HFSE and U-Th versus Zr and MgO. Contents of Th, U, and Ta increase with Zr (A) and decrease with MgO contents (B), whereas W does not. This suggests that the initial igneous trend for W is disturbed by later stage alteration, whereas the other HFSE are only little affected by alteration. Moreover, the co-variations of HFSE with Zr is stronger than with MgO, indicating potential late-stage alteration of Mg. MgO data from Neo, et al. 2009.

### 2.5.2 Origin of W-enrichment in different units of altered oceanic crust

The high downhole depth resolution in this study allows the evaluation of selective W enrichment in distinct portions of the AOC. Tungsten and HFSE concentrations are in general constant within the basalts. They appear to be broadly insensitive with respect to significant changes in the redox conditions of the hydrothermal fluids, their chemical composition, and the overall PT conditions between the lava and sheeted dike section (e.g. Alt, et al. 2010, Bach, 2003). It is still ambiguous where the distinct W enrichments in the transition zone and in parts of the gabbro section are exactly originating from. Several explanations are available, including partial melting processes, crystal fractionation, and hydrothermal alteration. Above, it was shown that it is unlikely that the concentration ratios of W vs. other HFSE and U-Th were significantly affected by partial melting or crystal fractionation. Thus, the influence of hydrothermal alteration on the observed W enrichment in the AOC will be further considered below.

The selective W enrichment is a ubiquitous feature of the studied segment of AOC. In fact, no selective W depletions have been found in any sample. To identify potential mineral carriers for W, this chapter is focussed on portions in the drill hole that are extreme enriched in W. In general, magmatic minerals such as olivine or pyroxene are unlikely candidates, as they exhibit very low D values for W (see above). In particular the transition zone is characterized by extremely high U and W concentrations (Table 2.1, and Neo et al., 2009). Both elements are selectively enriched over the fluid immobile Th and Ta. Uranium enrichment supersedes W enrichment resulting in  $U/Th > 10$  and  $W/U = 0.09$ . To constrain the magnitude and temporal evolution of hydrothermal alteration in various portions of the AOC in Hole 1256D, Harris et al. (2015) applied Sr-isotope systematics. In this work it could be shown that, although alteration was ubiquitous, intensive hydrothermal alteration and Sr-isotopic exchange was limited to discrete sections at the lava-dike transition zone and at the boundaries of the gabbroic intrusions, where dike margins provided fluid pathways (Harris, et al. 2015). The elevated  $^{87}Sr/^{86}Sr$  ratios in many altered sections provide further information of the fluid provenance in that seawater must have played an important role (Harris et al., 2015). The transition zone is characterized by particularly elevated  $^{87}Sr/^{86}Sr_{15\text{ Ma}}$  of ca. 0.7061, indicating extensive fluid-rock interactions, with mixtures of ambient seawater ( $^{87}Sr/^{86}Sr_{15\text{ Ma}}$  ca. 0.7088) and magmatic hydrothermal fluids ( $^{87}Sr/^{86}Sr_{15\text{ Ma}}$  ca. 0.7050, Harris et al., 2015). These findings indicate that the extreme local enrichments of U and W in the transition zone may potentially result from the mixing of downwelling seawater and upwelling hydrothermal fluids. Bach et al. (2003) have suggested that carbonate veins host significant amounts of U in ODP hole 504B. Such carbonate veins are an abundant component of the alteration assemblage in the transition zone of 1256D as well. Based on these findings, W may have potentially been incorporated in U bearing carbonates as well. Another available explanation is the incorporation of W in sulphides. With the limited data available for tungsten-mineral partition coefficients a firm conclusion cannot be drawn at this stage.

The application of  $^{87}\text{Sr}/^{86}\text{Sr}$  ratios in the granoblastic dikes is problematic, since the intrusion of the two gabbro bodies postdates the initial hydrothermal alteration and the vertical and lateral movement of the axial melt lens (Wilson et al., 2003, Alt et al., 2010, Harris et al., 2015, France et al., 2009) may have homogenized initial Sr isotope signatures (Harris et al. 2015). The measured  $^{87}\text{Sr}/^{86}\text{Sr}$  in this depth range are ca. 0.7039 which is only slightly elevated relative to 1256D MORB composition ( $^{87}\text{Sr}/^{86}\text{Sr}_{\text{fresh 1256D MORB}}$  0.70287). Samples 187-2 and 188-1 carry signs of hydrothermal alteration such as light greenish grey alteration halos around veins (Wilson et al., 2003). From  $\delta^7\text{Li}$  and  $\delta^{18}\text{O}$  isotope data and the mineral record it is known that these rock units have experienced alteration temperatures of 450 – 500°C, marking a transition from seawater dominated to rock dominated alteration (Gao et al., 2012).

In the gabbros themselves, Sr isotope data provide information on the history of hydrothermal fluid circulation. Here,  $^{87}\text{Sr}/^{86}\text{Sr}$  are elevated (ca. 0.7051, Harris et al., 2015) and are in the range of hydrothermal fluid compositions (ca. 0.705), but less radiogenic than 15 Ma seawater (ca 0.7088, McArthur et al., 2001). This observation indicates a nearly closed system in the gabbros, restricting the extensive fluid-rock reactions to the intrusive margins of both gabbro bodies (Harris et al. 2015). This feature is mirrored in the downhole variations of W concentration and other elements (Fig. 2.3), where W/Th, W/U and W/Ta are elevated along the intrusive dike margins. A potential mineral carrier for W from hydrothermal fluids may be abundant secondary epidote. Epidote is an abundant and well-known part of the hydrothermal alteration mineral assemblage, nevertheless their partitioning coefficients for W are not yet quantified. It is well known that epidotes can carry substantial amounts of W (Frei et al., 2004). It is thus speculated that precipitated epidote is one of the major mineral W sinks in the lower oceanic crust that lead to elevated W/Th, W/U, and W/Ta.

While fluid-rock interaction in the dike-gabbro transition is restricted to intrusive margins, it left the dike screen relatively unaffected (Harris et al., 2015). The observation of low W/Th, W/Ta, and W/U ratios in the lower dike screen (represented by sample 227 – 1) supports the model of France et al., (2009) and Koepke et al. (2011) that the dike screen rather constitutes a metamorphic overprinted xenolith than a block of the sheeted dike section that is isolated by dike intrusions. Strontium-isotope data published by Harris et al. (2015) do in principle not affect this conclusion, because the high temperatures of the gabbros and the fluid circulation induced alteration overprint initial Sr signatures.

### 2.5.3 Tungsten enrichment relative to U and Th enrichments

Uranium and Thorium have been regarded as the closest geochemical analogues to W in terms of magmatic fractionation behaviour (e.g., Palme & Rammensee 1981, Newsom et al. 1996). Thus, the higher W/U and W/Th ratios in AOC compared to fresh MORB point to a selective enrichment of W over these two elements (Fig. 2.8 A, B). If W/U and W/Th ratios are combined (Fig. 2.9C), most of the 1256D samples define a trend outside the fresh-MORB fields defined by König et al. (2008). Both element ratios points are highly correlated ( $R^2 = 0.985$ ). A remarkable outlier is sample 122-1, originating from the transition zone, where the extreme selective U enrichment leads to very low W/U ratios at moderately elevated W/Th. Hence, the trend is mainly controlled by W since U/Th is, except for the transition zone, relatively invariant at a near-canonical values of ca. 0.3 for the whole depth range. Moreover, a covariation of U or Th vs. U/Th could not be identified.

Above, explanations for the deviation of transition zone samples (significant U gain by alteration) and gabbroic samples (younger magma with Th excess) from the U-Th equiline were presented. A similar U enrichment in the transition zone was identified at hole 504B as well (Bach et al., 2003). Due to preserved  $^{230}\text{Th}$ -U disequilibrium, the U enrichment at the transition zone in hole 1256D potentially reflects relatively recent, off axis enrichment in U and possibly also in W.

U-Th disequilibria measurements were first employed to EPR samples by Newman et al. (1983) who found significantly elevated  $^{230}\text{Th}$  excesses and attributed these to a higher melt incompatibility of Th relative to U. In this regard, Turner et al. (2011) also observed  $^{230}\text{Th}$ - $^{238}\text{U}$  disequilibrium in off-axis segments further to the north at the EPR. As some of the lower gabbro samples display elevated  $^{230}\text{Th}$  excesses as well, the lower gabbro may likely contain portions that are significantly younger than the surrounding crust. An available explanation might the intrusion of a late doleritic dike (Harris et al., 2017) within the past 300 ka. This is in stark contrast to models presented by France et al., (2009) and Koepke et al. (2011) where the lower dike screen is regarded as large xenolith and both gabbros rather represent one unit. An alternative model could therefore also be that the gabbro is older than 300 kyrs, but the apparent  $^{230}\text{Th}$  excesses in the lower gabbro reflect young U removal by hydrothermal fluids.

#### 2.5.4 Comparison with ODP hole 504B

ODP hole 504B was drilled into crust formed at the EPR as well. It is located 200 km East of the Costa Rica Rift zone and is ca. 6 Ma old (Alt et al. 1996). The sedimentary cover of ca. 250 m is similar to 1256D (ca. 270 mbsf) but the effusive volcanic zone (VZ) at hole 504B is much thinner than at hole 1256D (570 mbsf vs. 750 mbsf). The volcanic section at 504B is predominantly composed of pillow lavas rather sheet and massive flows at 1256D (Alt et al. 1996). The thickness of the transition zone (TZ) differs also significantly between ca 57 m at 1256D and 209 m at 504B. Furthermore, though 504B is deeper (total depth ca 1850 mbsf), it has not reached the intrusive section (Alt et al. 1996). Although the same secondary minerals are present in both volcanic sequences, oxidation halos are much more abundant in the uppermost portions of hole 504B (Alt et al., 1996; Alt and Teagle, 2003; Bach et al., 1996; Teagle et al., 1996). The sequence of secondary mineral occurrence with depth in both sheeted dike complexes is similar, but the different thickness of the dike layers must reflect drastically different thermal gradients between the lavas and the underlying magma chambers (e.g., Alt et al., 1996, Bach et al., 2003).

In the samples from hole 1256D studied here, U is enriched in the transition zone, which agrees with the results of Neo et al., 2009 and with the study of 504B samples by Bach et al., 2003. The latter study of hole 504B identified extensive U enrichment in the upper portions of AOC and attributed it to a) abundant Fe-oxyhydroxides in the uppermost part of the crust and b) carbonate veins in lower parts. In contrast to results reported from ODP hole 504B, strong enrichments of U in the sheet and massive flows and within the transition zone of hole 1256D could not be identified here. The samples discussed here mostly originate from lithological deeper portions, where U is also not enriched in hole 504B (Bach et al., 2004). The elevated U concentration in upper portions of hole 504B (< ca. 820 mbsf) is attributed to carbonate-yielding veins (Bach et al., 2004). Although abundant carbonate + laumanite + anhydrite veins have also been identified in numerous samples of hole 1256D, U is not enriched over Th. Since the enrichment in U is attributed to low-T processes (e.g. Bach et al., 2003; Hart and Staudigel, 1982; Staudigel, 2013), it is highly likely that continuously increasing heat supply with downhole hole 1256D restricted the U enrichment to the uppermost oceanic crust which was not extensively studied here. Furthermore, the transition zone forms an effective barrier for later seawater influx (Wilson et al., 2006, Alt et al., 2010).



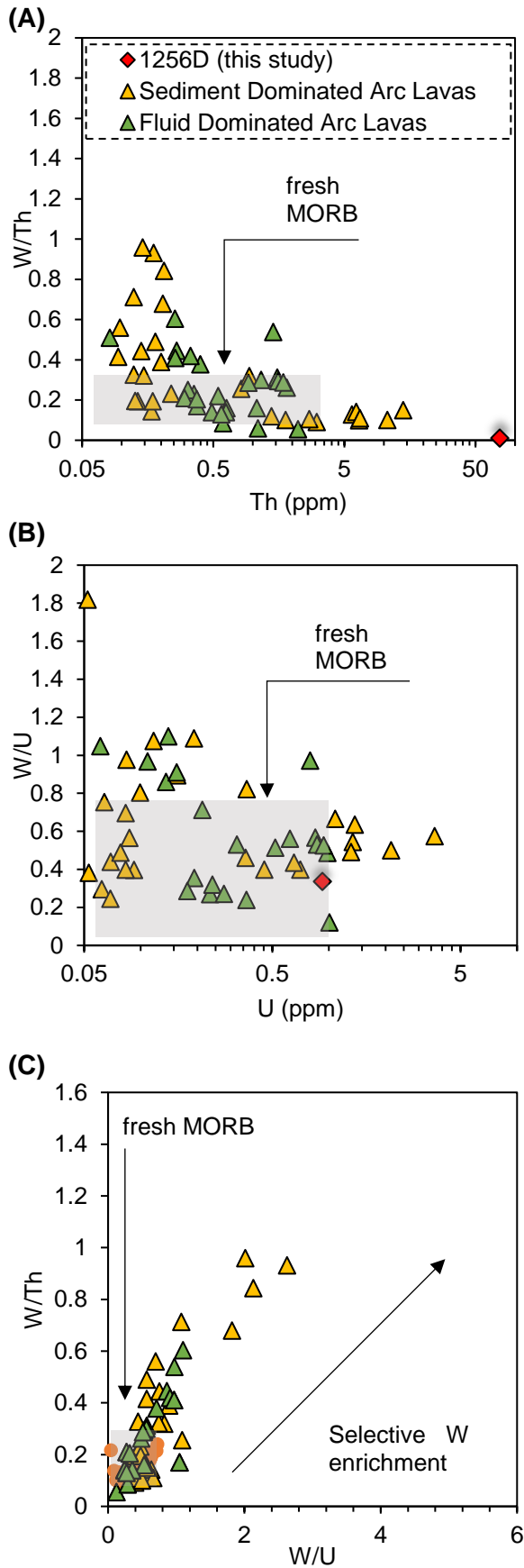


Figure 2.9: Systematics of W-Th-U for Leg 1256D samples in comparison to different types of arc lavas. Compared to fresh MORB (orange field, A, B), hole 1256D samples display elevated  $W/Th$  and  $W/U$  ratios at similar  $Th$  and  $U$  concentrations.

In  $W/Th$  vs.  $W/U$  space (C) samples from 1256D form a distinct array towards higher  $W/Th$  and  $W/U$  ratios than fresh MORB, indicating selective enrichment of  $W$  relative to  $U$  and  $Th$ . Some arc lavas display  $W/U$  and  $W/Th$  ratios even lower than MORB, indicating that  $W$  enrichment is absent, when nor significant amounts of pelagic sediment are subducted or in slab melt-dominated regimes. This indicates that the lower  $W/U$  ratios might be caused by the higher mobility of  $U$  that led to a lower  $W/U$  ratio compared to AOC values.

## 2.5.5 Tungsten enrichment in the AOC compared to arc settings

The finding of W enrichment in altered oceanic crust has important implications for understanding the behaviour of W during the subduction cycle. Previous surveys on the behaviour of W in arc lavas (König et al. 2008, 2011) have revealed that W behaves highly mobile in subduction zone systems, particularly, if fluids control the elemental budget in the sub-arc mantle. Tungsten enrichment in the subarc mantle is most pronounced in arcs where subducted sediments with high W concentrations are involved (e.g., Indonesia, Kermadec, Cyprus) and is less pronounced in arcs where negligible amounts of pelagic sediments are involved (e.g., W-Pacific arcs, König et al. 2011).

Compared to the AOC segment examined in this chapter, all arc lavas have in general lower Ta/W ratios at similar absolute Ta concentrations than fresh MORB ( $Ta/W_{Arc} < 2$ ,  $Ta/W_{MORB} > 4$ ; Fig. 2.7B). Samples from 1256D fill this gap with Ta/W ratios between 2 and 4. Like Ta, W shows selective enrichment relative to fresh MORB (Fig. 2.9 A & B) but not as pronounced as in arc lavas. When comparing arc lavas with different proportions of subducted sediments involved, it becomes obvious that the enrichment of W relative to Th and U is negligible in arcs where subducted mafic crust dominates the trace element budget and sediments are absent. For some of these arc segments (e.g., Solomon Islands, Kamchatka, Central Tonga) ratios of W/Th and W/U are at a similar range as fresh MORB or even lower (Fig. 2.8A & B). These arc magmas show no significant fluid-controlled W enrichment and were previously related to the presence of slab melts (König et al., 2010) or sediment-derived, melt-like components in their source (Sunda and Kermadec arc lavas, Turner and Foden, 2001; Wendt et al., 1997). This appears counterintuitive, as fluids from subducted, W-enriched AOC should significantly contribute to the trace element budget of arc rocks even though subducted sediments are negligible. A plausible explanation is that the elevated W/Th and W/U ratios observed here for rocks from hole 1256D are not representative for the whole AOC. There might be portions of the AOC where W is depleted which may not have been sampled by this study, e.g., the middle or lower oceanic crust or upper oceanic crust that underwent different alteration styles. Following the ever-decreasing selective W enrichment from the onset of granuloblastic dike overprint downwards, a possible root zone for W mobilization might be identified in the sheeted dyke section between the axial melt lens and the two gabbroic intrusions. This would at least argue for pervasive W enrichment in the upper oceanic crust, where the largest mass fraction of w should be located.

A second explanation for the excess W conundrum might therefore be that W is retained to a larger extent than U-Th during dehydration of AOC in subduction zones. Possible candidates for selectively retaining W are accessory phases like rutile, which is one of the few minerals W is compatible with (Klemme et al., 2005; Zack, 2002). Rutile is formed during high-pressure metamorphism of upper amphibolite facies to eclogite-facies grade. It is known to

carry significant portions of the HFSE budget in these rocks (Foley et al., 2000, Zack et al. 2002), but it is yet unconstrained how effective rutile is scavenging W from the oceanic crust during its formation. Moreover, available data for arc lavas demonstrated the overall mobility of W in subduction settings, ruling out that significant amounts of W are retained by rutile (König et al., 2008).

A third available explanation is that U-Th are mobilized in subduction zone components to a similar or even large extent than W, thus cancelling out the effects of selective W enrichment during oceanic crust alteration. It was demonstrated by Kessel et al. (2005) that supercritical subduction components formed at depths > 100 km below arc zones can mobilize substantial amounts of U and Th. As W behaves in similar to U in such settings (Bali et al., 2012), W is likely to be transported at a similar efficiency than U-Th, making it unlikely that U and Th are selectively mobilized over W.

Consequently, the results suggest that in the absence of substantial amounts of W-enriched subducted sediments, W is redistributed within the oceanic crust and enriched in its upper portions prior to subduction. Thus, dehydration of oceanic crust may selectively tap either W-enriched upper or W-depleted lower crustal levels which in many cases may buffer the effect of initial W enrichment in the upper to mid oceanic crust.

## 2.6 Conclusions

Samples from IODP hole 1256D can provide new insight into the behaviour of W during the alteration of the upper oceanic crust. Concentrations of high field strength elements like Nb-Ta, Zr-Hf and of Lu and U-Th are in line with previously published data for hole 1256D by e.g. Höfig et al. (2014) and Neo et al. (2009) and demonstrate the robustness of the newly developed sample digestion protocols applied here. Except for W, the variability of HFSE and U-Th in the effusive and intrusive section is limited and controlled by magmatic processes, a variation of concentrations with depth is not observed. Excluding W and U, most trace elements are depleted in the transition zone relative to the effusive section above and the intrusive section below. Along margins of intrusive gabbroic dikes, most trace elements are selectively enriched. Nevertheless, the cores of the gabbros remain at lower concentrations. Tungsten and U are strongly enriched in the transition zone. The deeper, sheeted dike section with granoblastic overprint is characterized by extreme selective W enrichment.

In the sample set, a strong enrichment in U is only found in the transition zone, whereas the effusive and intrusive section are characterized by canonical U/Th of ca. 0.3. This is different to ODP hole 504B, where U enrichment was found throughout the whole section, (Bach et al., 2004). The effusive section discussed in this study is significantly deeper than that in 504B, U enrichment is thus diminishing with depth.

Due to their similar incompatibility during silicate melting, Th, U, and Ta have been selected to provide a framework to quantify the selective mobility of W. Any deviations of W relative to U, Th and Ta are mainly caused by hydrothermal alteration. A selective W enrichment by a factor of up to 13 can be observed, as indicated by W/Th, W/U, and W/Ta ratios as high as 1.44, 4.14 and 1.75. The highest W concentrations are observed at the transition zone separating intrusive from effusive section (ca. 1300 mbsf), at the boundary between sheeted dike section and granoblastic dikes, as well as at the margins of granoblastic intrusions, also in line with more radiogenic Sr isotope compositions in these zones. With respect to the timing of W enrichment, it is evident from Th-U measurements, that most alteration likely occurred near-axis shortly after the formation of the oceanic crust, since no alteration younger than 350 ka is preserved in most rocks. This finding is in line with models of, e.g., Wilson, et al. (2006), Alt, et al. (2010), and Harris, et al. (2015) reporting multiple on-axis stages of alteration and mineralization in crust of 1256D. The absence of later-stage alteration potentially reflects fast sealing of the oceanic crust from seawater circulation by rapid sedimentation (> 30 m/ma, Tominaga et al., 2009).

By comparing the W/Ta, W/Th, and W/U ratios of AOC with those of unaltered MORB and arc lavas, it is striking that W is enriched in AOC at a similar order of magnitude as it is in some arc rocks. It can therefore be postulated that the selective enrichment of W observed in arc lavas (e.g., König, et al. 2008, 2011) is not solely caused by selective W mobility during

dehydration of the subducted slab but is at least partially inherited from alteration processes that occurred prior to subduction. Nevertheless, high W/Th and W/U ratios in arc settings cannot be straightforwardly explained by AOC alteration, because there are examples for arcs where subducted oceanic crust dominates the trace element budget, but the lavas do not show a selective enrichment of W relative to Th and U. In these cases, not only W is enriched by sub-arc processes, but also Th and U. Three models potentially explain this conundrum, (a) retention of W in rutile, (b) selective enrichment of subduction zone fluids in U and Th relative to W, and (c) unrepresentative sampling of AOC by hole 1256D, leaving W depleted portions in the oceanic crust unsampled.

The high-precision trace-element data show a continuously decreasing trend in W/Th, W/U, and W/Ta from the top of granoblastic dikes towards the lowest crustal levels. It is therefore tentatively suggested that the W enrichment originates from a root zone below the gabbroic intrusions. Consequently, dehydration during subduction of 1256D crust may sample both W enriched and W depleted crustal levels, thus diminishing the effects of selective W enrichment in upper and middle oceanic crust.

To further understand the global W cycle and the role of altered oceanic crust, more research on W mobility in lithological units deeper than hole 1256D is required, in particular in units of the lower oceanic crust like the massive gabbroic or ultramafic portions of the oceanic crust that provide a substantial portion of oceanic crust exposed on the seafloor.

**3. Extreme W enrichment during alteration of  
peridotites from the lower oceanic crust,  
IODP Leg 209**

### 3.1 Introduction

Tungsten acts as a highly incompatible element in the global geochemical cycle, similar to Th, U or Nb-Ta (e.g. Newsom et al., 1996; Newsom and Palme, 1984; Palme and Rammensee, 1981). Consequently, W/Th, W/U and W/Ta ratios are not significantly affected by magmatic processes and were taken as constant to mass balance the global W geochemical cycle (Arevalo and McDonough, 2008; Newsom et al., 1996; Noll et al., 1996). More recent studies could demonstrate that W may be selectively enriched in fluids, leading to selective W enrichment in arc lavas and the continental crust (Hulsbosch et al., 2016; König et al., 2008, 2011; Manning and Henderson, 1984). Thus, the long-standing view of W being a relatively immobile element in aqueous regimes (Noll et al., 1996) has changed over the last years. Furthermore, W is more efficiently removed from deep seawater than the chemically similar Mo (Sohrin et al., 1999), where the effective adsorption of W at the surfaces of Fe-Mn oxyhydroxides is one of the key processes (Kashiwabara et al., 2013).

Several studies even indicated W mobility during serpentinization and in sub-arc environments (König, et al., 2008, Peters et al., 2017, van de Löcht et al., 2018). Compared to intensive studies on mafic and felsic rocks (Arevalo and McDonough, 2008; König et al., 2008; 2011; Newsom et al., 1996; Noll et al., 1996), the oceanic crust, mainly due to its inaccessibility, has remained largely unexplored for elemental mass balances like that of W. In the above presented chapter, first indications on W enrichment in crust, formed at super-high spreading rates were presented. Nevertheless, the W inventory of deeper levels of peridotitic oceanic crust has so far been unexplored. Since altered oceanic crust (AOC) covers more than 60 % of the Earth's surface (Wilson et al., 2006), understanding the mobility of W during its alteration is a key question in understanding the global geochemical cycle of W. Altered oceanic crust is a geochemical sink for some elements (Alkali metals, Mg, S, U; Albarede and Michard, 1986) and source for, e.g., Ca, Mg, Si, Sr (Albarede and Michard, 1986; Bach et al., 2003; Hart and Staudigel, 1982; Huang et al., 2015). In particular serpentinization of peridotitic oceanic crust is known as major sink for Li (Ryan and Langmuir, 1987; Seyfried et al., 1984; Von Damm et al., 1985), B (Ryan and Langmuir, 1987, Smith et al., 1995) and K, Rb, Cs, Na (Hart and Staudigel, 1989, Staudigel, et al. 1995, Bach et al., 2001). Compared to similarly incompatible elements, the concentration of U is elevated in the uppermost volcanic zone and within the transition zone separating effusive from intrusive portions of the oceanic crust (e.g., Bach et al., 2004). In contrast to U, Th concentrations are invariable during alteration of oceanic basalts, similar to other immobile elements like Zr, Nb, Hf or Ta and the rare earth elements (REE) (Niu, 2004; Staudigel, 2013). In chapter 2 it is demonstrated that W is selectively enriched in moderately altered upper oceanic crust, it is thus promising to study alternative parts of altered oceanic crust.

Trace element distribution during alteration in mafic-ultramafic portions of oceanic crust is intimately linked to serpentinization. Seafloor serpentinization (< 150 meters below seafloor, mbsf) comprises a series of hydration reactions occurring when ultramafic rocks are exposed to aqueous fluids at  $T < \text{ca. } 350^\circ - 400^\circ\text{C}$ . Serpentinization is dominated by progressive alteration of olivine to lizardite and chrysotile ( $\pm$  brucite  $\pm$  talc  $\pm$  magnetite; e.g., Bach et al., 2004; Moody, 1976). Other prominent serpentinization reactions include the formation of chrysotile and brucite by the hydration of forsterite and the formation of chrysotile by the hydration of forsterite and talc (Caruso and Chernosky, 1979; Johannes, 1968; O'Hanley et al., 1989). As outlined in chapter 1, the extent of serpentinization is largely dependent on the porosity-permeability characteristics of the crust (Klein et al., 2015; Lamadrid et al., 2017). Endmembers of serpentinization in the presented sample suite may either be (a) isochemical addition of  $\text{H}_2\text{O}$  to the mineral fabric (water rock ratio  $< 1$ ) or (b) hydration of the mineral assemblage by trace element-enriched fluids of magmatic origin ( $w/r > 1$ , e.g. Kelemen et al., 2004, Paulick et al., 2006). In addition, intrusions of gabbroic dikes may also supply heat and incompatible trace elements to the alteration assemblage (France et al., 2009; Paulick et al., 2006). Dike intrusion may also lead to dehydration of already hydrated mantle portions and subsequent fluid generation with elevated trace element concentrations (e.g., Paulick et al., 2006; Harris et al., 2015). Late, low-grade oxidative alteration of the uppermost section of altered oceanic crust results in formation of Fe-oxyhydroxides, calcite and smectite and is typically associated with a prominent gain in U (Bach et al., 2001; Hart et al., 1999).

To assess the mobility of W during alteration of the lower oceanic crust, a coherent set of high-precision isotope-dilution (ID) data for high-field strength elements (HFSE) and U-Th for various portions of excessively altered abyssal peridotites formed in a magma starved, slow-spreading zone at the Mid-Atlantic Ridge (MAR), drilled during ODP Leg 209 is presented in this chapter. These drill cores offer a broad range of highly depleted peridotites with different alteration types and stages (Bach et al., 2004; Kelemen et al., 2004; Paulick et al., 2006). Alteration styles include a wide range of serpentinization types and intensities, covering serpentinization of only olivine to complete serpentinization of peridotite followed by replacement of serpentine by talc. Other alteration styles include various degrees of serpentine-brucite alteration and replacement of brucite by iowaite along with talc-tremolite alteration of pyroxene (Bach et al., 2004). Owing to the extremely low abundances of incompatible trace elements in ultramafic rocks, the here discussed dataset is the first comprehensive datasets for HFSE and U-Th for altered ultramafic rocks. The data are used to better understand incompatible trace element behaviour during alteration of the deeper oceanic crust and to better evaluate the role of altered oceanic crust during the global geochemical cycle of W.



## 3.2 Geological Overview of IODP Leg 209

### 3.2.1 Lithology and alteration styles at the drilled sites

ODP Leg 209 drilled highly serpentinized mantle peridotites and gabbroic rocks of the mid-Atlantic ridge (MAR) along the 15°20' fracture zone at 14°43' – 5°44' N and 47°30' – 44°30' W (Fig. 3.1). This section of the MAR is an example of a slow-spreading ridge (full rate ~ 25 mm/a), with little to no effusive magma production and large outcrops of lower-mantle peridotites (Kelemen et al., 2004). Thick lithosphere (10–20 km) in this region inhibits magma from reaching shallow levels beneath the ridge axis, causing plate formation only by extensional faulting (Schroeder et al., 2007). The studied section is young (< 5 Ma; Fujiwara et al., 2003) and has only seen little sediment deposition (Kelemen et al., 2004). In total, 19 holes have been drilled at 8 different sites (1268 – 1275) with the sites 1268 – 1272 being located south of the 15°20' N fracture zone and sites 1273, 1274, and 1275 being in the northwest of the fracture zone (Fig. 3.1, Kelemen et al., 2004). The focus on boreholes 1268 A, 1270 A, C & D, 1271 A & B, 1272 A, and 1274 was guided by the wide variety of alteration processes that were operating and by the available geochemistry (Bach et al., 2003; Godard et al., 2008; Kelemen et al., 2007; Paulick et al., 2006). In the following section, characteristic alteration effects and their influence on the trace element budget are summarized. More detailed descriptions are given in the ODP Initial Results Volume 209 (Kelemen et al., 2004).

Hole 1268 A mainly consists of intensively serpentinized harzburgite and dunite (ca. 75 vol. %) intersected by late magmatic dikes and gabbroic bodies (ca. 25 vol. %; Bach et al., 2004). As a result of fluid-dominated serpentinization at site 1268, REE patterns are U-shaped with mainly positive Eu anomalies. Additionally, S was added during serpentinization, resulting in the formation of secondary pyrite. The REE patterns show similarities to those of high-T black smoker fluids discharging from the nearby Logatchev hydrothermal field, suggesting similar compositions of the altering fluids (Bach et al., 2004; Paulick et al., 2006). An initial stage of fluid-dominated, greenschist-facies serpentinization was followed by pervasive talc alteration under static conditions at 350 – 400°C at pH ~ 4 – 5. In this temperature range is olivine still stable but orthopyroxene readily replaced by talc ± tremolite. This breakdown of pyroxene is a source of Si, facilitating talc formation (Bach et al., 2004). Late and pervasive talc alteration finally leads to whole-rock compositions close to pure talc (Kelemen et al., 2004) which is recorded by decreasing MgO/SiO<sub>2</sub>, loss on ignition (LOI), and Fe<sup>3+</sup> (Paulick et al., 2006). In talc-altered sections, LREE patterns are flat to slightly LREE enriched, with negative Eu anomalies. Talc alteration and gabbro intrusions are in close spatial relation, suggesting that gabbro emplacement and talc alteration are intimately linked (Paulick et al., 2006) and gabbro intrusion and dike formation may have revived the hydrothermal circulation.

Samples originating from site 1270 (holes A, C & D) are characterized by pervasive serpentinization and exsolution of ilmenite from titanomagnetite. The petrographic composition

is relatively uniform (~ 62 % harzburgite, 6 % dunite, and 32 % gabbro and gabbro-norite) and the proportion of gabbro to peridotite is similar to hole 1268A (Kelemen et al., 2007). The gabbros intruded at 600 – 900 °C, leading to fluid generation and intensive melt impregnation, resulting in elevated trace element concentrations (Kelemen et al., 2004). Where relict orthopyroxene is present it is locally replaced by talc ± tremolite in zones of mafic dike intrusions (Kelemen et al., 2004). Nevertheless, there was no extensive talc formation superseding serpentinization as recorded in hole 1268A. Minor amounts of carbonate veins are developed in holes 1270 C & D. Iron-oxyhydroxide veins are restricted to shallower portions and are interpreted to have formed during seafloor weathering under oxidizing conditions (Bach et al., 2004). Deeper carbonate and mineralized veins grade into talc-altered veins and indicate circulation of carbonate-rich fluids (Kelemen et al., 2004).

At site 1271 (A & B) dunites (A: ca. 98 vol.-%, B: ca. 56 vol.-%) comprise a greater proportion of the drilled crust than harzburgite (A: < 1 vol.-%, B: ca. 9 vol.-%, Kelemen et al., 2004). Like site 1270, this locality was subject to extensive serpentinization and high-T deformation (Kelemen et al., 2004). Talc alteration is restricted to deformation textures. Concentrations of incompatible elements are elevated compared to other holes from Leg 209, suggesting intensive interaction with gabbroic dikes comprising 2 % (1271A) and 21 % (1271B) of the drilled crust (Kelemen et al., 2004). The uppermost 10 meters are characterized by dunites with a yellowish green to grey groundmass hosting abundant black serpentine-magnetite veins, which is related to seafloor weathering reactions including brucite dissolution (Bach et al., 2004). Serpentine of site 1271 show U-shaped REE patterns and positive Eu-anomalies, which are likely caused by the formation of plagioclase during melt-rock interaction or result from hydrothermal alteration like in hole 1268A. Serpentinization itself happened under static conditions (Paulick et al., 2006).

Hole 1272A is subdivided into an intensively fractured zone with various lithologies, mainly fine-grained diabase and hypabyssal gabbro-diorite-diabase in the top 55 m, and a lower part mainly composed of harzburgite (ca. 95 vol. % vs. ca. 5 vol. % dunite). Hole 1272A harzburgites are characterized by low concentrations of immobile elements and are depleted in LREE (Paulick et al., 2006). No strong effects of metasomatic reactions are observed, revealing near pristine compositions. At fault gauges and in highly serpentinized samples, iowaite was formed in oxidizing conditions where Fe<sup>3+</sup> was balanced by Cl<sup>-</sup>. The overall alteration intensity decreases with depth in the harzburgites. Two types of gabbro intruded the 1272A section, one microlithic gabbro/diabase body and one single interval of gabbro-norites.

Of all examined sites, hole 1274A is the least altered with locally 35 % of its original mineral assemblage still preserved. The proportions of harzburgite (~ 77 vol.-%), dunite (~ 20 vol.-%) and gabbro (~3 vol.-%) are similar to sites 1268 and 1270. Serpentinization intensity increases with depth and is dominated by the formation of brucite, serpentine, and magnetite,

reflecting effects of local hydration and oxidation of olivine. The extent of serpentinization is reflected in its covariation with LOI values (Harvey et al., 2006). Late, low-grade oxidative alteration is reflected in Re-Os data which indicate a penetration depth of seawater of ca. 60 mbsf (Harvey et al., 2006). The concentrations of immobile elements are low and LREE are strongly depleted relative to MREE and HREE (Godard et al., 2008; Paulick et al., 2006). Positive correlations of  $\text{Al}_2\text{O}_3$ , Sc, Cr, and V reflect modal variations of pyroxene and olivine in the protolith (Paulick, et al. 2006). Despite their good preservation, the rocks contain 10 – 15 wt.%  $\text{H}_2\text{O}$  and iron in primary phases is often oxidized (Kelemen et al., 2004). The REE patterns of highly altered serpentinites resemble those of their least altered counterparts. The lower concentrations of HREE in 1272A compared to 1274A are explained by a more depleted precursor or by dilution effects due to serpentinization (Paulick, et al. 2006).

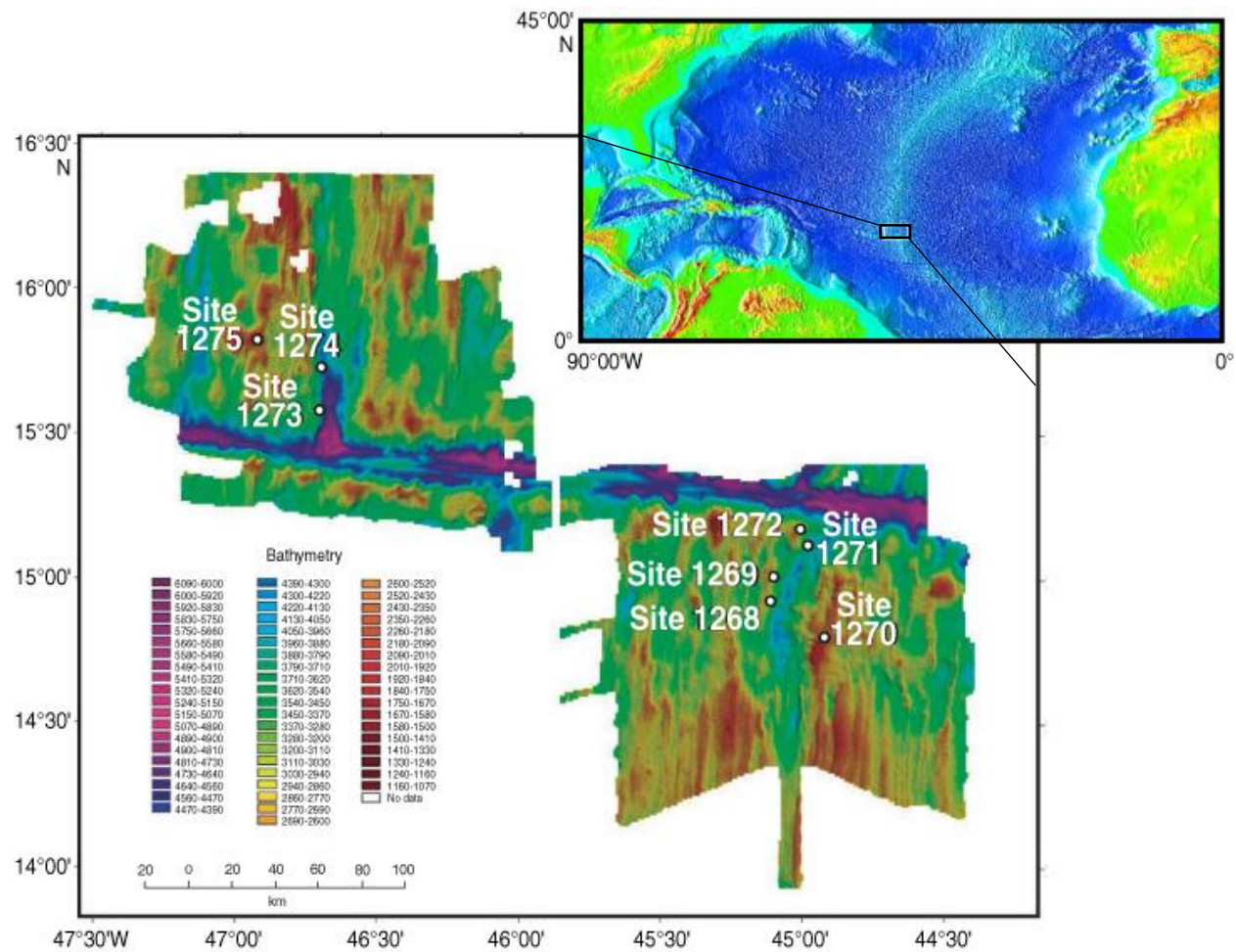


Figure 3.1: Location of the boreholes drilled at ODP Leg 209. Samples from drill sites 1268, 1270, 1271, 1272, 1274 were investigated in this chapter (Image from Kelemen et al., 2004).

### 3.2.2 Alteration effects common to all drilling sites

In Leg 209 rocks, predominant alteration styles include talc-alteration, fluid-dominated and rock-dominated serpentinization, melt-rock interaction and iowaite alteration (Table 3.1, Kelemen et al., 2004; Paulick et al., 2006). In the following, a brief overview of the specific alteration styles and the effect on geochemistry is given. Details are described in Kelemen et al. (2004), Bach et al., (2004), and Paulick et al. (2006).

Nearly all studied sites have been intruded by gabbros under granulite and amphibolite facies conditions. Sites 1270 and 1271 also provide geochemical evidence that small dikelets penetrated and modified the bulk rock geochemistry by the addition of incompatible elements (hereafter called melt-rock interaction, Paulick et al., 2006). Main serpentinization is recorded in an initial stage of high-T (> 350 °C) alteration in 1270 and 1271 peridotites by hydrothermal solutions triggering the disintegration of pyroxene and the formation of a first generation of talc and tremolite in gabbros. In general, serpentinization at samples from Leg 209 is defined by the formation of serpentine, magnetite and brucite. These phases may later be dissolved because of changes in the ambient fluid pH and changes of the silica activity and, thus, they are not always preserved (Bach et al., 2004). The initial stage of serpentinization and mafic dikelet intrusion is followed by pervasive serpentinization at ca. 250 °C under greenschist-facies conditions. Endmembers of fluid-rock interaction are fluid dominated serpentinization (water rock ratio  $w/r > 1$ ) at hole 1268A (addition of S) and rock dominated serpentinization (~ isochemical addition of H<sub>2</sub>O,  $w/r < 1$ , at sites 1272 & 1274). The other boreholes saw both alteration styles over time.

The last high-T alteration stage preserved in rocks from Leg 209 is talc alteration in hole 1268A. Fluid compositions changed to more oxidizing conditions, giving rise to the formation of hematite and iowaite under static conditions. Talc alteration is maintained by Silica metasomatism with Si released from pyroxene breakdown in gabbros and harzburgites undergoing high-T (> 350 °C), and low pH fluid-rock interaction (Bach et al., 2004). Consequences are lower MgO/SiO<sub>2</sub> ratios and flat REE patterns (Paulick et al., 2006). Silica metasomatism is close in space to gabbroic intrusions, suggesting their intrusion at greenschist facies condition into already serpentinized peridotites (Kelemen et al., 2004). Where brucite and clay minerals are abundant, seafloor weathering exerts a large control on the trace element budget as well (Bach et al., 2004). Moreover, oxidative alteration in the uppermost portion of oceanic crust results in strong enrichment in U.

### 3.3 Analytical Protocols

Sample selection for this chapter was guided by the petrographic descriptions of the Shipboard Scientific Party (Kelemen et al., 2004). The sample set covers a wide variety of alteration styles at the different sites. Concentrations of Lu, Zr, Nb, Hf, Ta, W, U and Th were determined at high precision by isotope dilution for 55 samples (Table 3.1). Because of the similar geochemical behaviour in nature W, Ta, U and Th were analysed together with Lu, Hf, Zr and Nb that allow identification of pristine magmatic trends (see chapter 1 and 2). Zirconium, Nb, Lu, Hf are also regarded as immobile during oceanic crust alteration (Niu, 2004; Staudigel, 2013), whereas, e.g., U is known to behave mobile at oxidized conditions (Hart and Staudigel, 1982). Combining the information from all HFSE therefore allows to better discriminate between pristine magmatic trends and alteration effects. To account for the extreme depletion of the peridotites of Leg 209, 200 mg of powdered sample were typically spiked with mixed HFSE ( $^{176}\text{Lu}$ ,  $^{94}\text{Zr}$ ,  $^{180}\text{Hf}$ ,  $^{180}\text{Ta}$ ,  $^{183}\text{W}$ ) and  $^{233/236}\text{U}$ - $^{229}\text{Th}$  tracers in pre-bombed Savillex<sup>®</sup> vials. The sample-spike mixture was tabletop-digested for 12 h in a 1:1 mixture of conc.  $\text{HNO}_3$  - conc. HF at 120°C. After evaporation to dryness, the samples were re-dissolved in 6 ml of a 2:3 mixture of conc.  $\text{HNO}_3$  – conc. HF and placed inside Parr<sup>®</sup> bombs for 36 h. Subsequently, 1 ml conc.  $\text{HClO}_4$  was added to the solution followed by an additional evaporation step. As gabbroic veins intruding peridotite in some localities contain zircon (Kelemen et al., 2007), these rocks were digested longer (108 h, method further described in chapter 2). The digested samples from both schemes were treated with 3 ml conc.  $\text{HNO}_3$  - trace HF (< 0.05N), evaporated and re-dissolved in 6 ml 6N HCl - trace HF for 12 h to achieve full sample/spike equilibrium. From the equilibrated sample solutions, a 1 ml, 16.6 %) aliquot for W purification was taken and W was separated after Kleine et al., 2004. The remaining sample solution underwent a three-stage ion exchange separation (Münker et al., 2001 and Weyer et al., 2002). The U-Th cut was collected in a 2 M HF rinse step in stage 2 of this protocol and loaded onto TRU-Spec ion exchange columns for separation of U from Th (Luo et al., 1997). All measurements were performed on a THERMO Neptune MC-ICP-MS at the University of Cologne. Blanks were better than 610 pg for Zr, 12 pg for Nb, 210 pg for Lu, 100 pg for Hf, 20 pg for U, 10 pg for Th, 25 pg for W and 20 pg for Ta. The external reproducibility was assessed by repeated measurements of 100, 150 and 200 mg splits BHVO-2 standard. The average 2 s.d. of all measured BHVO-2 splits is below 2 % for concentrations of Zr, Ta, W, Th, U, Lu, Hf and below 1 % for ratios Zr/Hf, Lu/Hf, U/Th, WTh and W/U.

Table 3.1: Downhole HFSE and U-Th variations in holes drilled at Leg 209. Alteration classification and LOI, MgO/SiO<sub>2</sub>, Fe<sup>2+</sup>/Fe<sup>3+</sup> values adapted from Paulick et al. 2006. Nd = not measured

Sample	Hole	Rock, Alt. Type	Depth (mbsf)	LOI (wt.-%)	MgO/SiO <sub>2</sub>	Fe <sup>2+</sup> /Fe <sup>3+</sup>	W/Th	W (ppb)	Zr (ppb)	Nb (ppb)	Ta (ppb)	U (ppb)	Th (ppb)	Lu (ppb)	Hf (ppb)
R-2-1	1268A	Du, talc alt.	14.10	5.93	0.5	1.29	18.5	46.1	111.2	17.5	3.70	26.9	2.49	147	3.284
R-2-2	1268A	Hz, FD serp.	15.67	11.78	0.9	0.94	4.22	13.0	244.8	15.8	< 0.5 ppb	24.4	3.08	8.30	221.5
R-2-3	1268A	Hz, talc alt.	20.49	4.68	0.5	4.89	0.965	9.33	632.1	49.4	5.73	5.85	9.67	8.19	14.99
R-2-4	1268A	Hz, FD serp.	25.06	11.55	0.9	0.56	29.2	49.3	34.89	4.68	1.06	2.96	1.69	3.72	1.005
R-2-5	1268A	Hz, FD serp.	25.24	12.70	0.9	6.49	9.38	35.4	100.3	22.3	1.21	3.69	3.77	11.6	9.604
R-2-6	1268A	Hz, talc alt.	28.04	4.58	0.5	3.78	1.69	6.97	478.8	49.4	2.06	2.56	4.12	15.6	12.97
R-2-7	1268A	Hz, talc alt.	44.28	4.36	0.5	7.47	0.268	2.16	889.3	52.2	< 0.5 ppb	5.69	8.07	14.8	21.16
R-2-8	1268A	Hz, talc alt.	54.18	4.63	0.5	6.52	40.8	15.7	18.74	4.59	< 0.5 ppb	8.78	0.386	1.98	< 0.5 ppb
R-2-9	1268A	Hz, talc alt.	59.38	5.51	0.5	3.55	1.97	10.0	649.4	53.0	3.14	6.26	5.11	2.04	16.49
R-2-10	1268A	Hz, FD serp.	68.66	12.27	0.9	1.84	> 0.203	17.1	259.2	36.7	< 0.5 ppb	< 0.5 ppb	84.1	3.97	5.642
R-2-11	1268A	Du, FD serp.	90.21	12.38	0.9	0.95	24.5	9.93	50.86	1.17	0.796	3.96	0.406	4.95	6.751
R-2-12	1268A	Du, FD serp.	94.15	12.23	1.0	0.35	57.8	503	8878	8.40	0.954	25.4	8.69	5.24	214.0
R-2-13	1268A	Hz, talc alt.	95.59	5.35	0.5	9.58	9.86	39.9	797.5	84.3	4.32	23.5	4.04	14.2	24.84
R-2-14	1268A	Du, FD serp.	97.68	11.92	1.0	0.48	>> 1	67.7	12.81	1.73	0.570	< 0.5 ppb	< 0.5 ppb	< 0.5 ppb	< 0.5 ppb
R-2-15	1268A	Du, FD serp.	99.88	12.42	0.9	0.66	2.69	21.6	47.03	1.62	0.650	0.600	8.00	3.04	0.1962
R-2-16	1268A	Du, FD serp.	103.33	11.84	0.9	0.65	>> 1	10.8	33.77	4.93	< 0.5 ppb	6.06	< 0.5 ppb	4.98	0.3162
R-2-17	1268A	Hz, talc alt.	104.24	5.01	0.5	1.42	>> 1	27.0	6.754	0.42	< 0.5 ppb	1.34	< 0.5 ppb	6.00	1.365
R-2-18	1268A	Hz, FD serp.	122.18	12.35	0.9	1.03	209	81.1	36.94	0.79	0.133	< 0.5 ppb	0.389	3.60	1.096
R-2-19	1270A	Hz, MRI, serp.	1.20	12.91	1.0	0.32	10.8	18.6	18.53	4.24	< 0.5 ppb	647	1.73	1015.6	0.6277
R-2-20	1270A	Hz, MRI, serp.	1.55	12.85	1.0	0.26	10.7	32.9	420.5	8.15	0.742	712	3.07	< 0.5 ppb	12.83
R-2-21	1270A	Hz, MRI, serp.	11.62	12.60	1.0	0.26	11.8	18.1	15.72	1.61	< 0.5 ppb	683	1.53	135	0.7237
R-2-22	1270C	Hz, MRI, serp.	12.90	12.62	0.9	0.32	0.678	57.5	nd	nd	nd	1.10 ppm	84.8	nd	nd
R-2-23	1270C	Hz, MRI, serp.	18.62	11.21	0.9	0.36	0.121	18.5	nd	nd	nd	1.26 ppm	153	nd	nd
R-2-24	1270D	Hz, MRI, serp.	0.69	12.83	0.9	0.33	3.13	322	1237	361	11.3	694	103	50.3	28.78
R-2-25	1270D	Hz, MRI, serp.	20.55	12.31	0.9	0.64	0.0857	39.8	1126	2.46 ppm	203	214	465	124	377.4
R-2-26	1270D	Hz, MRI, serp.	21.01	12.06	0.9	0.41	0.0918	38.5	2081	547	38.3	221	419	52.7	70.47
R-2-27	1270D	Hz, MRI, serp.	47.84	12.77	1.0	0.38	1.11	61.5	< 0.5 ppb	< 0.5 ppb	< 0.5 ppb	614	55.6	< 0.5 ppb	< 0.5 ppb
R-2-28	1270D	Hz, MRI, serp.	56.79	12.58	1.0	0.37	0.208	39.6	3677	617	45.6	1.04 ppm	190	121	155.7
R-2-29	1271A	Du, MRI, serp.	0.77	12.18	0.9	0.34	7.80	205	195.0	51.4	0.336	505	26.2	< 0.5 ppb	3.297
R-2-30	1271A	Du, MRI, serp.	0.96	11.66	0.9	0.26	5.57	119	< 0.5 ppb	< 0.5 ppb	< 0.5 ppb	381	21.4	< 0.5 ppb	< 0.5 ppb
R-2-31	1271A	Du, MRI, serp.	29.55	13.97	1.2	0.46	11.6	19.6	< 0.5 ppb	< 0.5 ppb	< 0.5 ppb	6.96	1.70	< 0.5 ppb	< 0.5 ppb
R-2-32	1271A	Du, MRI, serp.	30.31	13.72	1.2	0.43	3.25	29.1	622.2	32.2	0.830	81.4	8.94	< 0.5 ppb	21.47
R-2-33	1271B	Hz, talc alt.	0.51	7.98	n.a.	3.66	0.0722	13.2	< 0.5 ppb	< 0.5 ppb	< 0.5 ppb	781	183	< 0.5 ppb	< 0.5 ppb
R-2-34	1271B	Du, RD serp.	32.47	13.83	1.1	0.36	5.98	43.8	571.0	2.46	< 0.5 ppb	337	7.32	< 0.5 ppb	13.40
R-2-35	1271B	Du, RD serp.	36.35	11.73	1.0	0.32	80.3	41.5	< 0.5 ppb	< 0.5 ppb	< 0.5 ppb	616	0.517	< 0.5 ppb	< 0.5 ppb
R-2-36	1271B	Du, MRI, serp.	50.80	10.28	1.0	0.47	8.87	56.9	135.9	37.3	14.4	607	6.41	< 0.5 ppb	182.6
R-2-37	1271B	Du, MRI, serp.	56.63	12.82	1.0	0.37	0.926	50.7	4409	257	2.11	712	54.8	< 0.5 ppb	161.7
R-2-38	1271B	Du, MRI, serp.	85.11	14.55	1.2	0.62	12.8	71.1	824.5	33.7	2.27	20.1	5.56	9.10	18.51
R-2-39	1271B	Du, MRI, serp.	85.48	13.71	1.1	0.40	4.10	101	< 0.5 ppb	< 0.5 ppb	< 0.5 ppb	9.86	24.6	< 0.5 ppb	< 0.5 ppb
R-2-40	1272A	Olivine-Gabbro	18.18	0.77	0.1	3.24	0.0641	93.5	138.1 ppm	2.019 ppm	1.179 ppm	594	1459	360	3424
R-2-41	1272A	Diabase	38.06	0.88	0.1	3.73	0.151	187	119.7 ppm	1.708 ppm	1.004 ppm	391	1233	343	2964
R-2-42	1272A	Hz, RD serp.-iow.	62.34	14.12	1.0	0.57	64.1	8.15	19.01	2.49	< 0.5 ppb	10.2	0.127	5.12	9.598
R-2-43	1272A	Hz, RD serp.-iow.	99.17	14.60	1.1	0.55	> 37.6	6.67	< 0.5 ppb	< 0.5 ppb	< 0.5 ppb	< 0.5 ppb	0.178	< 0.5 ppb	< 0.5 ppb
R-2-44	1274A	Hz, least alt.	17.51	12.28	1.1	0.62	6.84	3.38	< 0.5 ppb	3.10	0.287	15.3	0.494	3.75	< 0.5 ppb
R-2-45	1274A	Hz, least alt.	18.01	9.87	1.1	1.06	13.4	6.33	6.447	< 0.5 ppb	< 0.5 ppb	1.53	0.471	4.79	0.2548
R-2-46	1274A	Hz, RD serp.	27.99	13.32	1.1	0.66	47.3	5.75	8.249	2.37	< 0.5 ppb	0.544	0.122	3.83	< 0.5 ppb
R-2-47	1274A	Hz, least alt.	33.06	10.48	1.0	1.05	28.4	4.81	< 0.5 ppb	4.16	0.273	2.45	0.169	9.15	< 0.5 ppb
R-2-48	1274A	Hz, RD serp.	40.72	13.95	1.2	0.45	41.4	9.45	< 0.5 ppb	1.16	12.1	179	0.228	1.44	0.0455
R-2-49	1274A	Hz, RD serp.	55.46	12.69	1.0	0.54	50.6	15.6	17.09	3.12	5.99	4.01	0.308	7.57	2.407
R-2-50	1274A	Hz, RD serp.	60.74	13.60	1.0	0.56	17.3	15.4	92.19	0.83	< 0.5 ppb	2.67	0.889	4.34	2.487
R-2-51	1274A	Hz, RD serp.	69.30	12.30	1.0	0.62	13.3	16.8	37.35	4.48	1.65	33.0	1.26	5.18	1.324
R-2-52	1274A	Hz, RD serp.	75.86	13.19	1.1	0.66	8.75	4.92	< 0.5 ppb	0.26	9.51	0.936	0.562	4.79	0.5507
R-2-53	1274A	Du, RD serp.	85.40	15.36	1.2	0.45	1.65	29.6	623.8	48.3	2.22	2.19	17.9	2.95	3.801
R-2-54	1274A	Hz, RD serp.	94.13	11.91	1.0	0.80	6.36	13.8	4.267	0.82	< 0.5 ppb	1.41	2.18	6.81	0.2541
R-2-55	1274A	Hz, RD serp.	131.96	13.74	1.0	0.72	2.53	20.4	1.901	164	13.2	6.92	8.05	30.6	58.78

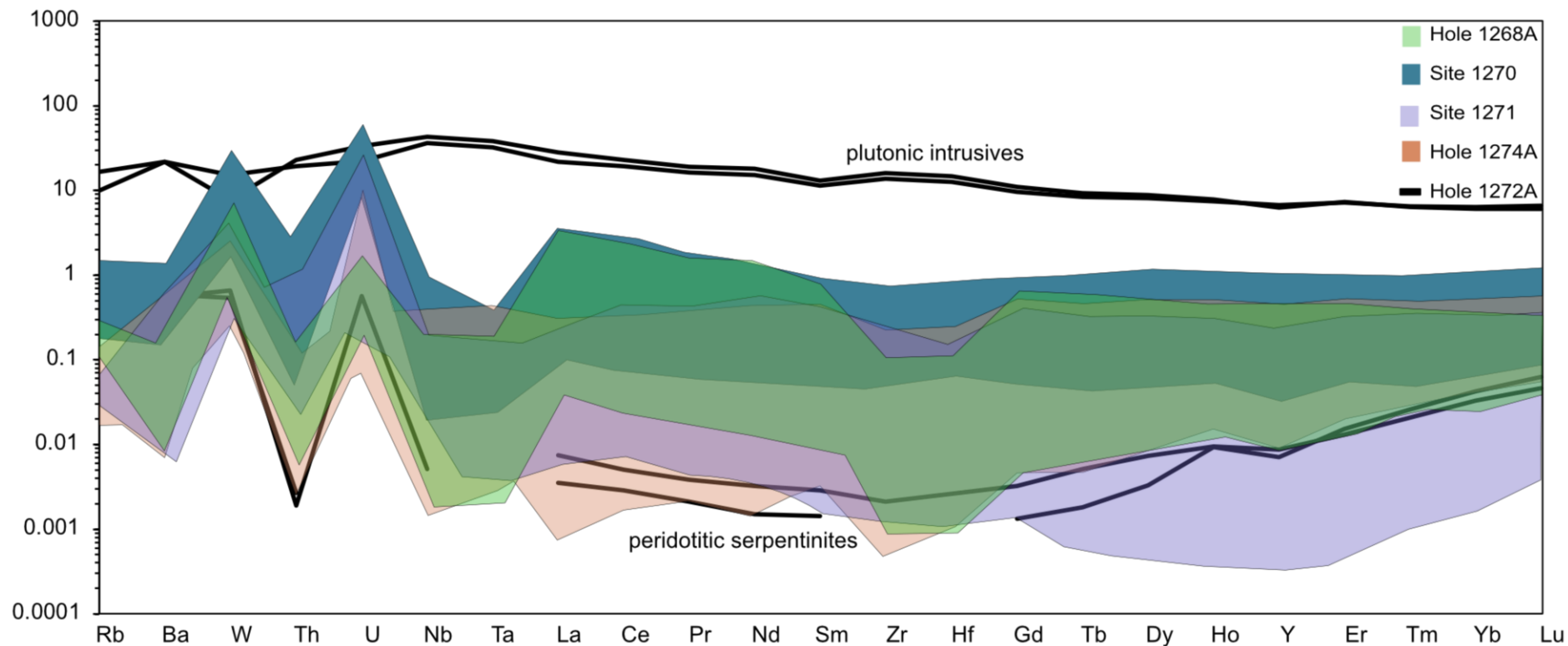


Figure 3.2: Trace element composition of ultramafic samples from the studied bore holes. Where possible, sites are grouped together (site 1270 comprises holes 1270A, C, D; site 1271 holes 1271A, 1271B). Troughs in Nb-Ta and Zr-Hf are characteristic for fluid induced REE enrichment. Data for W, Th, U, Nb, Ta, Zr, and Hf from this thesis, other data from Paulick et al., 2006.



## 3.4 Results

### 3.4.1 HFSE variations in Leg 209 drill holes

The sample suite comprises of 17 variably altered dunites, 36 harzburgites and 2 mafic intrusives. As a result of melt depletion, the concentrations of many measured trace elements are very low (Table 3.1, Fig. 3.2). Compared to the primitive mantle composition (Palme and O'Neill, 2013) Th, Nb, Ta, Zr, and Hf are depleted by a factor of up to 1000, similar to REE, whereas W and U are selectively enriched (Fig. 3.2). Characteristic troughs of Nb, Ta, Zr, and Hf in many samples indicate the later addition of REE by fluid alteration (Fig. 3.2). Based on previously published concentration data (Bach et al., 2004, Paulick et al., 2006) and petrographic descriptions by the shipboard party (Kelemen et al., 2004), the sample suite is divided into (mainly) fluid-dominated serpentized rocks from sites 1268, 1270, 1271, 1272, more pristine, rock-dominated serpentized peridotites from site 1274 as well as mafic intrusives from the top of hole 1272A.

The W concentrations in fluid-dominated serpentized samples from holes 1268A, and 1270 - 1272 vary between 5 – 60 ppb. Local enrichments of several hundred ppb have been identified in strongly veined samples from hole 1268A (R-2-12, 503 ppb), and in samples originating from shallow depths at hole 1270D (R-2-24, 322 ppb) and site 1271 (R-2-29, 205 ppb; R-2-30, 119 ppb). The concentration range of Zr spans from 30 to 800 ppb at these sites. Outliers to lower concentrations of less than 10 ppb have been identified in harzburgite of hole 1270D (R-2-27 < 0.5 ppb), the lower section of hole 1272A (R-2-42, 19.0 ppb, R-2-43 < 0.5 ppb) and in one harzburgite of 1268A (R-2-17 6.75 ppb). Furthermore, extremely low Zr contents of < 0.5 ppb have been identified in serpentinites from holes 1270D, 1271A and 1271B, in close spatial vicinity to more enriched samples with Zr contents between 30 – 800 ppb. Niobium concentrations vary between 20 – 80 ppb in this sample group. In general, the samples with extreme Zr abundances are also the most enriched (up to 2.46 ppm, R-2-25) and depleted (< 0.5 ppb, samples from site 1271) ones in Nb (Table 3.1). In most cases, Ta behaves like Zr and Nb and is also most enriched (up to 200 ppb, R-2-25) and depleted (< 0.5 ppb, site 1271) in the same samples, its typical concentration range is between 0.5 – 10 ppb. Uranium concentrations are highly variable and range from 2.64 – 25.4 ppb at site 1268A to 1.10 – 1.26 ppm at holes 1270C and 1270D. Extremely low U concentrations (< 10 ppb) have been identified in the lowest sections of holes 1271A and 1271B. Thorium concentrations range from < 0.25 ppb to as high as 465 ppb. Like U, Th concentrations at hole 1268A are low (< 10 ppb) and higher at sites 1270 and 1271. In marked contrast to U, Th concentrations at both sites are more variable with hole 1270A being similar in Th to 1268A (1.53 – 3.07 ppb) and 1270D being significantly higher in Th with 190 – 465 ppb. Lutetium and Hf concentrations behave like Zr-Nb, the general concentration range for Lu is 0.5 – 2 ppb. The highest concentrations of Lu were identified in harzburgites from 1270D (124 ppb) and melt-

impregnated harzburgites from 1270A (1.02 ppm). At site 1271, Lu concentration of only one sample was above the limit of detection (R-2-38, 9.1 ppb Lu). Hafnium concentrations at all holes typically range from 3 to 50 ppb, the highest Hf concentrations have been identified in samples from hole 1270D (e.g., R-2-25, 377.4 ppb), extremely low Hf concentrations below the detection limit have been identified at site 1271B as well (Table 3.1).

Hole 1272A was drilled into crust with an upper portion of igneous mafic rocks and a deeper portion of serpentinized harzburgite. The two mafic intrusive rocks exhibit significantly higher HFSE concentration (Tables 3.1 & 3.2, samples R-2-40 & -41) as their ultramafic counterparts. Tungsten concentrations are 93.5 and 187 ppb, respectively. Zirconium and Nb concentrations are in the range of MORB (Zr = 119.7 and 138.4 ppm, Nb = 1.708 and 2.019 ppm). Similar patterns are observed for Ta, Lu, and Hf (Table 3.1).

Rock dominated serpentinized peridotites of hole 1274A are characterized by extremely low HFSE concentrations. Tungsten concentrations in those samples range from 3.38 – 29.6 ppb. The lowest W concentrations < 10 ppb have been identified at the top of the section. Zirconium concentrations span a range from below the limit of detection up to 4.267 ppm in the lowermost section. The scatter is large, even on a limited depth scale. This was also observed for Niobium concentrations, and for Zr. Ta, Lu, and Hf. The Th concentrations range from 0.2 – 1 ppb, with excursions towards higher concentrations in the lowest part of the drill core. Conversely, U concentration data scatter from 0.544 ppb to 33.0 ppb, with no relationship to depth or alteration style. A sample with unusually high U concentration is R-2-48 with 179 ppb.

## 3.5 Discussion

### 3.5.1 Combined W-HFSE and U-Th systematics

As the drilled peridotites are among the most depleted ever encountered (Kelemen et al., 2004, Bach et al., 2004, Godard et al., 2006, Paulick et al., 2006), an evaluation based on element concentrations alone would be misleading. This is because alteration-mobile elements such as W or U would potentially be re-enriched to typical primitive mantle abundances whereas immobile elements such as Th and Ta are in most cases highly depleted relative to primitive mantle (PM). Zirconium is one of the HFSE considered to behave immobile during most fluid-related processes, and because of its incompatibility it is used as reference to trace the alteration influence on other elements (Niu, 2004). In Figure 3.3, elements of interest are plotted versus Zr. Tantalum and Th correlate with Zr abundances (C & D), indicating that they preserved their initial melt depletion characteristics during alteration. Conversely, abundances of W and to some extent of U (Fig 3.3 A and B) are extensively modified. These results are in accord with earlier studies showing the immobility of Th and Ta during alteration of abyssal peridotites (Niu, 2004; Polat et al., 2012). The further combination of high-precision concentration data with alteration proxies already proposed for rocks from Leg 209, e.g., LOI or  $MgO/SiO_2$  (Kelemen et al., 2004, Bach et al., 2004, Paulick et al., 2006) allows the further investigation of the impact of different alteration processes on the distribution of W and U. This is further discussed in section 3.6.2. At all studied sites, ratios of W/Th increase with decreasing Th concentrations (Fig. 3.4A). As Th preserved its initial melt depletion signature, it is highly unlikely that Th mobilization is controlling the distribution of W/Th. Rather, W gain is the controlling factor for W/Th, where there is a relatively small scatter in W contents, (one to two orders of magnitude) compared to Th (3-4 orders of magnitude, Fig. 3.4 A, B). Therefore, the addition of a broadly similar amount of W to rocks with various degrees of Th depletion caused by initial melt depletion is a plausible model.

In marked contrast to Th, U is extensively modified by oceanic crust alteration (e.g. Bach et al., 2004; Hart and Staudigel, 1982). Although U behaves mobile, the general melt depletion trend outlined above for W/Th (and W/Ta) is still preserved in W/U systematics (Fig. 3.4 D). Notably, samples from sites 1270 and 1271 display lower or similar W/U than primitive mantle at similar W concentrations but much more elevated U concentrations than in other holes (Fig. 3.4 D). This is because in these samples both U and W were initially gained during melt impregnation, and this has no effect on their relative abundance. Consequently, although U concentrations in the melt-impregnated samples were a priori the highest, secondary processes, such as low-T oxidative seafloor alteration led to further modification of U concentrations and a fractionation of U from W. The detailed mechanisms and characteristic features of each alteration style and drill site is further discussed below.

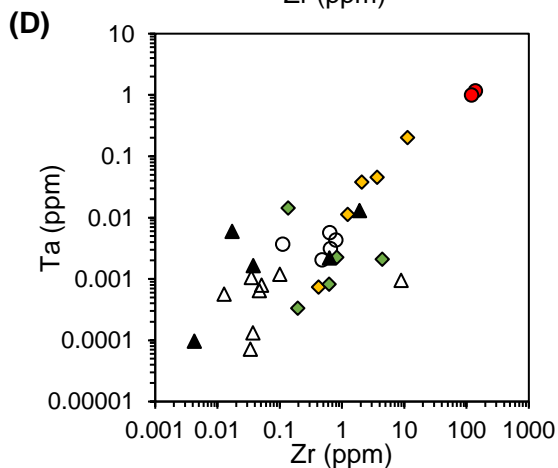
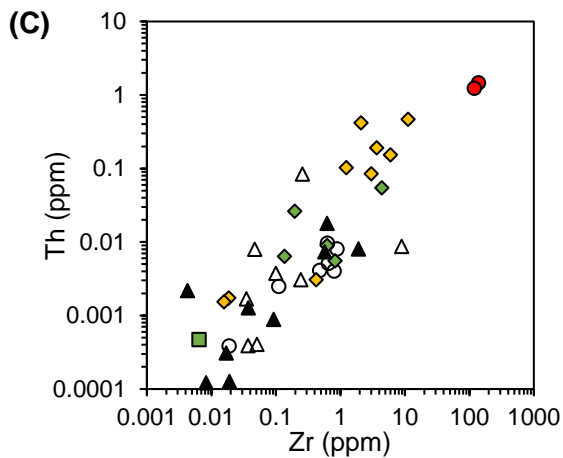
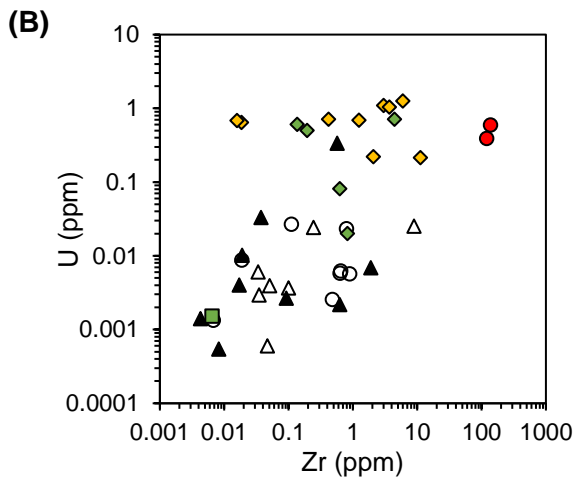
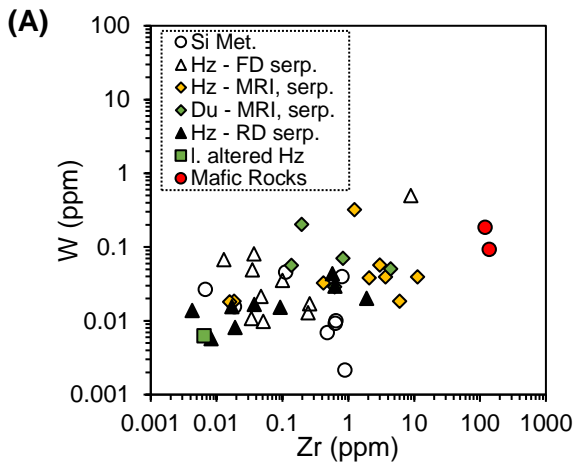


Figure 3.3:

Trace element co-variation diagrams for different HFSE and U-Th, illustrating the control of melt-depletion and hydrothermal overprint in peridotites of Leg 209. The lack of correlation between W-U and Zr contents illustrates that both W and U are enriched by secondary processes (A & B). If plotted versus Zr contents, Th and Ta display typical melt-depletion trends (C & D) characterized by melt-rock interactions samples (yellow diamonds) show similarly elevated U concentrations. Si Met. = Silica metasomatism ~ talc alteration; FD – Serp. = Fluid dominated serpentinization ( $w/r > 1$ ); RD – Serp. = Rock dominated serpentinization ( $w/r < 1$ ); MRI – Hz = harzburgite with signs of melt-rock interaction; MRI – Du = dunite with signs of melt-rock interaction; l. altered Hz = least altered harzburgite

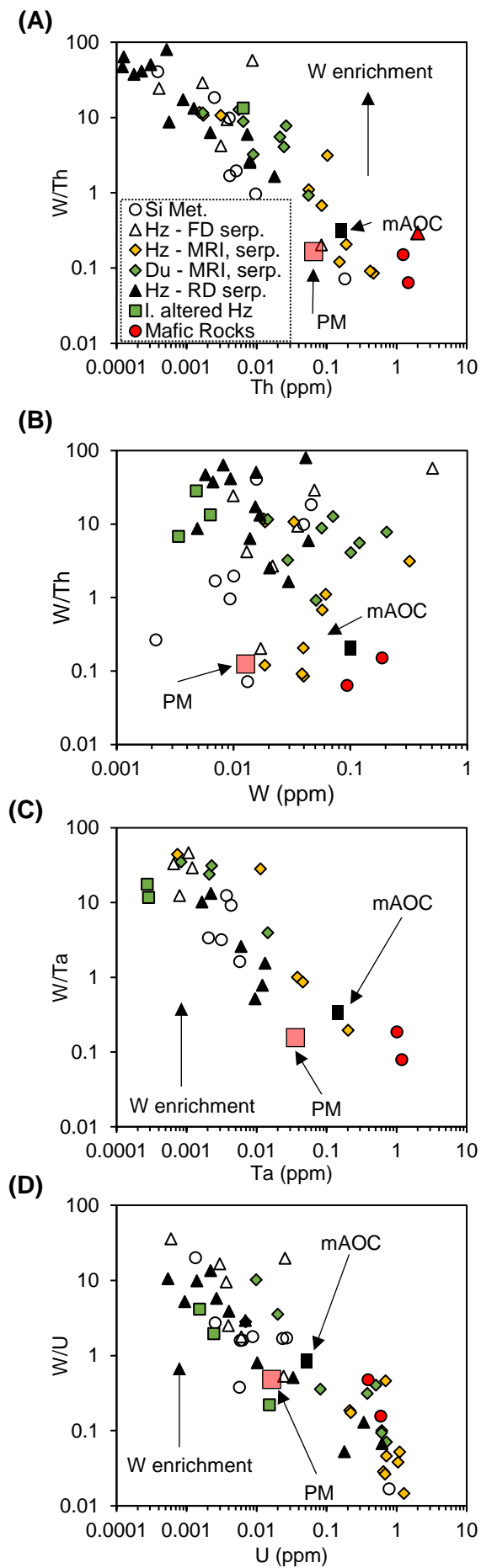


Figure 3.4:

Plots illustrating selective enrichment of W over Th, Ta, and U, discriminated by the main alteration processes. A similar amount of W is added to extremely Th depleted peridotite (A). Melt impregnated (MRI) samples have highest HFSE - concentrations. Rock - dominated serpentinized samples have not gained Th and are only affected by selective W enrichment (A). Simple correlations between W gain and W/Th are absent as the different alteration styles do not mobilize W to a similar extent (B). W/U preserves its initial W addition profile as W/Th does. Low-T seawater alteration is reflected in high U concentrations (D). Locally, this leads to sub-canonical W/U. mAOC = moderately altered oceanic crust from hole 1256D, PM = primitive mantle

### 3.5.2 Tungsten behaviour during different alteration styles and melt impregnation

#### 3.5.2.1 Progressive serpentinization at sites 1268, 1270 and 1271

Samples from 1268, 1270 and 1271 are characterized by pervasive serpentinization, melt rock-interaction and talc alteration, reflected in strong positive and negative Eu anomalies, and gain in LREE and HREE (Kelemen et al., 2004, Bach et al., 2004, Paulick et al., 2006). Additionally, the studied crust is strongly enriched in W, as reflected in supra-canonical ( $> 0.09$ , König et al., 2010) W/Th of as high as 12.8. Tungsten contents are highly variable and not correlated with U/Th (Fig. 3.5, 3.6). Thus, the progressive enrichments of W and U must be at least partially controlled by distinct processes. Tungsten concentrations are furthermore independent from alteration indicators such as MgO/SiO<sub>2</sub> and LOI, which can be expected as multiple alteration processes (e.g. serpentinization, melt-rock interaction, low-T seafloor weathering) were active at these sites and may offset each other (Bach et al., 2004; Kelemen et al., 2007, 2004; Vils et al., 2009). The lack of correlation may furthermore be caused by initial inhomogeneities in the orthopyroxene distribution, exerting control on the original Mg budget and the abundance of secondary talc veins which, in turn, have huge impact on W/Th (see below, Kelemen et al., 2004). The influence of relict pyroxene on trace element distribution is also demonstrated for other systems such as Li and B (Vils et al., 2009). Additionally, hydrothermal alteration is highly focused in veins, which implies a potential sample bias. In addition to serpentinization, hole 1268A is characterized by late pervasive talc formation (Bach et al., 2004, Kelemen et al., 2004), discussed in chapter 3.5.2.2.

Available sources for excess W at the above-named sites are hydrothermal fluids from deeper mantle portions, serpentinization or progressive enrichment by low-T seafloor alteration processes, such as brucite dissolution or shallow oxidative weathering. The observations that most samples have positive Eu anomalies argues for an important role of hydrothermal solutions, or alternatively for formation of plagioclase during melt impregnation. The latter process, would have also enriched immobile elements such as Th and is thus unlikely to cause selective W enrichment over Th. In contrast, examples for elevated W contents in hydrothermal fluids have already been identified by Kishida et al., (2004), at the Kairei Field, a mid ocean ridge hydrothermal field at the Indian Ridge. Thus, the flux of hydrothermal fluids likely explains the Eu, REE and W signatures. Apart from on-ridge venting, localized hydrothermal fluid flow may be triggered by the abundant intrusion of mafic dikelets which have been identified as source for particularly high REE concentrations at sites 1270 and 1271 (Paulick et al., 2006). Since melt impregnation itself does not fractionate U, Th, and W the dikelets are no hosts for elevated W/Th themselves. Nevertheless, the dikelets intruded in already partially serpentinized oceanic crust (Kelemen et al., 2004), and this may have led to local fluid generation with associated hydrothermal alteration. As W is significantly more mobile than Th (König et al., 2008), such fluid phases will most likely be enriched in W. It is therefore concluded

that the migration of these fluids resulted in progressive W gain in the alteration mineral assemblage.

Samples from shallow depths (< 1 mbsf, sample R-2-24, R-2-29, R-2-39) contain significantly elevated concentrations of W (119 – 322 ppb, W/Th 3.13 – 7.81) and U (214 – 694 ppb, U/Th 4.28 – 444). The sampled sections are characterized by mylonitization postdating melt intrusion and the formation of alternating layers of harzburgite and dunite with interfering serpentine-magnetite veins. Furthermore, late orange-coloured clay, composed of Fe-Mn-Mg-oxide weathering products, replaces serpentine. It is well known that Fe-oxyhydroxide clays act as a major sink for seawater U which causes extreme U enrichment over Th (Bach et al., 2003, 2001). The strong enrichment in U results in W/U below the primitive mantle value, even though both elements are significantly enriched over Th (Fig. 3.6 B, C). Samples R-2-24, R-2-29, R-2-39 share comparatively low ferrous-ferric iron ratios between 0.34 and 0.26, as a result of elevated Fe<sub>2</sub>O<sub>3</sub> contents (Paulick et al., 2006). The finding of both strongly elevated U and elevated Fe<sub>2</sub>O<sub>3</sub> contents is in agreement with other studies and related to oxidative weathering (Bach et al., 2003, 2001; Hart et al., 1999). The increasing U concentration is reflected in elevated U/Th with increasing U concentration (Fig. 3.5 A & B). The presented results show how during oxidative alteration in the uppermost oceanic crust, W is enriched along with U. These results highlight a potential seawater source of the excess W in the uppermost section of altered oceanic crust. The somewhat lower W enrichment relative to U might be explained by the significantly lower W abundances in seawater (0.011 ng\*g<sup>-1</sup>, Sohrin, 1987) compared to U (3.2 – 3.3 ng\*g<sup>-1</sup>, Delanghe et al., 2002; Chen et al., 1986, Ku et al., 1977). An efficient adsorption of W at the rock-water interface might therefore exhaust the fluid in W at comparatively shallow depths. A prominent example is sample R-2-23. This altered harzburgite from hole 1270C is characterized by substantial U gain (U/Th = 8.3), abundant carbonate veins but primitive mantle-like W and Th contents (Fig. 3.6). Prominent carbonate veins reported for both holes (Kelemen et al., 2004, Bach et al., 2004) thus most likely act as mineral host for U but potentially not for W. Some further evidence that the mineral composition of the uppermost crustal section exerts a large control on the W budget is sample R-2-33 from hole 1271B. This sample is strongly talc altered and characterized by extremely low W and W/Th whereas the U content is at a similar level as in other hole from sites 1270 and 1271.

By canonical W/U and W/Th and the absence of Eu-anomalies (Paulick et al., 2006), a zone of particularly weak alteration intensity has been identified in hole 1270D at a depth of 20 mbsf (R2-2-25 and R2-2-26). Nevertheless, contents of W, Th, and U are all elevated relative to PM, although W/Th and U/Th are near-canonical. It is therefore concluded that the elevated HFSE concentrations in these samples are the result of extensive melt impregnation that has not significantly fractionated W, Th, and U. Moreover, the samples are particularly high in Fe<sup>2+</sup>/Fe<sup>3+</sup> indicating the absence of prominent low-grade oxidative weathering. Both

harzburgites in fact yield slightly sub-canonical W/Th ( $< 0.09$ ) which may be caused by a slightly higher melt-incompatibility of Th. An alternative explanation for low W/Th in this section is leaching of W, which may be possible during initial talc formation at vein margins and as vein filling. Minor talc formation is described for the whole depth sequence (Kelemen et al., 2004). Nevertheless, it is possible by using W/Th systematics to discriminate between the effect of melt-rock interaction with little to now fluid interaction and melt-rock interaction with extensive fluid production during serpentinization.

In summary, it can be shown that progressive serpentinization might act as a sink for W. Strong W enrichment in serpentinites from other localities have been identified elsewhere, e.g., in earlier studies by Peters et al., (2017) on serpentinized peridotites. The recovered sample suite in Peters et al., 2017 mainly covers shallow samples, with evidence for W mobility during low-T serpentinization. As it shares strong U enrichment, the low-T oxidative weathering as outlined above might explain the strong W enrichment in these samples, as well. Strong W enrichment in serpentine has also been identified in fore-arc serpentinites from some 620 samples that were drilled or dredged during various Deep Sea Drilling Program (DSDP), International Ocean Drilling Program (IODP) and Ocean Drilling Program (ODP) campaigns (Peters et al., 2017).



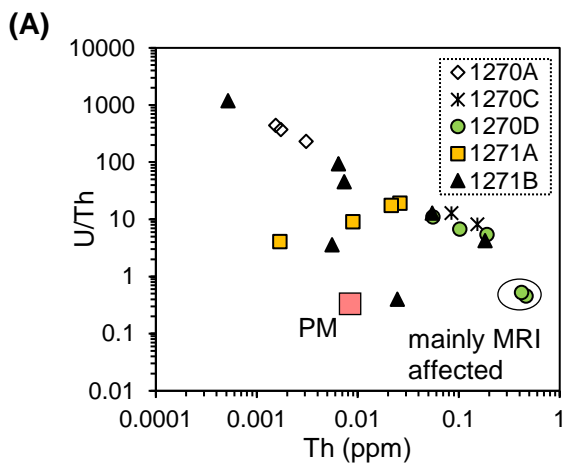
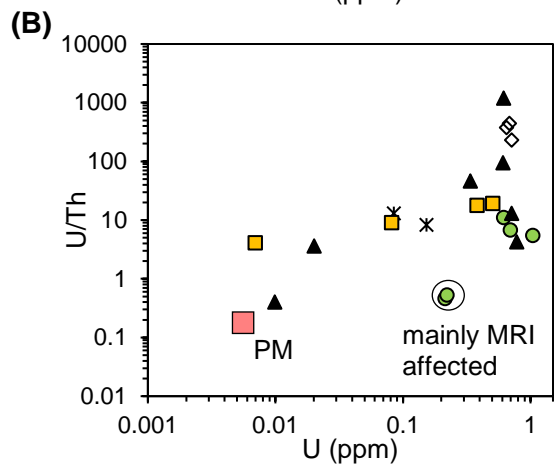


Figure 3.5:

Plots illustrating the extreme U enrichment over Th and locally W in samples from sites 1270 and 1271. Whereas Th is insensitive to mobilization during alteration, U is added during serpentinization and low-T seafloor weathering. Mainly melt-rock interaction (MRI)-affected samples are characterized by near-canonical U/Th and elevated Th and U.



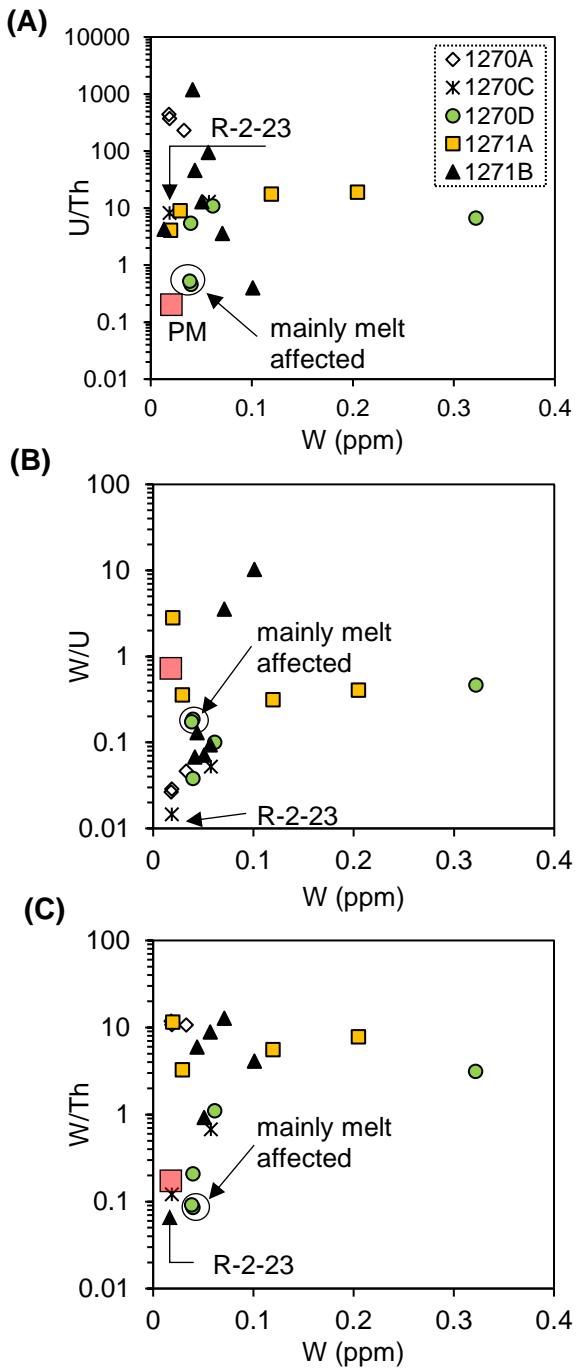


Figure 3.6:

Control of W contents on the variation of U/Th, W/U, and W/Th. Ratios of U/Th and W contents are controlled by different processes (A), and selective U enrichment is indicated by sub-canonical W/U (B). Relative to Th, W is still selectively enriched in most samples (C). Sample R-2-23 is a sample with strong U gain, when the altering most likely was already exhausted in W. Mainly melt affected samples symbolize the absence of strong late alteration or serpentinization.

### 3.5.2.2 Talc alteration at hole 1268A

The formation of talc in hole 1268A is mainly attributed to Si metasomatism of older serpentine at high temperatures ( $> 250 - 300$  °C, e.g. Bach et al., 2004; Kelemen et al., 2004, Paulick et al., 2006). In Si-metasomatized rocks, W/Th, W/Ta, and W concentrations correlate positively with LOI and MgO/SiO<sub>2</sub> ratios (Figure 3.7). As Ta or Th concentrations are not affected, it is highly likely that the decreasing of W/Th, W/Ta and W contents with LOI and MgO/SiO<sub>2</sub> mirrors W loss during progressive talc formation (Fig. 3.7). Uncorrelated W/U does not contradict this hypothesis as U may be similarly leached during talc formation along with W. In line with this view, U/Th are significantly lower in talc altered samples (Table 3.1). As outlined in previous studies (e.g., Paulick et al., 2006) talc altered samples of 1268A and 1271B are characterized by mainly negative Eu anomalies with only few exceptions. The negative Eu anomalies testify to intense hydrothermal activity, likely caused by evolved fluids of magmatic origin (Paulick et al., 2006). Importantly, the initial W/Th of talc altered and serpentized samples are relatively similar (Fig. 3.9). Based on the strong selective W enrichment over Th in serpentized peridotites and the decreasing W/Th with ongoing talc alteration W was enriched at very early stages of alteration, i.e. during serpentization and melt-rock interaction. Later, low-pH and high-T fluids leached W from the alteration mineral assemblage during talc alteration.

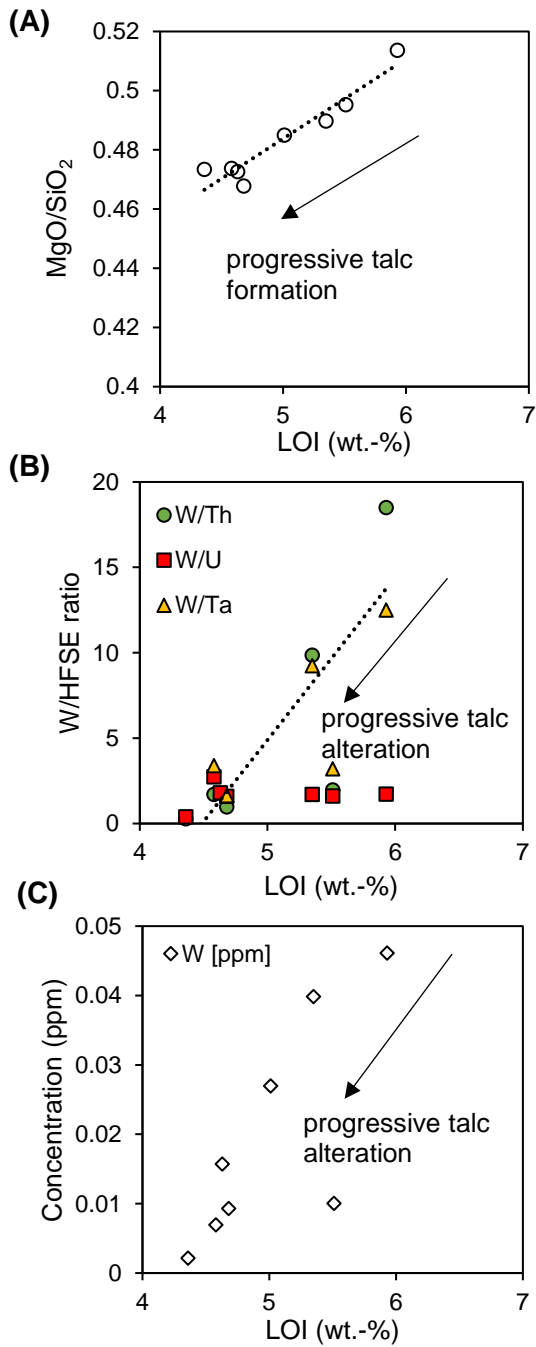


Figure 3.7:  
 Plots of  $MgO/SiO_2$ , W/Th, W/U, W/Ta and W content versus LOI for hole 1268A illustrating W loss during progressive talc alteration. (A). The observation that W/U shows no depletion trend demonstrates that U is modified by more processes than Ta, Th, and W (C).

### 3.5.2.3 Rock dominated serpentinization at holes 1272A and 1274A

Most samples from holes 1272A and 1274A were subject to rock-dominated (RD) serpentinization, i.e., near isochemical addition of H<sub>2</sub>O to the peridotites with water/rock ratios mainly < 1 (Jöns et al., 2010; Paulick et al., 2006). Elevated W/Th of 64 and 48 and U/Th ~ 80 in the samples highlight how W and U are selectively enriched over Th (Table 3.1, Figs. 3.9), although the absolute material exchange is limited in both holes. The samples are highly depleted in LREE with concentrations below 1% of the chondritic values whereas HREE concentrations are gradually increasing (Fig. 2.2, Paulick et al., 2006, Godard et al., 2006). Furthermore, positive and negative Eu anomalies ( $0.7 < \text{Eu}/\text{Eu}^* < 1.7$ ) could be identified, although they are not as pronounced as in other fluid-dominated serpentinized holes (e.g. 1268A,  $0.1 < \text{Eu}/\text{Eu}^* < 110$ , Paulick et al., 2006).

The presence of nontronite, iowaite and aragonite in serpentine muds from hole 1272A and 1274A indicates water-rock reactions continuing at low temperatures and under oxidizing conditions (Kelemen et al., 2004, 2007, Harvey et al., 2006, Bach et al., 2004, Prytulak et al., 2013). At hole 1274A, the maximum depth of penetration of oxidative fluids is still represented in a stepwise decline in W/Th and U/Th at 70 - 75 mbsf. Above this step, W/Th is well above 20 and decreases below at 3, U/Th decreases from > 10 to below 1. The identification of this step is in remarkable concordance with Re-Os data, suggesting a water penetration depth of ca. 60 m (Harvey et al., 2006). Thus, above > 60 – 70 mbsf, oxidative alteration dominates the alteration budget, below initial W enrichment during on-axis processes. As W is weakly correlated with LOI and LOI weakly reflects the extent of alteration in the sampled portions (Harvey et al., 2006) the W budget of 1274A possibly still mirrors progressive serpentinization even though strong oxidative weathering altered the rocks (Fig. 3.8). In contrast, no co-variation of LOI with increasing W/Th, nor W/U or W/Ta could be identified. The fact that W/Th and W/U are not correlated with W may be due to (a) analytical limitations regarding the extremely low Th concentrations (Table 3.1), (b) inhomogeneities in the trace element budget of the protoliths (i.e. caused by melt depletion or late melt-rock reaction with the associated precipitation of clinopyroxene (Godard et al., 2008)) or (c) multistage fluid activity. The coupling of elevated W/Th and U/Th with oxidative weathering highlights its importance for the W-U budget. In summary, even limited alteration has the potential to significantly enrich W in serpentinized rocks.

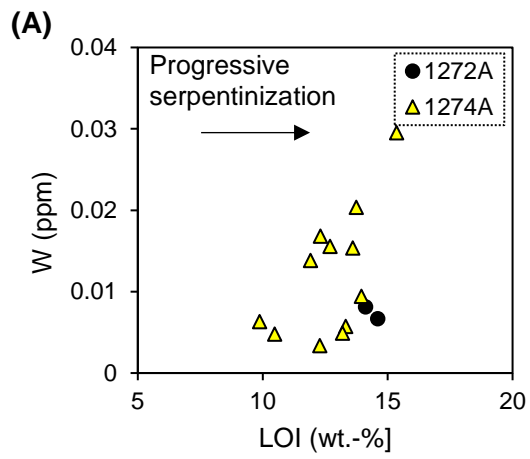
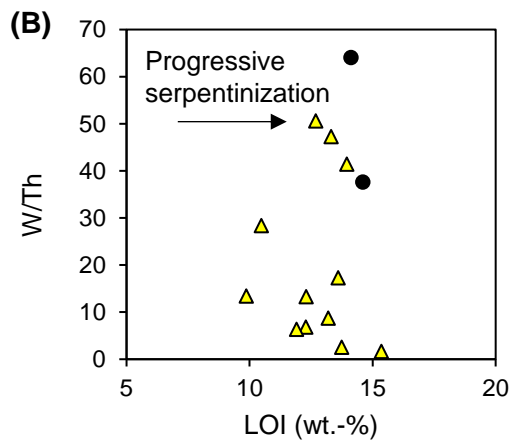


Figure 3.8:  
Plot illustrating the variation of W contents and W/Th with progressive serpentinization, as represented by LOI for holes 1272A and 1274A. Increasing W contents with increasing LOI are potentially linked to progressive serpentinization (A). In contrast, W/Th is not related to progressive serpentinization (B)



#### 3.5.2.4 Plutonic rocks of Hole 1272A

Samples R-2-40 and R-2-41 from hole 1272A are mafic rocks from a rotated tectonic block or a talus atop of the drilled section (Kelemen et al., 2004). The samples are clearly recognizable by their flat MORB-like trace element patterns and their significantly lower LOI (< 1 %) compared to the peridotitic samples (Table 3.1, Figure 3.2). In contrast to the studied peridotites, mafic intrusives show no positive W and U anomaly (Fig. 2.2). Based on their grain size, texture, and composition, all of the intrusives have been interpreted as having liquid compositions; none have a significant cumulate component (Kelemen et al., 2004), which is in contrast to e.g. 1256D intrusives (France et al., 2009). Their alteration mineral assemblage is dominated by pore-filling minerals like plagioclase, quartz, and amphibole (Kelemen et al., 2004). The concentration of HFSE is elevated (e.g. 93.5 – 187 ppb W, 1233- 1459 ppb Th, 391 – 594 ppb U, Table 3.1). Since W/Th (0.0641 – 0.151), W/U (0.16 – 0.48), and W/Ta (0.08 – 0.19) in the two dike samples display typical mantle-like values (Arevalo and McDonough, 2008; König et al., 2011), selective W enrichment by hydrous ocean-floor alteration is insignificant. This is in line with the reported absence of Eu anomalies (Paulick et al., 2006). Thus, these mafic rocks still have their initial, unmodified HFSE budget, also with respect to W and U. This observation demonstrates that basaltic alteration assemblages are less prone to W and U gain than ultramafic alteration assemblages. Their (sub-) canonical W/Th and W/Ta may indicate that mafic intrusives are the source region for selective W enrichment in altered oceanic crust. Significant sub-canonical W/Th are no necessary features of W sources in mafic dikelets as the extraction of is clearly not quantitative.

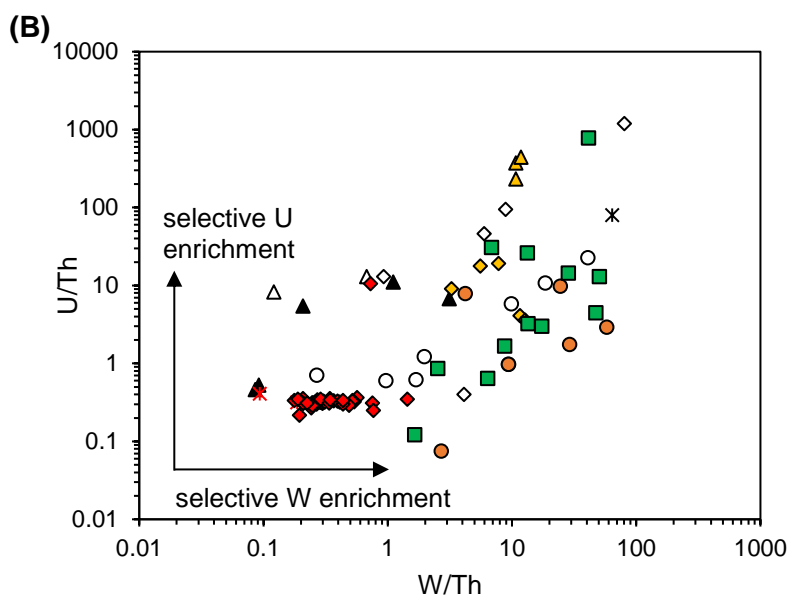
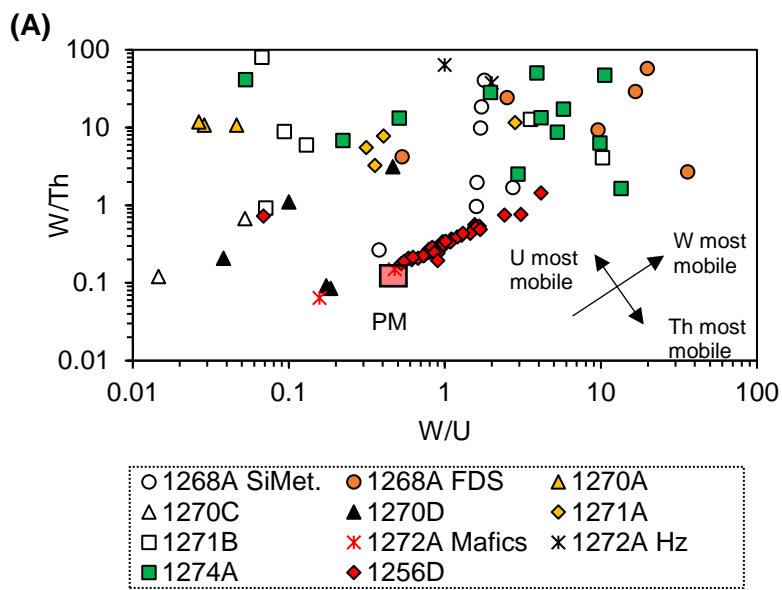


Figure 3.9:

Covariation diagrams for W/Th vs. W/U and U/Th vs. W/Th demonstrating how W in most studied samples of Leg 209 is selectively enriched by different processes. (A). In contrast, W in sample samples from hole 1256D (upper oceanic crust) is likely enriched by one specific process, thus maintaining co-variations between W/Th and W/U (Chapter 2). Uranium is the most mobile element at Leg 209 (A), although enriching processes are most likely independent.



### 3.5.3 Comparison with altered upper oceanic crust at hole 1256D

In chapter 2, W mobility in moderately altered upper oceanic crust drilled during various ODP/IODP campaigns at hole 1256D was outlined. In contrast to the crust presented here, hole 1256D was drilled into super-fast spreading ( $> 200$  mm/a) typical N-MORB crust (e.g. Wilson et al., 2006, Neo et al., 2009). Major lithologies are effusive and intrusive basalts and gabbros. Samples from hole 1256D also display selective W enrichment over similarly incompatible HFSE over the whole depth range drilled (750 m, Wilson et al., 2006, chapter 2). The strongest W enrichments were identified in portions where downward percolating seawater and upward migrating hydrothermal fluids mix, and in zones of intense high-temperature hydrothermal overprint in the sheeted dike section (Chapter 2). In comparison to Leg 209 samples, W concentration at hole 1256D is not as variable between different rock types and alteration styles.

Although absolute W concentrations are higher in the basaltic rocks of hole 1256D, selective W enrichment in all studied peridotites over other HFSE is much stronger at samples from Leg 209 (e.g.,  $W/Th_{1256D}$  0.321 – 1.52,  $W/Th_{Leg\ 209}$  = 0.1 - 200). Moreover, the extreme W concentrations in Leg 209 samples have particularly been identified in samples drilled from shallow depths  $< 1$  mbsf, which have not been recovered from hole 1256D (Wilson et al., 2006, chapter 2). The stronger degree of seawater alteration in Leg 209 peridotites as well as the excessive melt rock interactions led to a much larger scatter in elemental ratios of W-U-Th if compared to 1256D samples (Fig. 3.9 A). At site 1256, W was most likely enriched by one specific process (Fig. 3.9 A), leading to strongly coupled W/U and W/Th ratios. Conversely, W/U and W/Th in Leg 209 samples often show no significant correlation (Fig. 3.9 A), indicating the multi-stage processes outlined above and significant mobility of U. It is striking that strong selective W enrichment was identified at both sites under rock dominated conditions. Moreover, W and U mobilization during serpentinization and low-T oxidative seawater weathering in Leg 209 sections potentially obscure patterns of earlier selective W enrichment. This finding is in stark contrast to Hole 1256D samples, where W is the most mobile element. Only in one sample from the transition zone, U is enriched over W in the hole 1256D samples studied (Chapter 2, Fig. 2.3).

As described above, the geochemical characteristics like REE pattern of hole 1272A mafic intrusives are similar to fresh MORB composition and to gabbros from hole 1256D. The selective enrichment of W over U and Th is much stronger in mafic intrusives from site 1256 ( $W/Th_{Leg\ 209}$  = 0.06 – 0.15,  $W/Th_{1256D}$  0.19 – 0.44). Since U/Th is in a similar range at both sites ( $U/Th_{Leg\ 209}$  = 0.32 – 0.41,  $U/Th_{1256D}$  = 0.22 – 0.35) W is less mobile in plutonic environments of Leg 209. By decreasing W/Th, W/U and W/Ta with progressive depth, a hypothetical source of W at hole 1256D might be located immediately below the drilled gabbroic dikes that mark

the deepest section in the drill core (Chapter 2). This agrees with the observations of (sub)canonical W/Th in mafic intrusives of hole 1272A and single samples of hole 1270D.

Conclusively, although Leg 209 and hole 1256D sampled very distinct portions of upper and lower oceanic crust, respectively, selective W enrichment over similar incompatible HFSE is a ubiquitous feature of oceanic crust alteration. The main difference between the two groups of lithologies is that the ultramafic rocks of leg 209 appear to have undergone a much stronger and more complex modification of their W and U budgets.

### 3.5.4 Implications for the understanding of W enrichment in Arc Magmas

Subduction zones are important sites where crustal material is recycled into the Earth's mantle and play a key role for understanding the origin of volcanism, earthquakes, and global geochemical fluxes. Examples may be the light elements Li, Be and B which may be used as tracers for mass transfer in subduction zones (Marschall et al., 2007). They are readily mobilized by fluids and melts and display strong isotope fractionation (Li and B) in nature. All are enriched in sediments, altered oceanic crust and continental crust (Marschall et al., 2007). As consequence, island arc magmas are enriched in the named elements, as well (e.g. Ryan and Langmuir, 1993, 1987). Enrichment in arc lavas over fresh MORB has been identified for W as well. It could be demonstrated that W is considerably more mobile in arc magmatic settings as the similar melt-incompatible Th (König et al., 2008, 2011, Bali et al., 2012). It was also demonstrated before, that the subduction of basaltic crust formed at super-fast spreading rates carries W excess into the subduction factory (Chapter 2). The above presented results further underline that W fixation during oceanic crust alteration is a ubiquitous process, also within peridotitic oceanic crust. Thus, subduction of both kind of altered oceanic crust adds substantial amounts of W to the subduction factory. Subduction of altered oceanic crust and its sedimentary cover is accompanied by continuously progressive dehydration. Fluids arising from subducting crust cause partial melting in the mantle wedge and thus significantly contribute mobile elements to the developing arc magmas (e.g. Morris et al., 1990; Plank and Langmuir, 1993; Noll et al., 1996). Furthermore, late magmatic fluids, developed in relation to the emplacement of granitoid bodies e.g. at arc settings are known hosts for excessive W ore mineralization (Lassner and Schubert, 1999; Thompson et al., 1999; Yongbao et al., 2014). The generation of these magmas is largely dependent on the availability of fluids from the subducted slab. No mass balance calculation of the origin of W in magmatic bodies are available but future studies should include the input of W by subducted oceanic crust into the considerations. The implications of the presented chapter for recent arc systems is limited since most of today's subducted oceanic crust is of the fast-spreading ridge type, with magmatic crust dominating the chemical and isotopic budget (Vils et al., 2009). In contrast, the Jurassic/Cretaceous Tethys ocean floor was largely produced by slow-spreading ridges. Therefore, most exhumed and metamorphosed oceanic plates exposed on-land are relicts of slow-spreading ridges, and their chemical and isotopic signature should be largely similar to ODP Leg 209 (Vils et al., 2009). Thus, selective enrichment of W over Th, U and Ta identified at ODP Leg 209 should be present in Jurassic/Cretaceous oceanic plate that was subducted in Eocene times. Subduction of Tethys seafloor also contributed largely to magma generation and the formation of tungsten-tin deposits the Baiganhu District in Northern China (Yongbao et al., 2014).

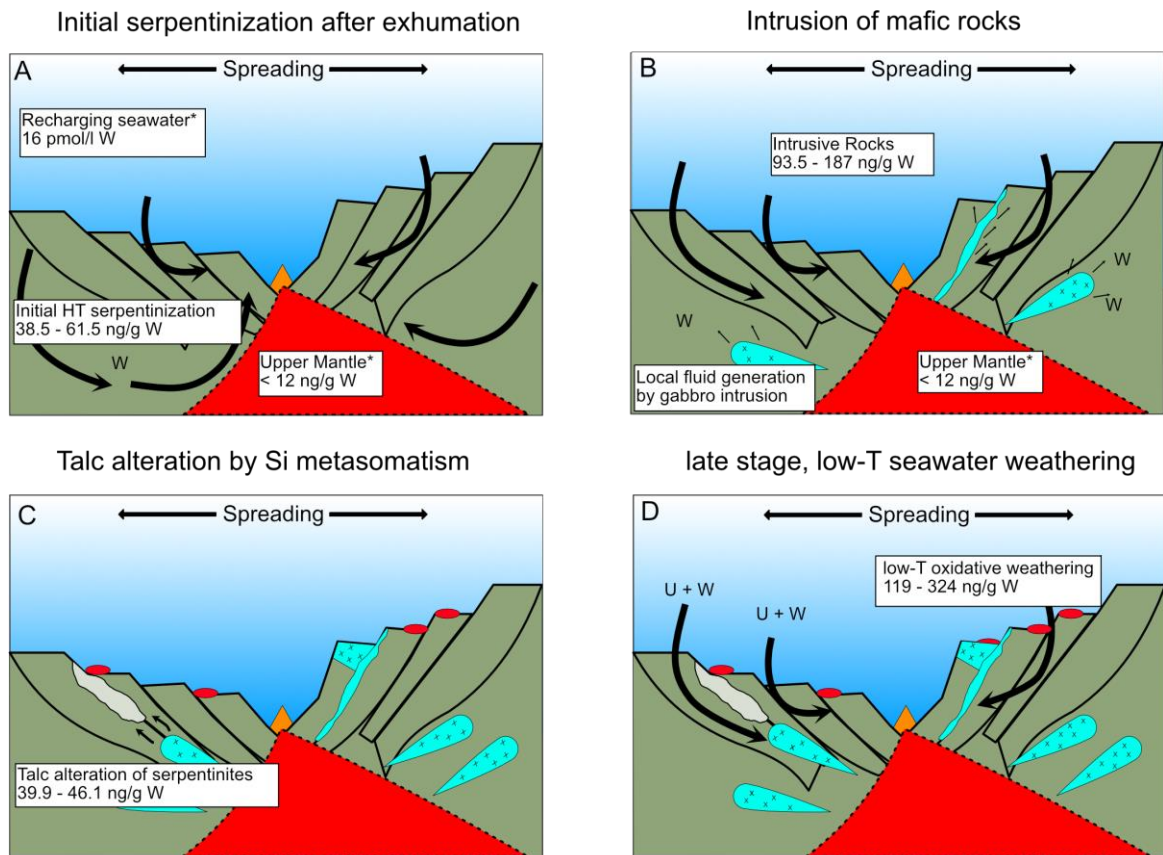


Figure 3.10:

Sketch illustrating the proposed succession of W enrichment events during alteration of peridotitic oceanic crust at Leg 209. In an initial serpentinization stage during exhumation, W is enriched by evolved HT fluids carrying W from ambient mantle rocks into altered portions of oceanic crust (A). Frequent intrusions of mafic melts lead to local dehydration and re-fertilization of the crust with additional W (B). The breakdown of pyroxenes in gabbros during hydrous alteration gave rise to the formation of low pH, HT fluids which locally (e.g., hole 1268A) lead to complete replacement of serpentine by talc. This process is reflected in decreasing W enrichment (C). Late, low-T oxidative surficial alteration of serpentinized peridotites is characterized by progressive enrichment of both U and W (D).

### 3.6 Conclusions

In this chapter the inventory of W, other HFSE and U-Th in extremely depleted and altered abyssal peridotites at ODP Leg 209, formed at the Mid-Atlantic Ridge was investigated. Relative to the similarly melt-incompatible elements U, Th, and Ta, W is enriched by factors of up to 200. The high variability of ratios like W/Th, W/Ta, W/U and of Eu anomalies indicates multiple alteration processes, often coupled with focused fluid flow.

A model for W enrichment at Leg 209 samples is presented in Figure 3.10. Initial W enrichment in Leg 209 samples during progressive serpentinization of altered oceanic crust is recorded in hole 1268A as well as in holes 1270 and 1271 (Fig. 3.10A). Since positive Eu anomalies and high W/Th occur in the same samples, the sources of the excess W are most likely deeper mantle portions tapped by hydrothermal fluids, similar to what has been identified in earlier studies (Chapter 2). The higher fluid mobility of W relative to Th ultimately resulted in elevated W/Th (Fig. 3.10B). Most Leg 209 samples have significantly higher W/Th than primitive mantle (PM) or moderately altered oceanic crust (mAOC) at site 1256 (Fig. 3.4). Hydrous alteration of pyroxenes resulted in the formation of low-pH, high aSiO<sub>2</sub> fluids (Allen and Seyfried, 2003, Bach et al., 2004). The interaction of these fluids with serpentinized peridotites resulted in talc replacement of serpentine (Fig. 3.10B). Locally, talc is also formed as vein filling (Kelemen et al., 2004). Whereas vein fillings are represented by locally decreasing MgO/SiO<sub>2</sub> ratios with only limited influence on the overall HFSE budget, pervasive talc alteration is characterized by decreasing W/Th and W contents with simultaneously decreasing MgO/SiO<sub>2</sub> and LOI (wt.-%). This observation indicates that talc alteration liberates W from altered ultramafic rocks. Intrusion of mafic dikelets pre- and postdates both serpentinization and talc alteration and results in pronounced melt-rock interaction (MRI). Within the mafic dikelets, W, Th, Ta and U are not fractionated (Fig. 3.10C). The intrusion led to local fluid generation which then resulted in selective W enrichment within the alteration mineral assemblage of the ultramafic host rocks. The last recorded alteration stage in the presented sample set is late, low-T, oxidative seawater weathering. The resulting orange Fe-Mg-oxyhydroxide alteration products are host for significant amounts of secondary W and U (Fig. 3.10D).

Collectively, two distinct sources of W enrichment have been identified in ultramafic rocks of Leg 209. First, seawater-derived W was added in zones of strong oxidative alteration in the core-top sections at sites 1270 and 1271, characterized by high Fe<sub>2</sub>O<sub>3</sub> content and strong U enrichment, and secondly, mantle-derived W, in samples from all other sites that underwent serpentinization and melt-rock interaction. The latter are often characterized by strong Eu anomalies, indicative for hydrothermal fluids and magma-related sources. As the alteration processes in Leg 209 were active over a wide temperature range, they might be reflected in changes in the stable W isotope composition (Kurzweil et al., 2019), which might be a

promising tool to identify W mobility in different thermal regimes. For example, high-T alteration in response to dikelet intrusions at sites 1270 and 1271 should result in a remarkably different stable W isotope composition as low-T serpentinization and seafloor weathering (chapter 3).

Combined with the observed strong W enrichment in altered upper oceanic crust (Chapter 2), the results of this chapter show that selective, fluid-induced W enrichment is a ubiquitous feature of altered oceanic crust which thus acts as a major sink in the global geochemical W cycle. It furthermore highlights how the subduction of variously altered oceanic crust influences the W budget in subduction zones. Contrary to expectation, ultramafic portions of altered oceanic crust can now be shown to be a major carrier of W in the global subduction cycle. The here discussed findings thus strongly suggest that the selective W enrichment found in many arc lavas may be inherited to a large extent from selective W enrichment in altered oceanic crust. It can furthermore be concluded that the here described chemical signature of elevated W/Th can be found in ophiolites all around the globe.

## **4. The stable W isotope composition of altered oceanic crust**

## 4.1 Introduction

Tungsten, Th, U, Nb and Ta are characterized by a similarly high incompatibility during mantle melting. Therefore, ratios of W/Th, W/U, W/Nb and W/Ta are not significantly fractionated during magmatic processes (e.g., Arevalo and McDonough, 2008; König et al., 2011; Newsom et al., 1996; Noll et al., 1996). In arc settings W behaves fluid mobile and is enriched relative to U, Th Nb and Ta (König et al., 2008, 2010). Selective W enrichments in arc lavas either result from the higher mobility of W in subduction zone components or, alternatively, from previous W enrichment in subducted material, e.g. altered oceanic crust. First high-precision W concentration data for an in-situ section of moderately altered basaltic crust (IODP hole 1256D) and strongly serpentinized abyssal peridotites (ODP Leg 209) have been reported in chapters 2 and 3 and revealed a ubiquitous W enrichment over U, Th and Ta. For example, W/Th range from 0.18 to 0.4 in moderately altered upper oceanic crust and up to >10 in strongly serpentinized abyssal peridotites (Chapter 2 & 3), much higher relative to the canonical W/Th value of 0.09 that was previously defined by fresh mid-ocean ridge basalt (MORB) analyses (König et al., 2011). The actual source of additional W in altered oceanic crust remains enigmatic. Potential sources include a) seawater W that is retained during alteration or serpentinization, b) on-ridge venting by hydrothermal fluids or c) local redistribution during various alteration processes.

Stable W isotopes represent a new tool that has the potential to clarify these questions, because different reservoirs may have different stable W isotope characteristics. The stable W isotope compositions of MORBs and OIBs show a very narrow range, proposing a stable W isotope composition of the Earth's mantle of  $\delta^{186/184}\text{W} = +0.085 \pm 0.019 \text{‰}$  (Kurzweil et al., 2019). Hence, partial melting has no resolvable influence on the stable W isotope composition (Kurzweil et al., 2019). In contrast to this homogenous mantle composition, arc lavas show regional variability, from mantle-like  $\delta^{186/184}\text{W}$  towards both lower and higher  $\delta^{186/184}\text{W}$  ( $\delta^{186/184}\text{W}$  between -0.009 and +0.195 ‰, Kurzweil et al., 2019, Mazza et al. 2020). The variation in stable W isotope compositions in arc lavas can be explained by a) fractionation during fluid generation by dehydrating, b) retention of heavy W isotopes in residual phases like rutile, c) subduction of isotopically light altered oceanic crust and d) subduction of isotopically heavy sediments (Kurzweil et al., 2019; Mazza et al., 2020). Ocean floor sediment of terrigenous origin, e.g., from the eastern Mediterranean ( $\delta^{186/184}\text{W} = +0.085 \text{‰} - +0.144 \text{‰}$ ) and Sunda-Arc ( $\delta^{186/184}\text{W} = +0.120 \text{‰} - +0.302 \text{‰}$ ) are indeed isotopically heavy (Kurzweil et al., 2019). Seawater is now known to have a heavy stable W isotope composition of  $\delta^{186/184}\text{W} = +0.545 \pm 0.051 \text{‰}$  (Kurzweil et al., 2020). The significance of isotope studies on the understanding of serpentinization and subduction zone processes was already demonstrated at Leg 209 and 1256D for e.g Li and B (Gao et al., 2012; Vils et al., 2009), Mg (Huang et al., 2015) and Re and Os (Harvey et al., 2006).



For altered oceanic crust, the potential W reservoirs mentioned above are likely distinct in their stable W characteristics, as the amount of equilibrium isotope fractionation is controlled by the extent of temperature differences, relative mass differences between isotopes and stiffness of the bonding environments (Bigeleisen and Mayer, 1947; Schauble, 2004; Urey, 1947). Thus, with increasing temperature, the extent of equilibrium isotope fractionation decreases by  $\sim 1/T^2$ . Moreover, at chemical equilibrium heavy isotopes of an element prefer stiffer bonds (Bigeleisen and Mayer, 1947; Schauble, 2004). Therefore, compounds with lower coordination number or higher oxidation states are preferred by heavier isotopes (Schauble, 2004). In the absence of redox changes, differences in coordination chemistry are the main factor driving stable W isotope fractionation (Kashiwabara et al., 2013). For example, in aqueous solutions with  $\text{pH} > 7$  tetrahedrally coordinated  $(\text{WO}_4)^{2-}$  is the most common W species (Cruywagen, 1999; Kishida et al., 2004). The protonated forms  $\text{HWO}_4^-$  and  $\text{H}_2\text{WO}_4$  are octahedrally coordinated and more common in acidic, low-pH environments (Cruywagen, 2000). As heavy isotopes preferentially partition into stronger bonding environments, this change in coordination is a possible mechanism in magmatic or hydrothermal environments that might cause stable W isotope fractionation. Moreover, the adsorption of W on abundant, submarine Fe-Mn oxide concretions is associated with a change from tetrahedral to octahedral coordination (increase in the coordination number from +4 in dissolved species to +6 in adsorbed species). As heavy isotopes prefer stiffer bonds, preferentially lighter W isotopes are absorbed (Kashiwabara et al., 2017). The adsorption of W on Fe-Mn oxide concretions is highly effective and potentially responsible for the relatively low W concentrations in seawater (Sohrin et al., 1987) and its high  $\delta^{186/184}\text{W}$ . Yet, these fractionations have only been identified in low-T surface processes. In arc settings, progressive dehydration of the subducted slab is proposed to release isotopically heavy W into the fluid phase, retaining light W in the altered oceanic crust (Mazza et al., 2020). In terrestrial realms, at  $f\text{O}_2$  above the quartz-fayalite-magnetite (QFM) buffer,  $\text{W}^{6+}$  is by far the most common W species.  $\text{W}^{4+}$  as a minor component has only been identified at reducing conditions during partial melting under QFM-2 conditions (Fonseca et al., 2014; O'Neill et al., 2008). Under these conditions, the compatibility of W increases by half an order of magnitude, since the  $\text{W}^{4+}$  species is significantly more compatible in minerals such as clinopyroxene, orthopyroxene and olivine (Fonseca et al., 2014).

In the following chapter, the first stable W isotope data for altered oceanic crust are presented. To investigate different types of alteration, samples from the above-described localities have been studied (Fig. 4.1). By combining high-precision stable W isotope data and high-precision isotope dilution (ID) measurements of W, U and Th concentrations, specific alteration processes changing the stable W isotope composition of oceanic crust are revealed. With respect to subduction zone dynamics, the understanding of stable W isotope composition of subducting oceanic crust is of great importance. Subduction of altered oceanic crust and parts of its sedimentary cover is accompanied by continuously progressive dehydration, water

ascending from the slab will be widely available in depths up to 150 – 200 km (Schmidt and Poli, 1998). Fluids arising from subducting crust will cause partial melting in the mantle wedge and thus significantly contribute mobile elements to the erupting magmas (e.g. Morris et al., 1990; Plank and Langmuir, 1993; Noll et al., 1996). The results presented here therefore also allow further inferences on the source of stable W isotope composition homogeneity in arc systems.

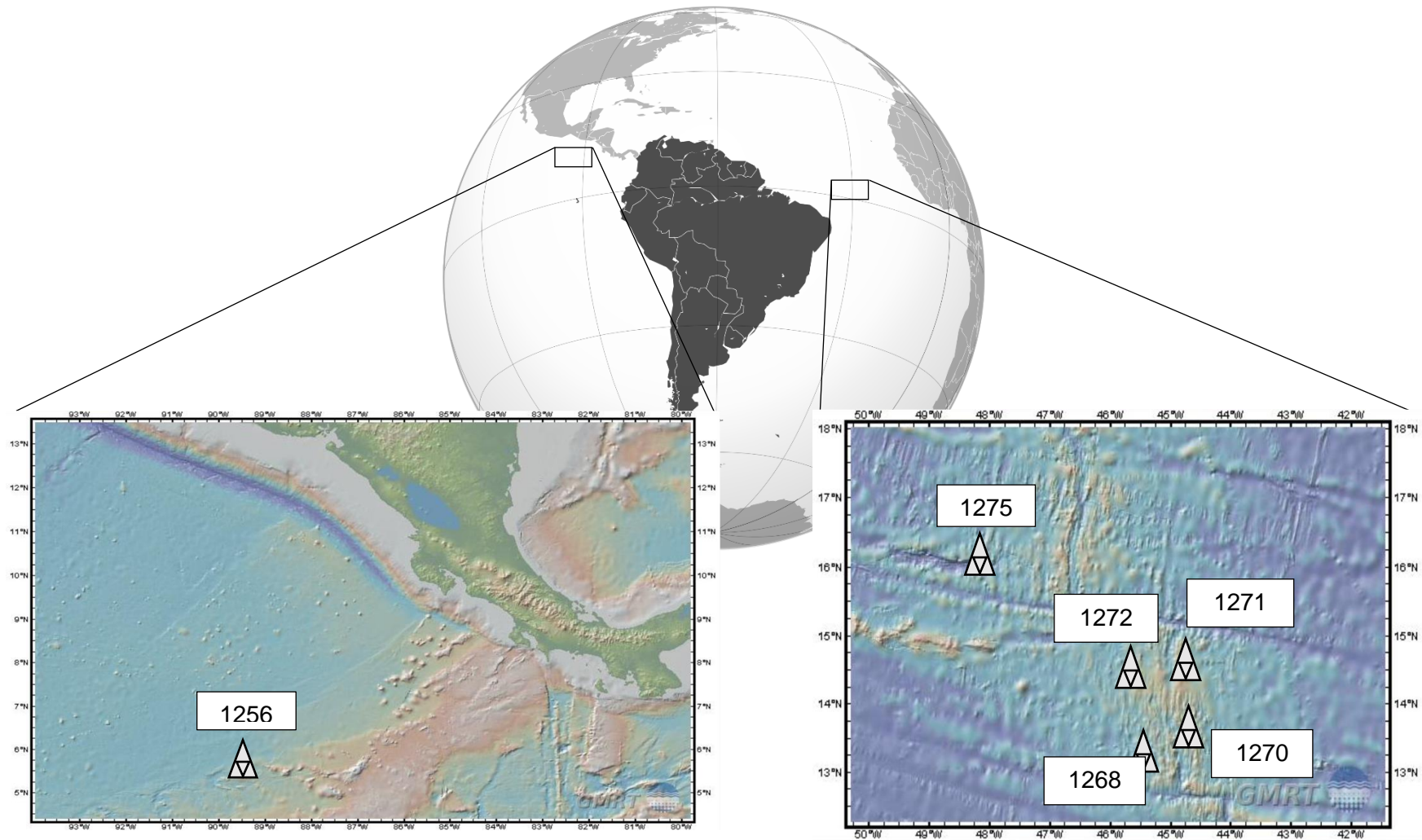


Fig. 4.1: Bathymetric maps of the sites investigated. The crust drilled at hole 1256D (left panel) was formed during an interval of superfast spreading at the East Pacific Rise at ca. 15 Ma. At Leg 209 (right panel), crust formed in a magma starved, slow spreading environment at ca. 5 Ma. A total of 5 holes of Leg 209 were studied. Data compiled from Ryan et al. (2009), World map: <https://bit.ly/39mk6MD>

## **4.2 Geological Overview**

### **4.2.1 Lithology and alteration styles at the investigated drilling sites**

In the following chapter, highly serpentinized abyssal peridotites that formed at slow spreading rates at the Mid-Atlantic Ridge (ODP Leg 209) and moderately altered effusive and igneous basalts that formed at super-fast spreading ridges from IODP hole 1256D (Fig 4.1., data compiled from Ryan et al., 2009) were investigated.

### **4.2.2 Lithology and elemental W systematics at hole 1256D**

The crust drilled in hole 1256D formed ~15 Ma ago during an interval of super-fast spreading with rates as high as 220 mm/a along the East Pacific Rise (EPR). Presently, the section is located at 6°44.1 N, 91°56.1 E (Wilson et al., 2006). The uppermost volcanic basement formed off-axis and is composed of a >75 m thick ponded lava flow followed downhole by effusive inflated sheet and massive flows. A 57 m thick transition zone below the extrusive rocks is characterized by intrusive contacts and sulphide-mineralized hyaloclastite breccias. The transition zone is underlain by intrusive basalts, the 350 m thick sheeted dike complex. The sheeted dike complex is cut by subvertical dikes with brecciated and mineralized chilled margins, testifying to intense hydrothermal activity (Alt et al., 2010). The transition from the intrusive section to the plutonic complex is defined by pervasive granoblastic overprinting of the lower dike section (granoblastic dikes, Alt et al., 2010). Two gabbroic intrusives that crosscut the granoblastic dikes at a depth of 1407 meters below sea level (mbsf) comprise the plutonic section. Stopped clasts from the granoblastic dikes were found within both gabbroic bodies (Koepke et al., 2008).

The whole studied section (800 – 1550 mbsf) was subject to deep-rooted hydrothermal alteration. On-axis alteration is characterized by hot, hydrothermal fluids and seawater migrating throughout the whole sheeted dike section. Fluid flow is mostly confined to discrete pathways as veins in zones of structural weakness or along gabbroic intrusions (Harris et al., 2015). In the transition zone and in the sheeted dike complex pervasive alteration is defined by a sub- to greenschist-facies mineral assemblage, mainly comprising chlorite and actinolite that formed at temperatures between 200 – 400°C. The transition zone represents a mixing zone between downwelling seawater-derived fluids and upwelling high temperature discharge fluids (Alt et al., 2010). During lateral crustal movement away from the spreading-centre, sheet and massive flows were further deposited on top of the intrusive section. Vein-related alteration in the transition zone is characterized by high degrees of recrystallization and a chlorite-smectite dominated mineralogy. Alteration intensity in the intrusive section below the transition zone is variable, vein related and pervasive. Typically 30 % of the original mineral assemblage is altered to (sub)greenschist facies minerals (Alt et al., 2010). With increasing depth (and temperature) the extent of alteration increases and actinolite becomes more common than

chlorite (below 1300 mbsf). Peak temperatures exceeding 400°C are indicated by hornblende formation below 1350 mbsf (Alt et al., 2010; Koepke et al., 2008). This early phase of alteration is caused by downward percolating seawater recharging the hydrothermal system. The seawater effect is recorded by strictly vein-related and elevated  $^{87}\text{Sr}/^{86}\text{Sr}$  in the whole sheeted dike section (Harris et al., 2015). After an initial stage of cooling and hydrothermal alteration, the emplacement of the two gabbro bodies led to contact metamorphism and the formation of granoblastic textures in the lower sheeted dike complex (~60 m) right above the gabbros. At peak conditions of granoblastic overprint, hydrous partial melting caused the intrusion of single crosscutting dikes and fluid circulation (Alt et al., 2010). The gabbroic bodies themselves were subject to intense later-stage hydrothermal alteration (Harris et al., 2015; Koepke et al., 2011). High spreading and sedimentation rates at hole 1256D led to a limited seawater recharge after ca. 5 Ma (Tominaga et al., 2009), resulting in only moderate but pervasive alteration of the fresh crust.

Selective W enrichment over U, Th, and Ta is a common feature in all portions of 1256D (Fig. 4.2, chapter 2). The enrichment is most prominent at lithological boundaries such as the transition zone (101 ng/g W, W/Th ca. 0.73) and in the top of the granoblastic dikes (> 100 ng/g W, W/Th 0.57 to 4.14). Below the granoblastic dikes W/Th continuously decrease with increasing depth (Fig. 4.2 A & B, chapter 2). Sub-canonical W/Th, W/U or W/Ta could not be identified anywhere in the analysed lithological section. In contrast to W/Th, U/Th remain uniform and only slightly elevated relative to fresh MORB (Chapter 2). Larger variations are restricted to the transition zone (U/Th up to 10.6) and the gabbroic intrusions (U/Th < 0.3). Along the contact of both gabbroic units, elevated W, W/Th, W/U, and W/Ta have been identified and were related to fluid circulation cells (Harris et al., 2015, chapter 2)

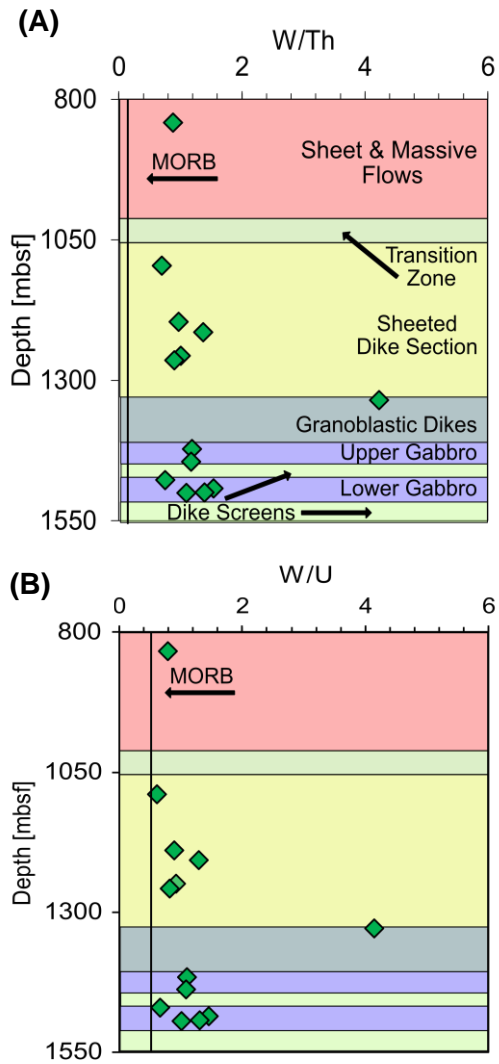


Fig. 4.2: Chemical and petrological variations in IODP hole 1256D. Tungsten is selectively enriched over Th and U, the W enrichment is most pronounced directly above the granoblastic dike section at ca. 1250 - 1330 mbsf (A-B). Below this point, the selective W enrichment decreases continuously (see also chapter 2).

### 4.2.3 Lithology and elemental W systematics at Leg 209 drill holes

Oceanic crust drilled during ODP Leg 209 comprises relatively young (< 5 Ma, Fujiwara et al., 2003) and highly serpentinized abyssal peridotites and gabbroic intrusives. They formed in a magma starved, slow-spreading setting (full rate ~ 25 mm/a; Kelemen et al., 2004) with little to no effusive magma production. Large outcrops of upper-mantle rocks are preserved at the Mid-Atlantic Ridge north and south of the 15°20' fracture zone. In the following section, characteristic alteration effects such as talc formation, serpentinization, and brucite dissolution with their specific influence on the trace element budget are briefly described. A more detailed description can be found in chapter 3 and in the ODP Initial Results Volume 209 (Kelemen et al., 2004).

Samples originating from site 1270 (holes A, C & D) are characterized by pervasive serpentinization and frequent manifestations of high temperature deformation such as mylonites and exsolution of ilmenite from titanomagnetite. The petrographic composition is ~ 62% harzburgite, 6% dunite, and 32% mafic intrusives (Kelemen et al., 2007). Relict orthopyroxene is locally replaced by talc ± tremolite in zones of mafic dike intrusions. Talc formation is abundant in the rock record of all holes from site 1270 but is strictly vein related. The intrusion of gabbroic dikelets lead to extensive melt impregnation resulting in elevated concentrations of W, U, Th, Ta, Zr, Nb, Ta, Lu, Hf (Paulick et al., 2006), where W/U, W/Th and U/Th were not changed in the dikelets themselves (Chapter 3). Since they intruded into (partially) serpentinized oceanic crust, its intrusion resulted into local fluid generation with associated elevated W contents (Chapter 3). Iron-oxyhydroxide veins are restricted to shallow crustal levels and are interpreted to have formed during seafloor weathering under oxidizing conditions (Bach et al., 2004). Minor carbonate veining is recorded in holes 1270 C & D, which indicates the circulation of carbonate-rich fluids. With increasing depth, talc filling dominates over carbonate vein mineralization. Correlations of W abundances, with W/Th, W/U, or U/Th are not observed. Locally strong U enrichment is related to oxidative weathering. Tungsten is mainly enriched over Th and Ta, resulting in W/Th between 0.210 – 10.7 (PM = 0.14) and W/Ta ranging between 0.2 – 44.4 (PM = 0.31). The enrichment of W is strongest in samples from shallow depths (< 2 mbsf, Fig. 3), that are strongly affected by oxidative weathering (Chapter 3). Only a zone at ~ 20 mbsf in hole 1270D is characterized by peridotites with (sub-) canonical W/Th (< 0.09). Thus, this section may represent a root zone for localized W redistribution (Chapter 3).

Hole 1268A mainly consists of intensively serpentinized harzburgite and dunite (ca. 75 vol.-%), intersected by late magmatic dikes and gabbros (ca. 25 vol.-%, Bach et al., 2004). An initial stage of fluid-dominated, greenschist facies serpentinization was followed by pervasive talc alteration under static conditions at 350 – 400°C at low pH of ~4 to 5. In this temperature range, olivine is still stable, but orthopyroxene is readily replaced by talc ± tremolite. The

breakdown of pyroxene in peridotites and intrusive rocks is a source of Si, facilitating talc formation (Bach et al., 2004). Intrusions of gabbros have been identified as driving force for fluid generation (Kelemen et al., 2004, Paulick et al., 2006). In discrete horizons, pervasive talc alteration modified whole-rock compositions close to pure talc (Kelemen et al., 2004). Geochemically, talc formation and fluid-dominated serpentinization can be distinguished by their MgO/SiO<sub>2</sub>. Talc alteration lowers the MgO/SiO<sub>2</sub> whereas serpentinization slightly increases MgO/SiO<sub>2</sub>. Furthermore, serpentinized peridotites are more enriched in W (W/Th 30 to 210) compared to talc altered samples (W/Th 0.1 to 40, Fig. 3 A & B). Lower W/Th in talc altered samples might indicate that W is not incorporated into the structure or adsorbed to the surface of talc but is leached from the rock matrix (Chapter 3).

The excessively serpentinized and high-T deformed crust at site 1271 (A & B) mainly comprises dunites (A: ca. 98%, B: 56%) with only minor portions of harzburgite (A: < 1%, B: ~ 9%, Kelemen, 2004). Talc alteration is rare and many sections were subject to excessive melt impregnation, leading to elevated incompatible element concentrations (Paulick et al., 2006). The uppermost 10 meters are made up of dunites with a yellowish-green to grey groundmass hosting abundant black serpentine-magnetite veins. The development of this macroscopic texture is related to seafloor weathering reactions including brucite dissolution (Bach et al., 2004). At hole 1271A brucite is an abundant phase, having formed coeval with serpentine (Bach et al., 2004). Its dissolution to Fe-oxyhydroxides at the crust-seawater transition is characteristic for site 1271. Phase relations indicate that reacting agents are characterized by high pH and low-*a*SiO<sub>2</sub>-fluids (Bach et al., 2004). Two dunites from depths < 1 mbsf show markedly high W concentrations of 207 and 120 ng/g, respectively. Their sub-canonical W/U of 0.41 and 0.31 are caused by selective U enrichment, also resulting in U/Th of 19.2 and 17.75. Ratios of W/Th in all studied samples are >> 3 and testify to substantial W enrichment over Th. As the dunites from deeper portions do not preserve U and W enrichment at of similar magnitude, the enrichments most likely formed in response to surface alteration processes like low-T oxidative alteration (Chapter 3).

Two mafic melt intrusives in hole 1272A have been examined for their stable W isotope compositions. The absence of olivine in these mafic melt intrusives limits the potential for hydration and they were thus selected as local mantle representatives. Both samples differ in their trace element characteristics. Sample R-2-41 is characterized by MORB-like W/Th, W/U and U/Th, whereas sample R-2-40 is depleted in W relative to Th (W/Th = 0.06) and U (W/U = 0.16). Thus, such a rock type may represent root zones for W enrichment observed elsewhere (Chapter 3).



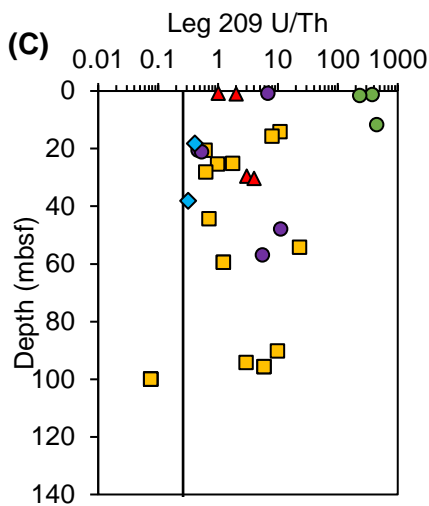
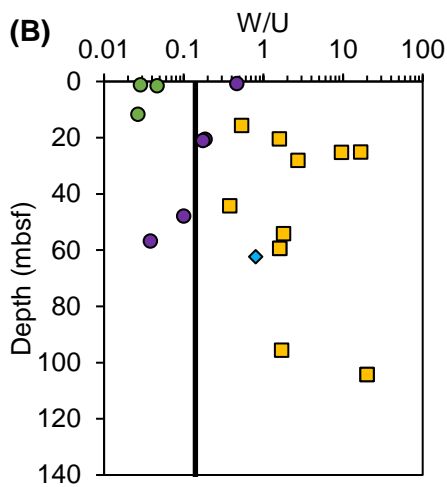
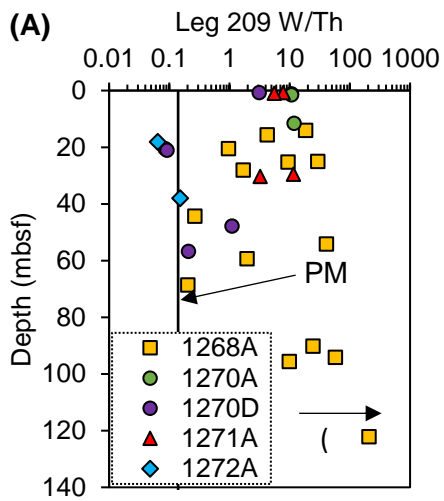


Figure 4.3: Downhole variations of W, U, and Th in IODP Leg 209, illustrating selective W enrichment over Th and U. At site 209, 5 sites have been drilled in total. Tungsten is enriched over Th in most samples, sub-canonical W/Th were only identified in serpentinized peridotites from holes 1270D and 1272A (A). Sub-canonical W/U are more common at sites 1270 in holes A and D (B). This is because U may behave as fluid-mobile element during oceanic crust alteration, it is selectively enriched over Th in most samples (B). The site 1270A samples being most enriched in U are also characterized by the highest U/Th (C). Further details are presented in chapter 3.

### 4.3 Analytical Protocol

For stable W isotope analyses, 31 samples from Leg 209 and hole 1256D were selected with known W concentrations that are representative for different alteration types, such as fluid-/rock dominated serpentinization, talc alteration, and seafloor weathering. The analytical protocol follows that of Kurzweil et al. (2018). Depending on the previously determined W concentrations, 50 – 600 mg of sample powder were weighed in pre-cleaned and pre-bombarded Savillex® beakers. An adequate amount of  $^{180}\text{W}$ - $^{183}\text{W}$  double spike was added to achieve an optimized W mixture of 60<sub>Sample</sub>:40<sub>Spike</sub>. The sample-spike mixture was tabletop digested for 48 h in 6 ml of a 3:2 mixture of conc. (14 N)  $\text{HNO}_3$  – conc. (24 N) HF at 120°C. For the zircon-bearing samples of hole 1256D (Neo et al., 2009; chapter 2), the first tabletop-digestion step was followed by evaporation to dryness and re-dissolution in 6 ml of a 3:1 mixture of conc. HF – conc.  $\text{HNO}_3$ . The samples were then placed in Parr® bombs for additional 36 h at 180°C. After evaporation, the samples were dissolved in 6 ml conc. HF and bombed for another 72 h at 180°C. Leg 209 peridotites were bombed once for 36 h in 8 ml of a 3:2 mixture of conc.  $\text{HNO}_3$  – conc. HF. Subsequently, samples from Leg 209 and hole 1256D were repeatedly dried down in conc.  $\text{HNO}_3$  and re-dissolved in 8 ml conc. (10 N) HCl at 120°C to break down fluorides which have potentially formed during previous digestion steps. After 48 h on the hotplate, the samples were dried and finally taken up in 10 ml 1 N HCl.

The chemical separation of W comprises a three-step column chemistry (BioRad AG 50W-X8, 200–400 mesh; BioRad AG 1-X8, 100–200 mesh; Eichrom TEVA), which is described in detail in Kurzweil et al. (2018). Tungsten isotope ratios were measured on a THERMO Neptune Plus MC-ICP-MS at the University of Cologne in freshly mixed 0.56 N  $\text{HNO}_3$  – 0.24 M HF. Sample and standard measurements were bracketed by acid-blank and on-peak-zero measurements. The yields of the chemical separation were typically > 60% and chemistry blanks ~ 160 pg, i.e., < 1% of the processed W. All stable W isotope data are given in  $\delta$ -notation relative to the NIST SRM 3163 standard, expressed in ‰ (eq. 2).

$$(2): \delta^{186/184}\text{W} = \left( \frac{\left( \frac{^{186}\text{W}}{^{184}\text{W}} \right)_{\text{Sample}}}{\left( \frac{^{186}\text{W}}{^{184}\text{W}} \right)_{\text{NIST SRM 3163}}} - 1 \right) * 1000$$

To account for instrumental drift and to assure long-term stability, NIST SRM 3163 and an Alfa standard solution were measured repeatedly in each sequence. The mean difference between both standard solutions was constant ( $\delta^{186/184}\text{W}_{\text{NIST SRM 3163 - ALFA 1256D Session}} = 0.059 \pm 0.008$  ‰,  $\delta^{186/184}\text{W}_{\text{NIST SRM 3163 - ALFA Leg 209 Session}} = 0.054 \pm 0.009$  ‰), in line with earlier data ( $0.054 \pm 0.007$  ‰; Kurzweil et al., 2019). The standard AGV – 2 was selected as geological

reference material and digested and processed along with the samples. Its stable W isotope composition was determined as  $\delta^{186/184}\text{W}_{\text{NIST SRM 3163 Leg 209 Session}} = +0.001 \text{ ‰}$  and  $\delta^{186/184}\text{W}_{\text{NIST SRM 3163 1256D Session}} = +0.005 \text{ ‰}$ , consistent with earlier studies ( $+0.016 \pm 16 \text{ ‰}$ , Kurzweil et al., 2018). The long-term external reproducibility of  $\pm 0.018 \text{ ‰}$  based on replicated measurements of geological reference materials is taken as error on the data and their graphical representation in figures (Kurzweil et al., 2018).

Concentration data for U, Th, Ta, Zr, Nb, Lu, and Hf have been determined by isotope dilution and MC-ICP-MS analyses at the University of Cologne. The digestion scheme follows the same procedure as described above and in chapter 2 & 3. Major element data are from Neo et al. (2009, 1256D) and Paulick et al. (2006, Leg 209).

Table 4.1: Measured stable W isotope and U-Th-W data for samples from hole 1256D and Leg 209. More high-precision isotope dilution data for the two sites are given in Chapter 2 & 3. Major element data for MgO/SiO<sub>2</sub> and Fe<sub>2</sub>O<sub>3</sub> are taken from Paulick et al., 2006. Du = dunite Hz = harzburgite.

Hole	Sample - No.	Rock & Alteration Type	Depth (mbsf)	W (ppm)	Th (ppm)	U (ppm)	W/Th	MgO/SiO <sub>2</sub>	Fe <sub>2</sub> O <sub>3</sub> (wt.-%)	$\delta^{186/184}$ ‰
1256D	087 - 1	sheet & massive flows	831.1	0.0375	0.138	0.0473	0.271	0.143	13.1	+0.065
1256D	134 - 2	upper dikes	1086.5	0.0404	0.202	0.0658	0.200	0.147	12.8	+0.076
1256D	155 - 2	upper dikes	1186.5	0.0565	0.201	0.0638	0.281	0.142	13.7	+0.063
1256D	159 - 1	upper dikes	1204.6	0.0802	0.195	0.0624	0.412	0.153	13.2	+0.077
1256D	168 - 4	upper dikes	1247.0	0.0645	0.222	0.0700	0.290	0.135	13.4	+0.059
1256D	170 - 3	upper dikes	1254.7	0.0272	0.105	0.0334	0.260	0.181	10.4	+0.059
1256D	187 - 2	upper dikes	1325.9	0.335	0.233	0.0809	1.44	-	-	+0.046
1256D	214 - 2	upper gabbro	1413.6	0.0479	0.131	0.0434	0.367	0.146	10.2	+0.088
1256D	220 - 1	upper gabbro	1435.9	0.0437	0.129	0.0402	0.338	0.167	10.8	+0.054
1256D	227 - 1	upper dike screen	1469.0	0.0439	0.211	0.0650	0.208	0.152	12.7	+0.116
1256D	230 - 1	lower gabbro	1483.7	0.0470	0.108	0.0324	0.437	0.152	15.2	+0.067
1256D	231 - 3	lower gabbro	1490.8	0.0412	0.0942	0.0315	0.437	0.174	11.2	+0.077
1256D	232 - 1	lower gabbro	1491.8	0.0325	0.0943	0.0321	0.345	0.175	11.2	+0.092
1268A	R-2-01	Du - talc alt.	14.1	0.0461	0.00249	0.0269	18.5	0.514	2.53	-0.040
1268A	R-2-04	Hz - FD serp.	25.1	0.0493	0.00169	0.00296	29.2	0.904	3.98	+0.032
1268A	R-2-12	Du - FD serp.	94.1	0.503	0.00869	0.0254	57.9	0.981	5.60	+0.042
1268A	R-2-13	Hz - talc alt.	95.6	0.0399	0.00404	0.0235	9.86	0.490	0.392	-0.117
1268A	R-2-18	Hz - FD serp.	122.0	0.0811	< 0.0001	< 0.001	208	0.912	2.95	+0.024
1270A	R-2-20	Hz - MRI, serp.	1.6	0.0329	0.00307	0.712	10.7	1.01	5.38	+0.114
1270D	R-2-24	Hz - MRI, serp.	0.7	0.324	0.103	0.694	3.16	0.891	5.84	+0.077
1270D	R-2-25	Hz - MRI, serp.	20.6	0.0398	0.465	0.214	0.0857	0.866	4.15	+0.104
1270D	R-2-26	Hz - MRI, serp.	21.0	0.0385	0.419	0.221	0.0918	0.917	5.10	+0.125
1270D	R-2-27	Hz - MRI, serp.	47.8	0.0615	0.0550	0.614	1.12	0.980	5.44	+0.055
1270D	R-2-28	Hz - MRI, serp.	56.8	0.0396	0.190	1.04	0.208	0.961	5.14	+0.097
1271A	R-2-29	Du - MRI, serp.	0.8	0.208	0.0262	0.505	7.91	0.945	9.03	-0.060
1271A	R-2-30	Du - MRI, serp.	0.9	0.119	0.0214	0.381	5.57	0.955	10.0	-0.071
1271A	R-2-31	Du - MRI, serp.	29.6	0.0196	0.00170	0.00696	11.6	1.19	6.24	-0.005
1271A	R-2-32	Du - MRI, serp.	30.3	0.0291	0.00894	0.0814	3.25	1.17	6.70	+0.002
1272A	R-2-40	Olivine-Gabbro	18.2	0.0935	1.46	0.594	0.0641	0.112	2.29	+0.070
1272A	R-2-41	Diabase	38.1	0.187	1.23	0.391	0.151	0.143	1.81	+0.074

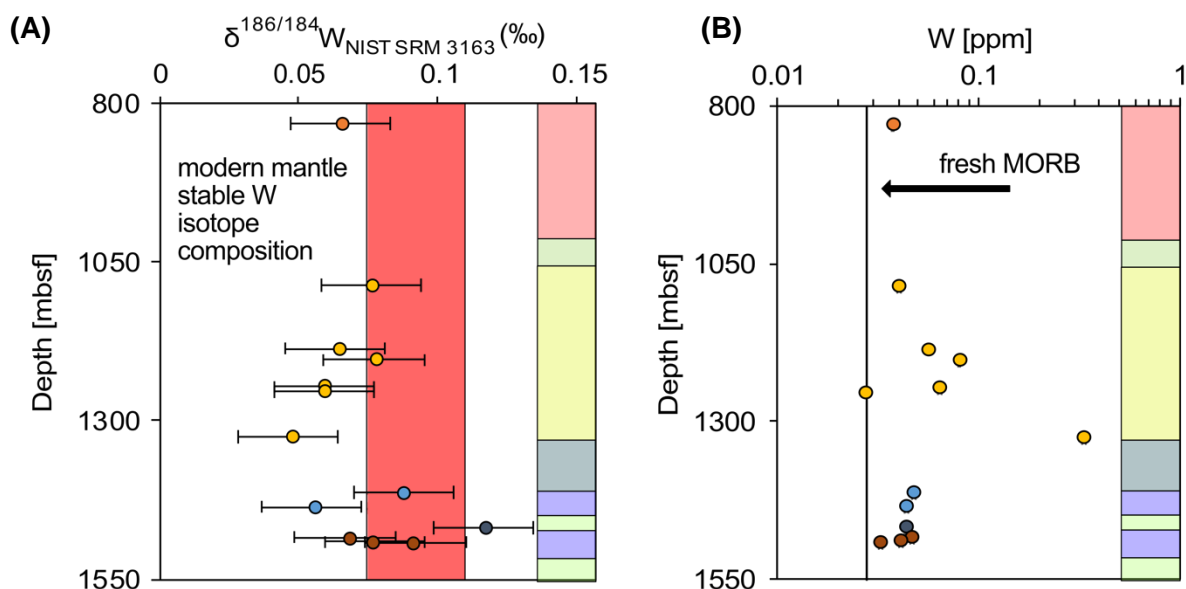


Figure 4.4: Downhole variation of stable W isotope compositions (A) and W concentrations (B) determined for hole 1256D. The stable W isotopic compositions of the sheet and massive flows (S&MF) largely overlap with the mantle array (red) as defined by Kurzweil et al., 2019. With increasing depth in the sheeted dike complex (yellow), the W isotope compositions become lighter and decrease to minimum values of  $\sim 0.046 \pm 0.18$  ‰. Simultaneously, the W concentrations rise to a maximum value of 335 ppb (B). The lower section is characterized by mantle-like W isotope compositions and lower W concentrations. The stratigraphy is colour-coded as in Fig. 4.2.

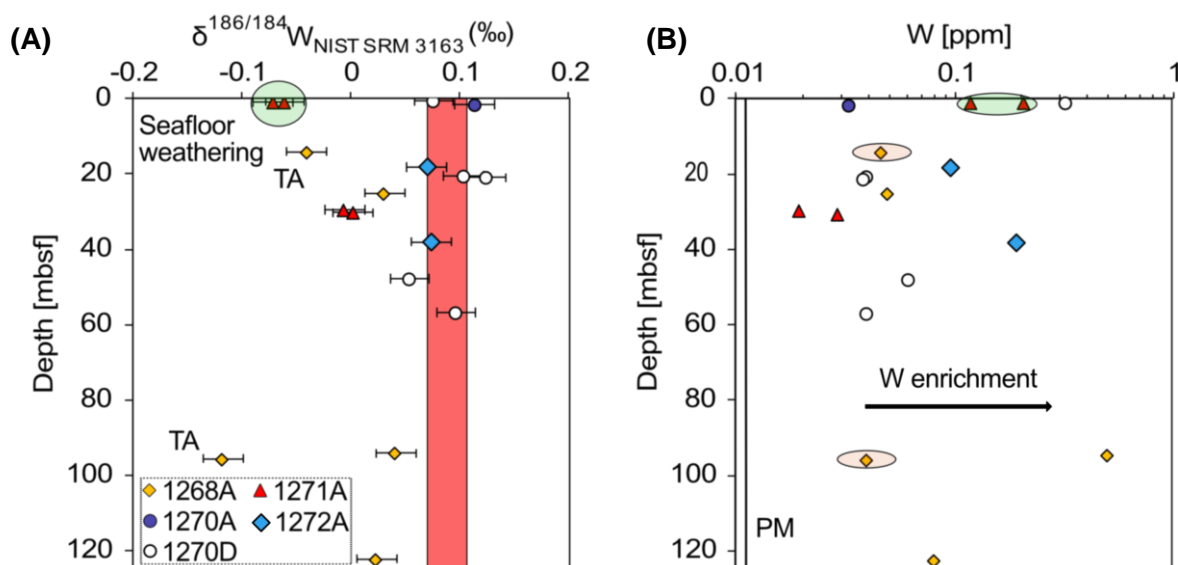


Figure 4.5: Downhole variation of stable W isotope compositions (A) and W concentrations (B) measured for various holes of ODP Leg 209. Fluid-dominated, serpentinized and Si metasomatized rocks (TA, red encircled) from hole 1268A and extensively serpentinized peridotites from 1271A are significantly lighter in their W isotope compositions than the mantle value (red bar). In contrast, melt-impregnated and serpentinized peridotites from hole 1270D and mafic intrusions from 1272A plot well within the mantle array (A). The W concentrations are much more diverse in samples from Leg 209 than in hole 1256D (B). Tungsten concentrations are especially elevated close to the seawater-rock interface (pale green field).

## 4.4 Results

### 4.4.1 Stable W isotope patterns at different drilling sites

The results of stable W isotope measurements are given in Table 4.1. In general, most samples from hole 1256D are characterized by mantle-like stable W isotope compositions. The sample from the effusive sheet and massive flow section at hole 1256D shows a  $\delta^{186/184}\text{W} = +0.074$  ‰, which is within error of the typical MORB value of  $+0.088 \pm 0.017$  ‰ (Kurzweil et al., 2019). The stable W isotope composition of 5 sheeted dike section samples is very uniform and MORB-like, with a tendency towards lighter values ( $\delta^{186/184}\text{W} = +0.052$  to  $+0.083$  ‰). Only one sample of the sheeted dike section has a lighter  $\delta^{186/184}\text{W}$  of  $+0.046$  ‰ which is resolvable from the MORB value. The gabbros are defined by  $\delta^{186/184}\text{W}$  values of  $+0.054$  ‰ to  $+0.116$  ‰, which is barely resolvable from the MORB range (Fig. 4.4 A & B, Table 4.1).

Seventeen samples covering 5 holes from Leg 209 (Mid-Atlantic Ridge) have been selected for stable W isotope analyses (Fig. 4.5 A & B, Table 4.1). Two samples from the mafic intrusive section of the upper part of hole 1272A show  $\delta^{186/184}\text{W}$  of  $+0.075$  ‰ and  $+0.080$  ‰, again overlapping with the MORB range. Likewise, the stable W isotope compositions of site 1270 serpentinized harzburgites are mainly defined by MORB-like  $\delta^{186/184}\text{W}$  between  $+0.077$  and  $+0.114$  ‰. Only samples from hole 1270D with canonical W/Th (R-2-25 & -26) have slightly elevated  $\delta^{186/184}\text{W}$  of  $+0.109$  ‰ and  $+0.130$  ‰. Talc altered samples from hole 1268A show  $\delta^{186/184}\text{W}$  that are significantly lower, between  $-0.035$  ‰ and  $-0.111$  ‰. Fluid-dominated serpentinized peridotites from the same hole range in  $\delta^{186/184}\text{W}$  from  $+0.029$  ‰ to  $+0.047$  ‰, also significantly lighter than the stable W composition of MORBs. Likewise, shallow ( $< 1$  mbsf), intensely seafloor-weathered dunites of hole 1271A are also characterized by low  $\delta^{186/184}\text{W}$  values ( $-0.054$  ‰ and  $-0.065$  ‰). Similarly, both samples (R-2-31 & -32) from greater depths (ca. 30 mbsf) that are intensively talc-veined are also significantly lighter than the mantle value ( $\delta^{186/184}\text{W} = -0.005$  and  $+0.002$  ‰).

## 4.5 Discussion

### 4.5.1 The source of W in altered oceanic crust

All studied samples are elevated in W/Th compared to fresh MORB, indicating relative W enrichment by fluids and excluding secondary gain of W by melt overprint (during melting, Th is similarly incompatible as W, e.g. Arevalo et al., 2008; König et al. 2011). The stable W isotope composition of the sample suite indicates large internal variability with a clear tendency towards low  $\delta^{186/184}\text{W}$  values when compared to MORBs (Fig. 4.4). Potential sources for W gain include hydrothermal fluids, terrigenous sediments, and seawater. The high  $\delta^{186/184}\text{W}$  value of seawater ( $0.545 \pm 0.051$  ‰, Kurzweil et al., 2020) and high  $\delta^{186/184}\text{W}$  values of pelagic sediments (+0.085 to +0.302 ‰, Kurzweil et al., 2019) make these reservoirs highly unlikely sources for additional W. Features that need to be explained by a successful model are (1) the overall excesses of W and (2) the mantle-like stable W isotope signatures in rocks which carry excess W.

Regardless of their strong W enrichment, 1256D samples mainly show MORB-like  $\delta^{186/184}\text{W}$  values with a weak tendency towards lower values only in the sheeted dike section, clearly indicating a magma-related W source (Fig. 4.4). The proposed model for stable W isotope fractionation at drill hole 1256D is illustrated as a sketch in Fig. 4.6. High temperatures (> 700°C) prevailing during initial fluid induced alteration at the spreading centre and suppressed resolvable isotopic variations in these rocks (Fig. 4.6 A). This is because the extent of equilibrium isotope fractionation usually decreases with increasing temperature (Schauble, 2004). Moreover, as outlined in chapter 2, the lack of samples that show relative W depletion (e.g. sub-canonical W/Th) suggests an external source of W. The deepest gabbroic bodies from the proposed root zone of hydrothermal activity (Wilson et al., 2006, Alt et al., 2010, Koepke et al., 2011, Harris et al., 2015) are enriched in W due to intense hydrothermal alteration (Chapter 2) and thus represent an unlikely origin for selective W addition in the upper sections. Based on the decreasing W enrichment downhole (Chapter 2, Fig. 2.3) deeper crustal portions with mantle-like W isotope compositions, located between the gabbroic intrusions and the axial melt potentially have supplied the W (Fig. 4.6B). Further drilling of hole 1256D may recover deeper rock portions that are depleted in W and display the source for the ubiquitous W enrichment in the studied section of oceanic crust. Variation in the stable W isotope composition is mainly restricted to later alteration, discussed in section 4.5.2.1.

In search for a root zone of the excess W in Leg 209 samples the dataset was screened for samples with sub-canonical W/Th. The only samples with slightly (sub-)canonical W/Th are the intrusive olivine-gabbros from site 1272A and peridotites from hole 1270D that also shows a MORB-like W concentration and stable isotope composition. A proposed model for stable W isotope fractionation in peridotitic altered oceanic crust is illustrated as a sketch in Figure 4.7.

For the peridotite samples with canonical W/Th, it was already demonstrated in chapter 3 that they originate from a zone of minor alteration intensity. In chapter 3 it was also demonstrated how intrusions of mafic dikes potentially result in local fluid production and subsequent W enrichment in the host rocks. As these dikes intruded at ca. 700 °C (Kelemen et al., 2004), the developing fluids most likely do not fractionate stable W isotopes (Figs. 4.5, 4.7A). Moreover, the resulting mineral assemblage formed also under high-T conditions. Thus, this alteration would produce W gain with a MORB stable W isotope signature. This hypothesis is in concordance with the presented data in Table 4.1 for holes 1270 and 1271. Significant stable W isotope fractionation is only to be found in samples strongly affected by late stage alteration, discussed further below in section 4.5.2.2.

Another likely W source is low grade, oxidative seafloor weathering which adds significant amounts of U and W to the rock fabric (Chapter 3). These weathering products have very light stable W isotope compositions of  $\delta^{186/184}\text{W}$  between -0.071 and +0.002 ‰ (Fig. 4.7D). Two processes are potentially responsible for the W gain within the altered mineral assemblage, (a) earlier W enrichment as recorded in serpentinites from deeper levels of hole 1271 and other sites from Leg 209 or (b) adsorption of W from low-T fluids. As serpentinization has no strong influence on the stable W isotope composition, it represents an unlikely source for W excess. Thus, fixation of light W isotopes from a low-T fluid due to changes in coordination chemistry from +4 in the fluid phase to +6 in the adsorbed phase is the most likely scenario. Although seawater is known to be extremely high in  $\delta^{186/184}\text{W}$  (Kurzweil et al., 2020), it may still represent a plausible source for W as the fractionation associated with coordination changes is particularly strong (Kashiwabara et al., 2017). A simple line between W enrichment and the stable isotope composition cannot be drawn (Fig. 4.8 A). This is most likely caused by the several alteration styles offset each other and the complex and long history of exhumation at the site of Leg 209.



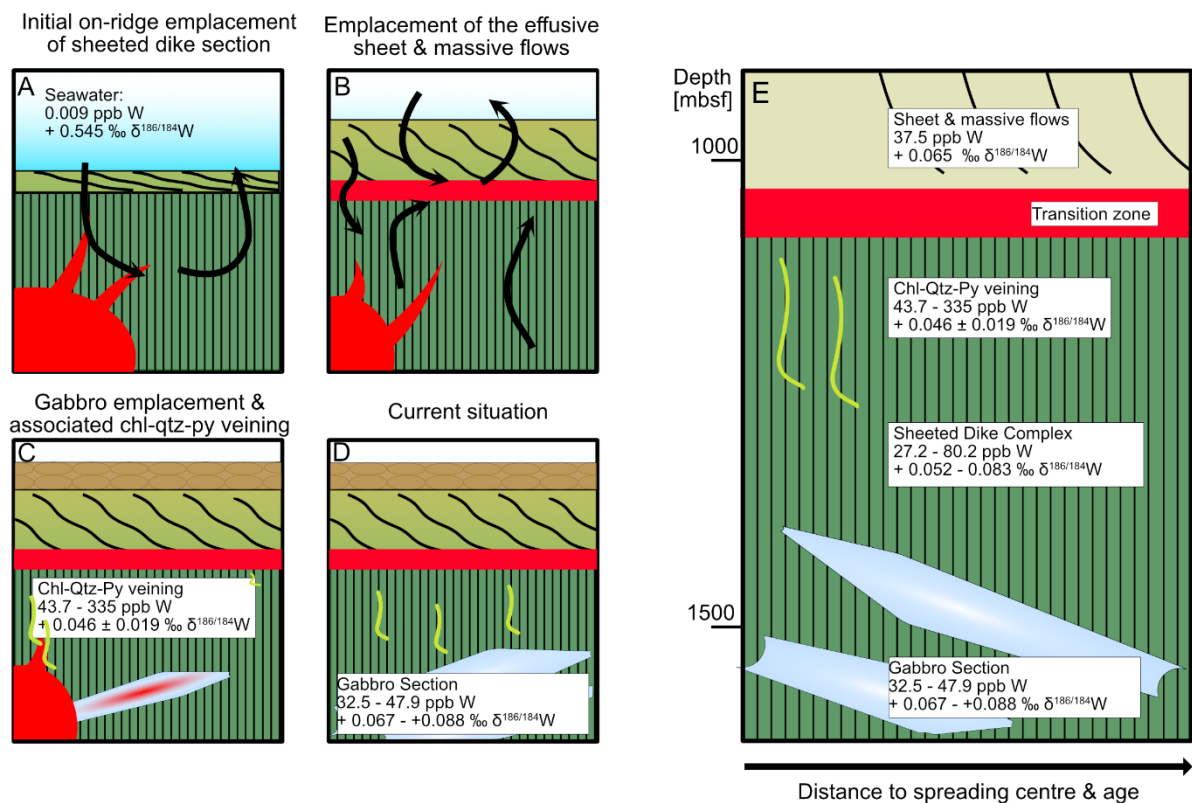


Figure 4.6: Development of the current stable W isotope composition of altered oceanic crust at hole 1256D. Initial interaction of seawater with the sheeted dike section resulted in W enrichment which, due to the high-T environment, is not reflected in stable W isotope fractionation (A). The thickening of the effusive sheet & massive flow unit led to the formation of the transition zone inhibiting fluid exchange between sheet & massive flows and lower crustal levels (B). Late veining in response to intrusion of gabbroic melt resulted in lighter stable W isotope composition (C). The gabbroic section itself shows mantle-like stable W isotope composition, as it was emplaced in a high temperature environment (E).

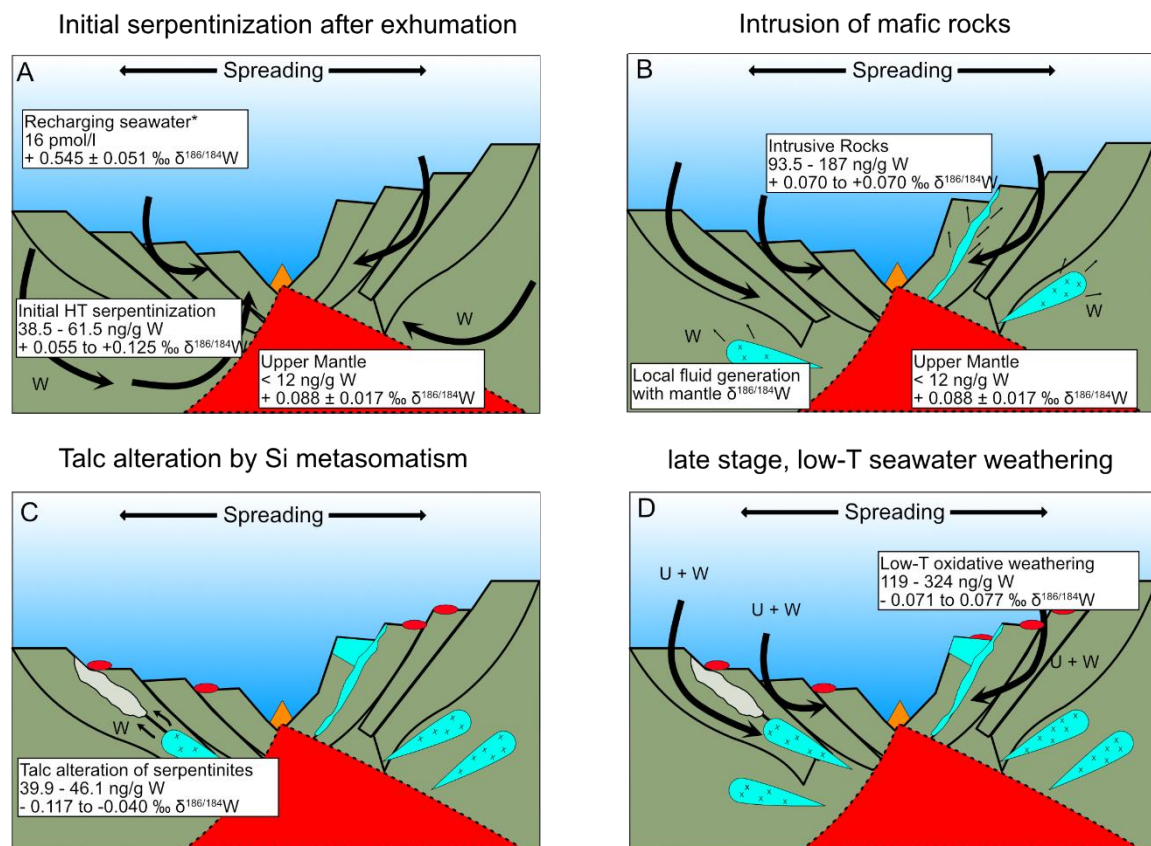


Figure 4.7: Succession of W enrichment events and changes in the stable W isotope composition during alteration of peridotitic oceanic crust at Leg 209. In an initial stage during serpentinization, W is enriched by evolved high-T fluids carrying W from deeper sources into the accessible section of altered oceanic crust. These processes are not reflected in stable W isotope compositions (A). Frequent intrusions of mafic melts lead to local dehydration and re-fertilization of the crust with additional W (B). Low pH, high-T fluids locally (hole 1268A) led to complete replacement of serpentine by talc, associated with leaching of isotopically heavy W (C). Late, low-T oxidative surface alteration of serpentinized peridotites is characterized by progressive enrichment of U and W and decreasing  $\delta^{186/184}\text{W}$  (D).

## 4.5.2 The effect of different alteration styles on the stable W isotope composition

### 4.5.2.1 Hole 1256D

MORB-like  $\delta^{186/184}\text{W}$  values in most 1256D samples suggest that the process accounting for W enrichment during alteration did only marginally fractionate W isotopes. Moreover, the earliest recorded metamorphism along the spreading centre (Fig. 4.6 A & B) or in response to gabbroic dike intrusions (Fig. 4.6 C & D) are unlikely to cause significant stable W isotope fractionation because of the prevailing high-T environment.

Some samples from the sheeted dike section exhibit a tendency towards lighter stable W compositions, but only one sample is resolvably lighter than MORB (Figs. 4.4 A, 4.6 C). This sample is located at the interface between the granoblastic dikes and the sheeted dike section. This section is characterized by abundant chlorite-quartz-pyrite veins, which formed at temperatures as low as 250 °C (Alt et al., 2010, chapter 2, Table 4.1, Sample 187-2). Samples from higher crustal levels that are also characterized by slightly lower  $\delta^{186/184}\text{W}$  are intensively fractured and intersected by abundant veins of chlorite, anhydrite, pyrite, and minor quartz as well. This veining is restricted to initial on-axis cooling at temperatures around 200°C (Alt et al., 2010, Gao et al., 2012, Fig. 4.9 C). In the named section, alteration at ~ 200°C is also strongly reflected in the highest  $\delta^7\text{Li}$  and the lowest  $\delta^{18}\text{O}$  (Gao et al., 2012). With Li isotopes it was furthermore demonstrated that the alteration was under rock-dominated conditions ( $w/r < 1$ , Gao et al., 2012). It is highly likely, that this late-stage alteration at relatively low temperatures caused the preferential sequestration of isotopically light W in chlorite-anhydrite-pyrite veins. If so, the remaining fluid might be isotopically heavy, similar as in fluid-controlled arc settings (Kurzweil et al., 2019; Mazza et al., 2020).

#### 4.5.2.2. Leg 209

Mafic intrusive olivine-gabbro and diabase drilled at hole 1272A have MORB-like  $\delta^{186/184}\text{W}$  values of +0.070 ‰ and +0.074 ‰ and canonical W/Th of 0.09, highlighting that these portions are only slightly affected by hydrous alteration. Consistent with earlier studies (Kurzweil et al., 2019), the MORB-like  $\delta^{186/184}\text{W}$  values support that melt generation even in magma starved settings has no implications on the stable W isotope compositions (Fig. 4.7A). Mafic intrusives that were drilled at hole 1272A potentially represent the enriching component for W-rich peridotites from sites 1270 that were strongly affected by melt-rock interaction (Fig. 4.7B). In support of this view, the 1270 peridotites have  $\delta^{186/184}\text{W}$  values within the MORB range indicating that melt impregnation only marginally affected stable W isotope compositions. As presented earlier in chapter 3, dehydration in response to dikelet-intrusion may have led to localized fluid generation where W is selectively enriched over Th. If, despite the high temperatures, isotope fractionation occurred, potentially due to changes in coordination chemistry, the stable W isotope composition in the altered samples must have been initially significantly heavier than today. In this scenario, progressive serpentinization, with preferred fixation of lighter stable W isotopes potentially leads to lower  $\delta^{186/184}\text{W}$ , which might explain the wide scatter from + 0.055 to +0.125  $\delta^{186/184}\text{W}$  in samples from site 1270 (Table 4.1).

Peridotites from hole 1268A were subject to multiple stages of fluid-dominated serpentinization and locally intense, late-stage, pervasive talc alteration during Si metasomatism (Bach et al., 2004, Paulick et al., 2006; chapter 3). Serpentinized and talc-altered peridotites in Leg 209 are characterized by strongly positive Eu-anomalies (17.1 – 148), which reflect excessive overprinting by hydrothermal fluids (Bach et al., 2004, Paulick et al., 2006). This hydrothermal overprinting also accounts for selective W enrichment as indicated by elevated W/Th (29.2 – 208). Talc altered serpentinites from site 1268A show  $\delta^{186/184}\text{W}$  values between +0.024 ‰ and +0.042 ‰ that are significantly lower than the  $\delta^{186/184}\text{W}$  range of MORBs and serpentinites from site 1270 (Fig. 4.5), indicating resolvable stable W isotope fractionation during talc alteration (Figs. 4.5, 4.7C). Initial stages of talc alteration during Silica metasomatism are recorded over the whole depth range drilled at site 1268A (Kelemen et al., 2003, Bach et al., 2004, Paulick et al., 2006). The trigger phase for Silica metasomatism is a low pH fluid, of which the Si originates from the breakdown of pyroxene in peridotites and gabbros (Bach et al., 2004). As talc is a  $\text{Mg}^{2+}$ -layered silicate,  $\text{Fe}^{2+}$  is better incorporated into its crystal structure than  $\text{Fe}^{3+}$  (Deer et al., 2013). Thus, the grade of talc formation is reflected in systematically lowered  $\text{MgO}/\text{SiO}_2$  with simultaneously decreasing  $\text{Fe}^{3+}$  (wt.-%) and  $\text{Fe}_{\text{tot}}$  (wt.-%). Indeed, a negative co-variation of  $\text{Fe}^{3+}$  with W/Th and  $\delta^{186/184}\text{W}$  is observed (Fig. 4.9). This strongly suggests that the progressive formation of talc by Si metasomatism cause lighter  $\delta^{186/184}\text{W}$  due to the preferential leaching of heavy W isotopes. In summary, for hole 1268A

successive alteration events, involving initial serpentinization resulted in increasing W/Th but still MORB-like  $\delta^{186/184}\text{W}$ . The subsequent interaction with high  $a\text{SiO}_2$  fluids then caused preferential leaching of heavy stable W isotopes, reflected in decreasing  $\delta^{186/184}\text{W}$  and increasingly lower W/Th (Fig. 4.8B).

Dunites from site 1271A have experienced multiple stages of alteration (Kelemen et al., 2007, Paulick et al., 2006, Kelemen et al., 2004, Bach et al., 2004). As a result, all samples are enriched in W and U (Chapter 3). With progressive oxidative alteration, as reflected by increasing  $\text{Fe}_2\text{O}_3$  (wt.-%), the stable W isotope composition is lowered from  $\delta^{186/184}\text{W}$  of -0.002 ‰ to -0.071 ‰ (Fig. 4.9). As products of low-T oxidative seafloor weathering are known hosts for W (Chapter 3) and U (Bach et al., 2001, Hart et al., 1999), their formation is associated with fixation of isotopically light W (Fig. 4.10 D). Furthermore, the lowest  $\delta^{186/184}\text{W}$  originate from the uppermost drilled portions (< 1 mbsf), which is best accessible to seawater in a low-T weathering environment. This finding is in accord to the identification of stable U isotope fractionation in zones of oxidative alteration (Andersen et al., 2015). The significance of Fe-oxyhydroxides in these environments as controlling factor of stable isotope fractionation has been outlined in earlier studies, e.g., by Kashiwabara et al. (2017). They demonstrated how the change in W specification between dissolved  $\text{WO}_4^{2-}$  and adsorbed W lead to preferred fixation of isotopically light W, resulting in seawater with increasingly heavy stable W isotope composition. Whereas their study focuses on Fe-Mn crusts at the seafloor, the here presented results show further evidence for stable W isotope fractionation in low-T, oxidative alteration settings.

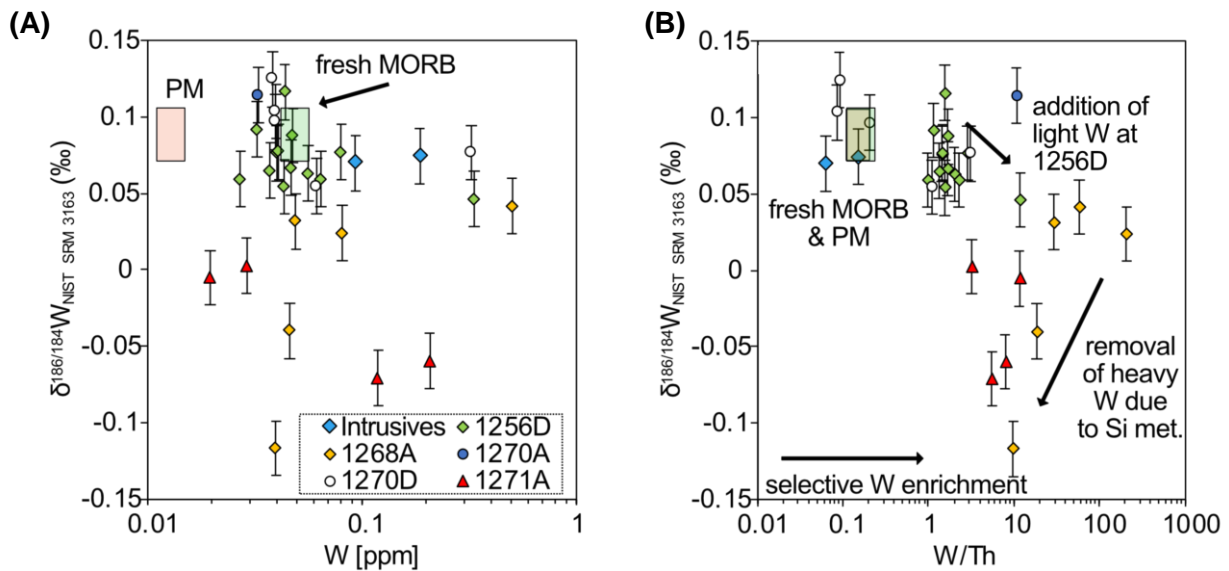


Figure 4.8: Co-variations of measured stable W isotope compositions with W concentrations and W/Th ratios. Neither the basaltic crust at hole 1256D, nor the serpentinized abyssal peridotites from Leg 209 show co-variations between their stable W isotope composition and W concentrations (A). At hole 1256D, stable W isotope compositions become lighter with increasing W/Th (B, Si met. = Silica metasomatism). In contrast, Leg 209 serpentinized samples of holes 1270A and D and insignificantly altered mafic rocks overlap with the mantle array, independent of their W/Th. In the extremely isotopically light peridotites of 1271A and 1268A, no connection between selective W enrichment and a lightening stable isotope composition is recorded (B). Two peridotites with elevated stable W isotope composition and one mafic dike are depleted in W and thus may hint at the sites where the W enriching the oceanic crust is originating from.

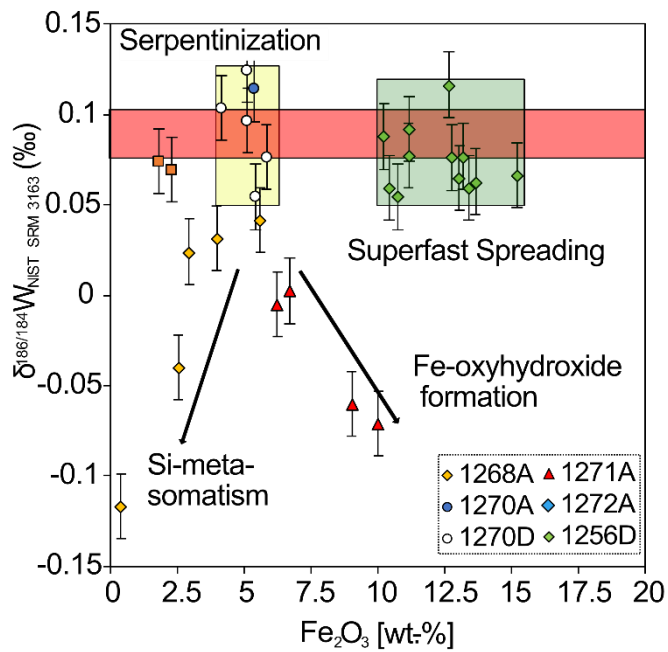


Figure 4.9: Effect of different late stage alteration processes, on the stable W isotopic compositions. Late stage pervasive talc alteration in hole 1268A is characterized by decreasing  $\text{Fe}_2\text{O}_3$  concentrations (Paulick et al, 2006). With increasing degree of alteration, the stable W isotope compositions become lighter, showing that heavy W is preferentially leached out. Seafloor weathering at site 1271A is, in contrast, mirrored by increasing  $\text{Fe}_2\text{O}_3$  concentration and increasingly light W isotope compositions. The two samples with the lightest W compositions both originate from very shallow depths (< 2 mbsf) and, thus, were most prone to weathering. Oceanic crust samples from hole 1256D show elevated  $\text{Fe}_2\text{O}_3$  due to their advanced magmatic evolution.

Since alteration intensity ceased relatively early (Alt et al., 2010, Harris et al, 2015), the overall alteration intensity is limited and stable W isotope fractionation is of lower magnitude.  $\text{Fe}_2\text{O}_3$  data for Leg 209 samples from Paulick et al., 2006.  $\text{Fe}_2\text{O}_3$  data for hole 1256D from Neo, et al., 2006.

#### 4.5.3 Implications on the source of seawater stable W isotope signature

The W concentration in seawater is significantly lower compared to the chemical similar Mo (Sohrin et al., 1999, 1987). Tungsten in seawater is furthermore isotopically very heavy ( $+0.545 \pm 0.051\text{‰}$ , Kurzweil et al., 2020). In earlier studies, it was shown how effective surface adsorption on Fe-Mn oxyhydroxides (Kashiwabara et al., 2017) potentially contributes to the heavy isotope signature of seawater W. The influence of oceanic crust alteration yet remains untested. Available examples for well-established isotope systems in seawater are Mo and U stable isotope fractionations (Andersen et al., 2015; Freymuth et al., 2015; Weyer et al., 2008). Under the oxygenated conditions of the modern ocean, dissolved U occurs as oxidized U(VI) and forms soluble uranyl carbonate complexes, resulting in a concentration of  $3.2 \text{ ng} \cdot \text{g}^{-1}$  (Ku et al., 1977) and a homogeneous  $\delta^{238}\text{U}$  of  $-0.390 \pm 0.010 \text{‰}$  (Andersen et al., 2015). Fractionation occurs when U is incorporated during oxidative alteration of oceanic crust and is characterized by  $\delta^{238}\text{U}$  between  $-0.436 \text{‰}$  and  $0.145\text{‰}$  whereas anoxic alteration results in significantly heavier signatures, averaging  $+0.164 \text{‰} \pm 0.086 \text{‰}$  (Andersen et al., 2015). Thus, stable U isotopes can be used as tracer to track RedOx conditions during oceanic crust alteration. In contrast to seawater W, seawater U is a major source of excess U in altered oceanic crust. In the sample set presented here only excursions to lower  $\delta^{186/184}\text{W}$  ( $-0.117$  to  $+0.077 \text{‰}$ ) from the mantle value of  $+0.085 \pm 0.019 \text{‰}$  (Kurzweil et al., 2019) have been identified. Heavier stable W isotope compositions could not be detected. It is thus concluded that changes in coordination during (a) adsorption of W at low-T seawater alteration and (b) leaching of heavy stable W isotopes during talc alteration results in fluids which get increasingly heavy during progressive alteration. Fluid flow through oceanic crust is one of the major mass fluxes on Earth, in total  $3.5 \cdot 10^{12} \text{ kg} \cdot \text{a}^{-1}$  of hot, black smoker fluids and  $6.4 \cdot 10^{14} \text{ kg} \cdot \text{a}^{-1}$  of cold ( $\sim 20 \text{ °C}$ ) fluids from colder venting circulate through the oceanic crust (Elderfield and Schultz, 1996). Hence, leaking of alteration fluids into the oceans over time led to an increasingly heavier  $\delta^{186/184}\text{W}$  composition of seawater. Important parameters to clarify in future studies are the isotopic state of hydrothermal vent fluids and the share of talc alteration and oxidative weathering in altered oceanic crust as both have potentially huge implications on the stable W composition of seawater. Based on the data presented here, it is likely that hydrothermal fluids are high in  $\delta^{186/184}\text{W}$  as well. Apart from talc alteration or low-grade oxidative weathering, numerous alteration processes (brucite dissolution, sulphide precipitation, saponite replacement) affect the mineral assemblage on smaller scales. The impact of those processes is unconstrained, yet. Moreover, it is still unclear which of Earth's geochemical reservoirs contributes in which proportion to the stable W isotope composition of the seawater. A remarkable difference between the isotopic systems of W and Mo is the fixation of heavy stable Mo isotopes in the most oxidative altered, parts of oceanic crust, indicating the incorporation of isotopically heavy, seawater-derived Mo into the upper crust during alteration (Freymuth et al., 2015). In contrast to W, isotope fractionation of Mo is limited during late-stage alteration (Freymuth et al., 2015)



#### 4.5.4 Implications for the understanding of the behaviour of W in subduction zones

Subduction zones are important areas of element recycling and redistribution between Earth's crust and mantle. Furthermore, the prograde dehydration of subducting serpentinites has been demonstrated to contribute significantly to the fluid budget of the subarc mantle (e.g. Morris et al., 1990; Plank and Langmuir, 1993; Noll et al., 1996; Inglis et al., 2017; Scambelluri and Philippot, 2001). It was shown before, how the isotope signatures of B, Li and Sr (Vils et al., 2009) and Cu (Wang et al., 2019) of the subducted slab is still reflected in the arc magma composition. Surveys on the behaviour of W in arc lavas (König et al. 2008, 2011) have revealed that W behaves highly mobile in subduction zone systems, particularly, if fluids from the subducted slab control the elemental budget in the sub-arc mantle. Tungsten enrichment in arc magmas is most pronounced where subducted sediments with high W concentrations are involved (e.g., Indonesia, Kermadec, Cyprus) and is less pronounced in arcs where negligible amounts of pelagic sediments are involved (e.g., W-Pacific arcs, König et al. 2011). During fluid enrichment, ratios of W/Th, W/U and W/Ta are elevated to various extents, depending on the type of subduction component involved (König et al., 2008, 2011; Bali et al., 2012). Since W mobilization by dehydration most likely causes stable isotope fractionation and subducted crust is, as showed above, light in stable isotopes, W isotope data provide a powerful tool for investigating material transport from the slab into the mantle wedge, and ultimately arc magmas (Mazza et al., 2020). Recent studies demonstrated that the range in  $\delta^{186/184}\text{W}$  values of arc lavas is significantly larger when compared to MORBs and OIBs (e.g., Kurzweil et al., 2019, Mazza et al., 2020). This larger variability was attributed to variable stable W isotope compositions of different subduction components, retention of light W in residual phases or to stable W isotope fractionation processes during subduction (Kurzweil et al., 2019, Mazza et al., 2020).

In some arc lava suites, where the W budget is controlled by melts from subducted mafic crust,  $\delta^{186/184}\text{W}$  values are close to the upper mantle value or only slightly elevated (e.g., Papua New Guinea, New Britain, +0.079 to +0.133 ‰; Kurzweil et al., 2019). In arc suites, where the W budget is controlled by subducted pelagic sediments (e.g., Sunda, Cyprus),  $\delta^{186/184}\text{W}$  values are significantly higher (Kurzweil et al., 2019). Consistently, most sediments being recycled into subduction zone show heavy stable W isotope compositions (Kurzweil et al., 2019). The element budget of Sunda arc lavas in Kurzweil et al. (2019) shows a large regional variability from sediment dominated (West Java) to being dominated by fluids from altered oceanic crust (Central/East Java, Handley et al., 2014). Whereas West Java volcanoes are characterized by MORB/OIB-like  $\delta^{186/184}\text{W}$  values between +0.061 and +0.081 ‰ (Kurzweil et al., 2019), low  $\delta^{186/184}\text{W}$  values (down to - 0.009 ‰) in some volcanoes from Central/East Java cannot be explained by the influence of isotopically heavy sediments. These low values require an alternative explanation. One suggestion is that the local subduction of basaltic basement (Roo Rise) affects the element budget of Central/East Java volcanoes (Handley et al., 2014) and possibly lowered the  $\delta^{186/184}\text{W}$  in the respective lavas (Kurzweil

et al. 2019). The here presented new data that show light stable W isotope compositions in Si-metasomatized and seafloor-weathered parts of altered oceanic crust may thus confirm that the subduction of altered oceanic crust (Roo Rise) had indeed lowered the stable W isotope composition of some arc lavas of Central/Eastern Java volcanoes. Alternatively, it was suggested that isotopically heavy W was preferentially mobilized by fluids, leaving the dehydrated slab with a light signature that is then tapped by arc lavas (Kurzweil et al., 2019; Mazza et al., 2020). Indeed, observations from arc lavas in Japan, Izu and Sangihe suggested that decreasing  $\delta^{186/184}\text{W}$  seem to correlate with increasing distance from the trench (Mazza et al., 2020).

In summary, not only subduction zone processes have an impact on the stable W isotope composition of arc magmas, but also inherited signatures from subduction components. A closer look at stable W isotope fractionation in altered oceanic crust reveals that isotope fractionation only occurs during low-T oxidative alteration and during high-T talc formation, but not during high-T serpentinization or melt intrusion. If the light W isotope signatures of arc lavas are indeed inherited from subducted altered oceanic crust, this would imply (1) that the major part of the W inventory underwent low-T or talc alteration and that (2) a significant amount of isotopically heavy W was transferred from oceanic crust to seawater. Better resolving the mass balance of W in seawater might therefore ultimately help to constrain mass fluxes from alteration of oceanic crust and also the W isotope budget of altered oceanic crust entering the subduction factory. Furthermore, future research needs to clarify how much of the oceanic crust is affected by low-T alteration processes or talc alteration. Answering this question might also help to constrain the total mass fluxes between the subducted slab and the mantle wedge below island arcs.

## 4.6 Conclusions

In this chapter, the first stable W isotope data for different types of altered oceanic crust are presented. The sample set comprises highly serpentinized abyssal peridotites, formed at slow-spreading rates, from ODP Leg 209 of the Mid-Atlantic Ridge, and moderately altered, mainly basaltic crust that formed at the super-fast spreading East-Pacific Rise of IODP hole 1256D (Kelemen et al., 2004, Wilson et al., 2006). Applying the  $^{180}\text{W}$ - $^{183}\text{W}$  double spike protocol, significant W isotopic variations that can be linked to distinct alteration processes in different types of altered oceanic crust have been resolved.

Samples from the effusive sheet and massive flows, gabbroic intrusions, and the separating basaltic layer of hole 1256D mainly show MORB-like isotope compositions ( $\delta^{186/184}\text{W}$  between +0.059 ‰ and +0.116 ‰). Tungsten enrichment in these rocks is related to on-ridge hydrothermal fluid flow which transports W from deeper levels into the intrusive and extrusive section with only negligible effects on the stable W isotope compositions. Only one sample from the sheeted dike complex with a  $\delta^{186/184}\text{W}$  of +0.046 ‰ is slightly isotopically lighter than MORB. These findings indicate that the formation of minerals from late chlorite-quartz-pyrite veining preferentially incorporated light stable W isotopes.

The stable W isotopic signatures of highly serpentinized peridotites from site 1270 drilled in ODP Leg 209 show  $\delta^{186/184}\text{W}$  between +0.077 and +0.104 ‰, which is close to the MORB value of  $0.088 \pm 0.17$  ‰. This indicates only small and not resolvable stable W isotope fractionation during mobilization (leaching) and secondary enrichment (serpentinization). In contrast, high temperature alteration during Si metasomatism and low temperature seafloor weathering of already W-enriched oceanic crust caused significant and resolvable stable W isotope fractionation. Talc alteration during Si metasomatism at high temperatures ( $> 400^\circ\text{C}$ ; Bach et al., 2004, Paulick et al., 2006) is characterized by decreasing  $\text{Fe}_2\text{O}_3$  (Paulick et al., 2006) coupled with decreasing W/Th and decreasing  $\delta^{186/184}\text{W}$  values relative to the host serpentinite (Fig. 4.9). Thus, the transformation of serpentine to talc by hot, low-pH and high  $a\text{SiO}_2$  fluids releases isotopically heavy W to a circulating fluid. At low-T oxidative seafloor alteration,  $\text{Fe}_2\text{O}_3$  contents increase but  $\delta^{186/184}\text{W}$  decreases (Fig. 4.9). Seafloor alteration is thus associated with the preferred retention of isotopically light W, leaving behind isotopically heavy fluids. Based on the ubiquitous mantle-like or lighter stable W isotope composition of the altered oceanic crust, the missing isotopically heavy counterpart is most likely the hydrothermal fluid itself. Thus, leaking of low- and high-T hydrothermal waters that interacted with oceanic crust are a likely source for the heavy stable W isotope composition of seawater.

Most parts of altered oceanic crust selectively gained W as indicated by elevated W/Th. The source of this additional W could be hydrothermal fluids, seawater and cover sediments. Seawater W and sedimentary W can be excluded as source as both are isotopically heavy.

Thus, the W source in altered oceanic crust is most likely to be found in the deeper crust, where W is leached out and precipitated in the serpentinized portions of altered oceanic crust at slow spreading zones (Leg 209) and in deep, plutonic regions of super-fast spreading zones (Hole 1256D). Moreover, frequent intrusions of mafic dikes have fed the system with additional W. Potential root zones of W enrichment have in common that they are predominantly affected by high-temperature processes which is not necessarily reflected in the stable isotope record. Indeed, some samples in Leg 209 that meet these criteria and show canonical W/Th, but no stable W isotope fractionation were identified.

In summary, it is proposed that altered oceanic crust has a somewhat lighter stable W isotope composition relative to fresh MORBs or OIBs. This has important implications on the understanding of stable W isotope characteristics in arc settings. The presented data show, that the tendency to lighter stable W isotope compositions in some arc lavas is not unambiguously related to subduction zone processes but can also originate from the dehydrated crust itself. A better understanding of the mass balance of the W stable isotope budget of seawater and the oceanic crust-seawater interface would help constrain fluxes between altered oceanic crust, seawater and arc lavas.

The precise study of the stable W isotope composition may be a future tool to investigate the prevailing alteration styles in oceanic crust. Its application to vein-minerals or secondary sulphides can furthermore help clarifying the behaviour of W during alteration on smaller scales.

# Bibliography

- Albarede, F., Michard, A., 1986. Transfer of continental Mg, S, O and U to the mantle through hydrothermal alteration of the oceanic crust. *Chem. Geol.* 57, 1–15.
- Allen, D.E., Seyfried, W.E., 2005. REE controls in ultramafic hosted MOR hydrothermal systems: An experimental study at elevated temperature and pressure. *Geochim. Cosmochim. Acta* 69, 675–683. <https://doi.org/10.1016/j.gca.2004.07.016>
- Allen, D.E., Seyfried, W.E., 2003. Compositional controls on vent fluids from ultramafic-hosted hydrothermal systems at mid-ocean ridges: An experimental study at 400°C, 500 bars. *Geochim. Cosmochim. Acta*. [https://doi.org/10.1016/S0016-7037\(02\)01173-0](https://doi.org/10.1016/S0016-7037(02)01173-0)
- Alt, J.C., 2004. Alteration of the upper oceanic crust: mineralogy, chemistry, and processes, in: Davis, E.E., Elderfield, H. (Eds.), *Hydrogeology of the Oceanic Lithosphere*. Cambridge University Press, pp. 495–533.
- Alt, J.C., Laverne, C., Coggon, R.M., Teagle, D.A.H., Banerjee, N.R., Morgan, S., Smith-Duque, C.E., Harris, M., Galli, L., 2010. Subsurface structure of a submarine hydrothermal system in ocean crust formed at the East Pacific Rise, ODP/IODP Site 1256. *Geochemistry, Geophys. Geosystems* 11, 1–28. <https://doi.org/10.1029/2010GC003144>
- Alt, J.C., Laverne, C., Vanko, D.A., Tartarotti, P., Teagle, D.A.H., Bach, W., Zuleger, E., Erzinger, J., Honnorez, J., Pezard, P.A., Becker, K., Salisbury, M.H., Wilkens, R.H., 1996. 34. Hydrothermal alteration of a section of upper oceanic crust in the eastern equatorial pacific: A synthesis of results from site 504 (DSDP Legs 69, 70, and 83, and ODP Legs 111, 137, 140, and 148), in: *Proceedings of the Ocean Drilling Program, Scientific Results*. pp. 417–434.
- Alt, J.C., Teagle, D.A.H., 2003. Hydrothermal alteration of upper oceanic crust formed at a fast-spreading ridge: Mineral, chemical, and isotopic evidence from ODP Site 801. *Chem. Geol.* 201, 191–211. [https://doi.org/10.1016/S0009-2541\(03\)00201-8](https://doi.org/10.1016/S0009-2541(03)00201-8)
- Alt, J.C., Teagle, D.A.H., 1999. The uptake of carbon during alteration of ocean crust [10.1016/S0016-7037\(99\)00123-4](https://doi.org/10.1016/S0016-7037(99)00123-4): *Geochimica et Cosmochimica Acta* | ScienceDirect.com. *Geochim. Cosmochim. Acta* 63, 1527–1535. [https://doi.org/10.1016/S0016-7037\(99\)00123-4](https://doi.org/10.1016/S0016-7037(99)00123-4)

- Andersen, M.B., Elliott, T., Freymuth, H., Sims, K.W.W., Niu, Y., Kelley, K.A., 2015. The terrestrial uranium isotope cycle. *Nature* 517, 356–359. <https://doi.org/10.1038/nature14062>
- Andrews, A.J., 1980. Saponite and celadonite in layer 2 basalts, DSDP Leg 37. *Contrib. to Mineral. Petrol.* 73, 323–340. <https://doi.org/10.1007/BF00376627>
- Arevalo, R., McDonough, W.F., 2008. Tungsten geochemistry and implications for understanding the Earth's interior. *Earth Planet. Sci. Lett.* 272, 656–665. <https://doi.org/10.1016/j.epsl.2008.05.031>
- Arnórsson, S., Óskarsson, N., 2007. Molybdenum and tungsten in volcanic rocks and in surface and <100 °C ground waters in Iceland. *Geochim. Cosmochim. Acta* 71, 284–304. <https://doi.org/10.1016/j.gca.2006.09.030>
- Bach, W., Alt, J.C., Niu, Y., Humphris, S.E., Erzinger, J., Dick, H.J.B., 2001. The geochemical consequences of late-stage low-grade alteration of lower ocean crust at the SW Indian Ridge: Results from ODP Hole 735B (Leg 176). *Geochim. Cosmochim. Acta* 65, 3267–3287. [https://doi.org/10.1016/S0016-7037\(01\)00677-9](https://doi.org/10.1016/S0016-7037(01)00677-9)
- Bach, W., Bernhard, P.E., Hart, S.R., Blusztajn, J.S., 2003. Geochemistry of hydrothermally altered oceanic crust: DSDP/ODP Hole 504B-Implications for seawater-crust exchange budgets and Sr-and Pb-isotopic evolution of the mantle. *Geochemistry, Geophys. Geosystems* 4, 40–55. <https://doi.org/10.1029/2002GC000419>
- Bach, W., Erzinger, J., Alt, J.C., Teagle, D.A.H., 1996. Chemistry of the Lower Sheeted Dike Complex, Hole 504B (Leg 148): Influence of Magmatic Differentiation and Hydrothermal Alteration, in: *Proceedings of the Ocean Drilling Program, 148 Scientific Results*. <https://doi.org/10.2973/odp.proc.sr.148.114.1996>
- Bach, W., Garrido, C.J., Paulick, H., Harvey, J., Rosner, M., 2004. Seawater-peridotite interactions: First insights from ODP Leg 209, MAR 15°N. *Geochemistry, Geophys. Geosystems* 5. <https://doi.org/10.1029/2004GC000744>
- Bali, E., Keppler, H., Audetat, A., 2012. The mobility of W and Mo in subduction zone fluids and the Mo-W-Th-U systematics of island arc magmas. *Earth Planet. Sci. Lett.* 351–352, 195–207. <https://doi.org/10.1016/j.epsl.2012.07.032>

- Bennett, C.L., Halpern, M., Hinshaw, G., Jarosik, N., Kogut, A., Limon, M., Meyer, S.S., Page, L., Spergel, D.N., Tucker, G.S., Wollack, E., Wright, E.L., Barnes, C., Greason, M.R., Hill, R.S., Komatsu, E., Nolte, M.R., Odegard, N., Peiris, H. V., Verde, L., Weiland, J.L., 2003. First-Year Wilkinson Microwave Anisotropy Probe ( WMAP ) Observations: Preliminary Maps and Basic Results . *Astrophys. J. Suppl. Ser.* 148, 1–27. <https://doi.org/10.1086/377253>
- Bigeleisen, J., Mayer, M.G., 1947. Calculation of Equilibrium Constants for Isotopic Exchange Reactions. *J. Chem. Phys.* 15, 261–267. <https://doi.org/10.1063/1.1746492>
- Carbotte, S.M., Macdonald, K.C., 1994. The axial topographic high at intermediate and fast spreading ridges. *Earth Planet. Sci. Lett.* 128, 85–97. [https://doi.org/10.1016/0012-821X\(94\)90137-6](https://doi.org/10.1016/0012-821X(94)90137-6)
- Carlson, R.L., Hilde, T.W.C., Uyeda, S., 1983. The driving mechanism of plate tectonics: Relation to age of the lithosphere at trenches. *Geophys. Res. Lett.* 10, 297–300. <https://doi.org/10.1029/GL010i004p00297>
- Caruso, L.J., Chernosky, J.V.J., 1979. The stability of lizardite. *Can. Mineral.*
- Cruywagen, J.J., 1999. Protonation, Oligomerization, and Condensation Reactions of Vanadate (V), Molybdate(VI), and Tungstate(VI). *Adv. Inorg. Chem.* 49. <https://doi.org/0898-8838/00>
- Deer, W.A., Howie, R.A., Zussman, J., 2013. Talc, in: *An Introduction to the Rock-Forming Minerals*. Mineralogical Society, London, pp. 204–207.
- Dziony, W., Koepke, J., Holtz, F., 2008. Data report: petrography and phase analyses in lavas and dikes from Hole 1256D (ODP Leg 206 and IODP Expedition 309, East Pacific Rise) 309. <https://doi.org/10.2204/iodp.proc.309312.201.2008>
- Elderfield, H., Schultz, A., 1996. Mid-ocean ridge hydrothermal fluxes and the chemical composition of the ocean. *Annu. Rev. Earth Planet. Sci.* 24, 191–224. <https://doi.org/10.1146/annurev.earth.24.1.191>
- Elthon, D., 1981. Metamorphism in oceanic spreading centres, in: Emiliani, C. (Ed.), *The Oceanic Lithosphere*. Wiley, New York, pp. 285–303.
- Flower, M.F.J., 1981. Thermal and kinematic control on ocean-ridge magma fractionation: contrasts between Atlantic and Pacific spreading axes. *J. Geol. Soc. London.* 138, 695–712. <https://doi.org/10.1144/gsjgs.138.6.0695>

- Foley, S.F., Barth, M.G., Jenner, G.A., 2000. Rutile/melt partition coefficients for trace elements and an assessment of the influence of rutile on the trace element characteristics of subduction zone magmas. *Geochim. Cosmochim. Acta* 64, 933–938. <https://doi.org/0016-7037/00>
- Fonseca, R.O.C., Mallmann, G., Sprung, P., Sommer, J.E., Heuser, A., Speelmanns, I.M., Blanchard, H., 2014. Redox controls on tungsten and uranium crystal/silicate melt partitioning and implications for the U/W and Th/W ratio of the lunar mantle. *Earth Planet. Sci. Lett.* 404, 1–13. <https://doi.org/10.1016/j.epsl.2014.07.015>
- France, L., Ildefonse, B., Koepke, J., 2009. Interactions between magma and hydrothermal system in Oman ophiolite and in IODP Hole 1256D: Fossilization of a dynamic melt lens at fast spreading ridges. *Geochemistry, Geophys. Geosystems* 10. <https://doi.org/10.1029/2009GC002652>
- France, L., Koepke, J., Ildefonse, B., Cichy, S.B., Deschamps, F., 2010. Hydrous partial melting in the sheeted dike complex at fast spreading ridges: Experimental and natural observations. *Contrib. to Mineral. Petrol.* 160, 683–704. <https://doi.org/10.1007/s00410-010-0502-6>
- Frei, D., Liebscher, A., Franz, G., Dulski, P., 2004. Trace Element Geochemistry of Epidote Minerals. *Rev. Mineral. Geochemistry* 56, 553–605. <https://doi.org/1529-6466/04/0056-0012>
- Freyruth, H., Vils, F., Willbold, M., Taylor, R.N., Elliott, T., 2015. Molybdenum mobility and isotopic fractionation during subduction at the Mariana arc. *Earth Planet. Sci. Lett.* <https://doi.org/10.1016/j.epsl.2015.10.006>
- Fujimaki, H., 1986. Partition coefficients of Hf, Zr, and REE between zircon, apatite, and liquid. *Contrib. to Mineral. Petrol.* 94, 42–45. <https://doi.org/10.1007/BF00371224>
- Fujiwara, T., Lin, J., Matsumoto, T., Kelemen, P.B., Tsucholke, B.E., Casey, J.F., 2003. Crustal evolution of the mid-atlantic ridge near the fifteen-twenty fracture zone in the last 5 Ma. *Geochemistry, Geophys. Geosystems* 4. <https://doi.org/10.1029/2002GC000364>
- Gale, A., Dalton, C.A., Langmuir, C.H., Su, Y., Schilling, J.G., 2013. The mean composition of ocean ridge basalts. *Geochemistry, Geophys. Geosystems* 14, 489–518. <https://doi.org/10.1029/2012GC004334>



- Gao, Y., Vils, F., Cooper, K.M., Banerjee, N., Harris, M., Hoefs, J., Teagle, D.A.H., Casey, J.F., Elliott, T., Laverne, C., Alt, J.C., Muehlenbachs, K., 2012. Downhole variation of lithium and oxygen isotopic compositions of oceanic crust at East Pacific Rise, ODP Site 1256. *Geochemistry, Geophys. Geosystems* 13. <https://doi.org/10.1029/2012GC004207>
- Godard, M., Lagabrielle, Y., Alard, O., Harvey, J., 2008. Geochemistry of the highly depleted peridotites drilled at ODP Sites 1272 and 1274 (Fifteen-Twenty Fracture Zone, Mid-Atlantic Ridge): Implications for mantle dynamics beneath a slow spreading ridge. *Earth Planet. Sci. Lett.* 267, 410–425. <https://doi.org/10.1016/j.epsl.2007.11.058>
- Handley, H.K., Blichert-toft, J., Gertisser, R., Macpherson, C.G., Turner, S.P., Zaennudin, A., Abdurrachman, M., 2014. Insights from Pb and O isotopes into along-arc variations in subduction inputs and crustal assimilation for volcanic rocks in Java, Sunda arc, Indonesia. *Geochim. Cosmochim. Acta.* <https://doi.org/10.1016/j.gca.2014.04.025>
- Harper, C.L., Jacobsen, S.B., 1996. Evidence for  $^{182}\text{Hf}$  in the early Solar System and constraints on the timescale of terrestrial accretion and core formation. *Geochim. Cosmochim. Acta.* [https://doi.org/10.1016/0016-7037\(96\)00027-0](https://doi.org/10.1016/0016-7037(96)00027-0)
- Harris, M., Coggon, R.M., Smith-Duque, C.E., Cooper, M.J., Milton, J.A., Teagle, D.A.H., 2015. Channelling of hydrothermal fluids during the accretion and evolution of the upper oceanic crust: Sr isotope evidence from ODP Hole 1256D. *Earth Planet. Sci. Lett.* 416, 56–66. <https://doi.org/10.1016/j.epsl.2015.01.042>
- Harris, M., Coggon, R.M., Wood, M., Smith-Duque, C.E., Henstock, T.J., Teagle, D.A.H., 2017. Hydrothermal cooling of the ocean crust: Insights from ODP Hole 1256D. *Earth Planet. Sci. Lett.* 462, 110–121. <https://doi.org/10.1016/j.epsl.2017.01.010>
- Hart, S.R., Blusztajn, J., Dick, H.J.B., Meyer, P.S., Muehlenbachs, K., 1999. The fingerprint of seawater circulation in a 500-meter section of ocean crust gabbros. *Geochim. Cosmochim. Acta.* [https://doi.org/10.1016/s0016-7037\(99\)00309-9](https://doi.org/10.1016/s0016-7037(99)00309-9)
- Hart, S.R., Staudigel, H., 1982. The control of alkalis and uranium in seawater by ocean crust alteration. *Earth Planet. Sci. Lett.* 58, 202–212. [https://doi.org/10.1016/0012-821X\(82\)90194-7](https://doi.org/10.1016/0012-821X(82)90194-7)
- Harvey, J., Gannoun, A., Burton, K.W., Rogers, N.W., Alard, O., Parkinson, I.J., 2006. Ancient melt extraction from the oceanic upper mantle revealed by Re-Os isotopes in abyssal peridotites from the Mid-Atlantic ridge. *Earth Planet. Sci. Lett.* <https://doi.org/10.1016/j.epsl.2006.02.031>

- Höfig, T.W., Geldmacher, J., Hoernle, K., Hauff, F., Duggen, S., Garbe-Schönberg, D., 2014. From the lavas to the gabbros: 1.25km of geochemical characterization of upper oceanic crust at ODP/IODP Site 1256, eastern equatorial Pacific. *Lithos* 210–211, 289–312. <https://doi.org/10.1016/j.lithos.2014.08.013>
- Huang, J., Ke, S., Gao, Y., Xiao, Y., Li, S., 2015. Magnesium isotopic compositions of altered oceanic basalts and gabbros from IODP site 1256 at the East Pacific Rise. *Lithos*. <https://doi.org/10.1016/j.lithos.2015.06.009>
- Hulsbosch, N., Boiron, M.C., Dewaele, S., Muchez, P., 2016. Fluid fractionation of tungsten during granite-pegmatite differentiation and the metal source of peribatholithic W quartz veins: Evidence from the Karagwe-Ankole Belt (Rwanda). *Geochim. Cosmochim. Acta* 175, 299–318. <https://doi.org/10.1016/j.gca.2015.11.020>
- Inglis, E.C., Debret, B., Burton, K.W., Millet, M.A., Pons, M.L., Dale, C.W., Bouilhol, P., Cooper, M., Nowell, G.M., McCoy-West, A.J., Williams, H.M., 2017. The behavior of iron and zinc stable isotopes accompanying the subduction of mafic oceanic crust: A case study from Western Alpine ophiolites. *Geochemistry, Geophys. Geosystems*. <https://doi.org/10.1002/2016GC006735>
- Johannes, W., 1968. Experimental investigation of the reaction forsterite + H<sub>2</sub>O  $\rightleftharpoons$  serpentine + brucite. *Contrib. to Mineral. Petrol.* <https://doi.org/10.1007/BF00389413>
- Jöns, N., Bach, W., Klein, F., 2010. Magmatic influence on reaction paths and element transport during serpentinization 274, 196–211. <https://doi.org/10.1016/j.chemgeo.2010.04.009>
- Kadko, D., 1993. An assessment of the effect of chemical scavenging within submarine hydrothermal plumes upon ocean geochemistry. *Earth Planet. Sci. Lett.* 120, 361–374. [https://doi.org/10.1016/0012-821X\(93\)90250-D](https://doi.org/10.1016/0012-821X(93)90250-D)
- Kashiwabara, T., Kubo, S., Tanaka, M., Senda, R., Iizuka, T., Tanimizu, M., Takahashi, Y., 2017. Stable isotope fractionation of tungsten during adsorption on Fe and Mn (oxyhydr)oxides. *Geochim. Cosmochim. Acta* 204, 52–67. <https://doi.org/10.1016/j.gca.2017.01.031>
- Kashiwabara, T., Takahashi, Y., Marcus, M.A., Uruga, T., Tanida, H., Terada, Y., Usui, A., 2013. Tungsten species in natural ferromanganese oxides related to its different behavior from molybdenum in oxic ocean. *Geochim. Cosmochim. Acta* 106, 364–378. <https://doi.org/10.1016/j.gca.2012.12.026>

- Kearey, P., Klepeis, K.A., Vine, F.J., 2009. Global tectonics, Wiley-Blackwell.  
<https://doi.org/10.1038/236261b0>
- Kelemen, P.B., Kikawa, E., Miller, D.J., 2007. Leg 209 Summary: Processes in a 20-km-Thick Conductive Boundary Layer beneath the Mid-Atlantic Ridge, 14°–16°N. Proc. Ocean Drill. Program, 209 Sci. Results 209.  
<https://doi.org/10.2973/odp.proc.sr.209.001.2007>
- Kelemen, P.B., Kikawa, E., Miller, D.J., 2004. Leg 209 Summary. Proc. Ocean Drill. Program, Initial Reports 209, 139. <https://doi.org/doi:10.2973/odp.proc.ir.209.101.2004>
- Kessel, R., Schmidt, M.W., Ulmer, P., Pettke, T., 2005. Trace element signature of subduction-zone fluids, melts and supercritical liquids at 120-180 km depth. *Nature* 437, 724–727.  
<https://doi.org/10.1038/nature03971>
- Kirkland, C.L., Smithies, R.H., Taylor, R.J.M., Evans, N., McDonald, B., 2015. Zircon Th/U ratios in magmatic environs. *Lithos* 212–215, 397–414.  
<https://doi.org/10.1016/j.lithos.2014.11.021>
- Kishida, K., Sohrin, Y., Okamura, K., Ishibashi, J. ichiro, 2004. Tungsten enriched in submarine hydrothermal fluids. *Earth Planet. Sci. Lett.* 222, 819–827.  
<https://doi.org/10.1016/j.epsl.2004.03.034>
- Klein, F., Grozeva, N.G., Seewald, J.S., McCollom, T.M., Humphris, S.E., Moskowitz, B., Berquó, T.S., Kahl, W.A., 2015. Fluids in the Crust. Experimental constraints on fluid-rock reactions during incipient serpentinization of harzburgite. *Am. Mineral.*  
<https://doi.org/10.2138/am-2015-5112>
- Kleine, T., Mezger, K., Münker, C., Palme, H., Bischoff, A., 2004. <sup>182</sup>Hf-<sup>182</sup>W isotope systematics of chondrites, eucrites, and martian meteorites: Chronology of core formation and early mantle differentiation in Vesta and Mars. *Geochim. Cosmochim. Acta* 68, 2935–2946. <https://doi.org/10.1016/j.gca.2004.01.009>
- Kleine, T., Münker, C., Mezger, K., Palme, H., 2002. Rapid accretion and early core formation on asteroids and the terrestrial planets from Hf-W chronometry. *Nature* 418, 952–955.  
<https://doi.org/10.1038/nature00982>
- Klemme, S., Prowatke, S., Hametner, K., Günther, D., 2005. Partitioning of trace elements between rutile and silicate melts: Implications for subduction zones. *Geochim. Cosmochim. Acta* 69, 2361–2371. <https://doi.org/10.1016/j.gca.2004.11.015>

- Koepke, J., Christie, D.M., Dziony, W., Holtz, F., Lattard, D., MacLennan, J., Park, S., Scheibner, B., Yamasaki, T., Yamazaki, S., 2008. Petrography of the dike-gabbro transition at IODP Site 1256 (equatorial Pacific): The evolution of the granoblastic dikes. *Geochemistry, Geophys. Geosystems* 9. <https://doi.org/10.1029/2008GC001939>
- Koepke, J., France, L., Miller, T., Faure, F., Goetze, N., Dziony, W., Ildefonse, B., 2011. Gabbros from IODP Site 1256, equatorial Pacific: Insight into axial magma chamber processes at fast spreading ocean ridges. *Geochemistry, Geophys. Geosystems* 12. <https://doi.org/10.1029/2011GC003655>
- König, S., Münker, C., Hohl, S., Paulick, H., Barth, A.R., Lagos, M., Pfänder, J., Büchl, A., 2011. The Earth's tungsten budget during mantle melting and crust formation. *Geochim. Cosmochim. Acta* 75, 2119–2136. <https://doi.org/10.1016/j.gca.2011.01.031>
- König, S., Münker, C., Schuth, S., Garbe-Schönberg, D., 2008. Mobility of tungsten in subduction zones. *Earth Planet. Sci. Lett.* 274, 82–92. <https://doi.org/10.1016/j.epsl.2008.07.002>
- König, S., Schuth, S., Luguet, A., 2010. Boninites as windows into trace element mobility in subduction zones 74, 684–704. <https://doi.org/10.1016/j.gca.2009.10.011>
- Ku, T.L., Knauss, K.G., Mathieu, G.G., 1977. Uranium in open ocean: concentration and isotopic composition. *Deep. Res.* [https://doi.org/10.1016/0146-6291\(77\)90571-9](https://doi.org/10.1016/0146-6291(77)90571-9)
- Kurzweil, F., Archer, C., Wille, M., Schoenberg, R., Münker, C., Dellwig, O., 2020. The stable tungsten isotope composition of seawater and Mn-rich sediments from the Baltic Sea, in: *Goldschmidt 2020 Abstract*.
- Kurzweil, F., Münker, C., Grupp, M., Braukmüller, N., Fechtner, L., Christian, M., Hohl, S. V., Schoenberg, R., 2019. The stable tungsten isotope composition of modern igneous reservoirs. *Geochim. Cosmochim. Acta* 251, 176–191. <https://doi.org/10.1016/j.gca.2019.02.025>
- Kurzweil, F., Münker, C., Tusch, J., Schoenberg, R., 2018. Accurate stable tungsten isotope measurements of natural samples using a 180W-183W double-spike. *Chem. Geol.* 476, 407–417. <https://doi.org/10.1016/j.chemgeo.2017.11.037>
- Lamadrid, H.M., Rimstidt, J.D., Schwarzenbach, E.M., Klein, F., Ulrich, S., Dolocan, A., Bodnar, R.J., 2017. Effect of water activity on rates of serpentinization of olivine. *Nat. Commun.* <https://doi.org/10.1038/ncomms16107>

- Lassner, E., Schubert, W.-D., 1999. Tungsten: properties, chemistry, technology of the element, alloys, and chemical compounds. Kluwer Academic / Plenum Publishers, New York, Boston, Dordrecht, London, Moscow.
- Laverne, C., Grauby, O., Alt, J.C., Bohn, M., 2006. Hydroschorlomite in altered basalts from Hole 1256D, ODP Leg 206: The transition from low-temperature to hydrothermal alteration. *Geochemistry, Geophys. Geosystems* 7, 1–29. <https://doi.org/10.1029/2005GC001180>
- Luo, X., Rehkämper, M., Lee, D.C., Halliday, A.N., 1997. High precision  $^{230}\text{Th}/^{232}\text{Th}$  and  $^{234}\text{U}/^{238}\text{U}$  measurements using energy-filtered ICP magnetic sector multiple collector mass spectrometry. *Int. J. Mass Spectrom. Ion Process.* [https://doi.org/10.1016/s0168-1176\(97\)00136-5](https://doi.org/10.1016/s0168-1176(97)00136-5)
- Macdonald, K.C., 1982. Mid-Ocean Ridges: Fine Scale Tectonic, Volcanic and Hydrothermal Processes Within the Plate Boundary Zone. *Annu. Rev. Earth Planet. Sci.* 10, 155–190. <https://doi.org/https://doi.org/10.1146/annurev.ea.10.050182.001103>
- Manning, D.A.C., Henderson, P., 1984. The behaviour of tungsten in granitic melt-vapour systems. *Contrib. to Mineral. Petrol.* 86, 286–293. <https://doi.org/10.1007/BF00373674>
- Marschall, H.R., Altherr, R., Rüpke, L., 2007. Squeezing out the slab - modelling the release of Li, Be and B during progressive high-pressure metamorphism. *Chem. Geol.* 239, 323–335. <https://doi.org/10.1016/j.chemgeo.2006.08.008>
- Mazza, S.E., Stracke, A., Gill, J.B., Kimura, J.I., Kleine, T., 2020. Tracing dehydration and melting of the subducted slab with tungsten isotopes in arc lavas. *Earth Planet. Sci. Lett.* 530, 115942. <https://doi.org/10.1016/j.epsl.2019.115942>
- McArthur, J.M., Howarth, R.J., Bailey, T.R., 2001. Strontium isotope stratigraphy: LOWESS version 3: Best fit to the marine Sr-isotope curve for 0-509 Ma and accompanying look-up table for deriving numerical age. *J. Geol.* 109, 155–170. <https://doi.org/10.1086/319243>
- Michael, P.J., Langmuir, C.H., Dick, H.J.B., Snow, J.E., Goldstein, S.L., Graham, D.W., Lehnert, K., Kurras, G., Jokat, W., Mühe, R., Edmonds, H.N., 2003. Magmatic and amagmatic seafloor generation at the ultraslow-spreading Gakkel ridge, Arctic Ocean. *Nature* 423, 956–961. <https://doi.org/10.1038/nature01704>
- Michard, A., Albarède, F., Michard, G., Minster, J.F., Charlou, J.L., 1983. Rare-earth elements and uranium in high-temperature solutions from east pacific rise hydrothermal vent field (13 °N). *Nature.* <https://doi.org/10.1038/303795a0>

- Moody, J.B., 1976. Serpentinization : a review 125–138.
- Morris, J.D., Leeman, W.P., Tera, F., 1990. The subducted component in island arc lavas: Constraints from Be isotopes and B-Be systematics. *Nature* 344, 31–36. <https://doi.org/10.1038/344031a0>
- Müller, R.D., Sdrolias, M., Gaina, C., Roest, W.R., 2008. Age, spreading rates, and spreading asymmetry of the world's ocean crust. *Geochemistry, Geophys. Geosystems* 9, n/a-n/a. <https://doi.org/10.1029/2007GC001743>
- Münker, C., Pfänder, J.A., Weyer, S., Büchl, A., Kleine, T., Mezger, K., 2003. Evolution of planetary cores and the Earth-Moon system from Nb/Ta systematics. *Science* (80-. ). <https://doi.org/10.1126/science.1084662>
- Münker, C., Weyer, S., Scherer, E., Mezger, K., 2001. Separation of high field strength elements (Nb, Ta, Zr, Hf) and Lu from rock samples for MC-ICPMS measurements. *Geochemistry, Geophys. Geosystems* 2. <https://doi.org/10.1029/2001GC000183>
- Neo, N., Yamazaki, S., Miyashita, S., 2009. Data report: bulk rock compositions of samples from the IODP Expedition 309/312 sample pool, ODP Hole 1256D. *Proc. Integr. Ocean Drill. Program, Sci. Result* 309/312, 312. <https://doi.org/10.2204/iodp.proc.309312.204.2009>
- Newman, S., Finkel, R.C., MacDougall, J.D., 1983. <sup>230</sup>Th-<sup>238</sup>U disequilibrium systematics in oceanic tholeiites from 21°N on the East Pacific Rise. *Earth Planet. Sci. Lett.* 65, 17–33. [https://doi.org/10.1016/0012-821X\(83\)90186-3](https://doi.org/10.1016/0012-821X(83)90186-3)
- Newsom, H.E., Palme, H., 1984. The depletion of siderophile elements in the Earth's mantle: new evidence from molybdenum and tungsten. *Earth Planet. Sci. Lett.* 69, 354–364. [https://doi.org/10.1016/0012-821X\(84\)90194-8](https://doi.org/10.1016/0012-821X(84)90194-8)
- Newsom, H.E., Sims, K.W.W., Noll, P.D., Jaeger, W.L., Maehr, S.A., Beserra, T.B., 1996. The depletion of tungsten in the bulk silicate earth: Constraints on core formation. *Geochim. Cosmochim. Acta* 60, 1155–1169. [https://doi.org/10.1016/0016-7037\(96\)00029-4](https://doi.org/10.1016/0016-7037(96)00029-4)
- Niu, Y., 2004. Bulk-rock major and trace element compositions of abyssal peridotites: Implications for mantle melting, melt extraction and post-melting processes beneath Mid-Ocean ridges. *J. Petrol.* 45, 2423–2458. <https://doi.org/10.1093/petrology/egh068>
- Noll, P.D., Newsom, H.E., Leeman, W.P., Ryan, J.G., 1996. The role of hydrothermal fluids in the production of subduction zone magmas: Evidence from siderophile and chalcophile trace elements and boron. *Geochim. Cosmochim. Acta* 60, 587–611.

- O'Hanley, D., Chernosky, J., Wicks, F., 1989. The stability of lizardite and chrysotile. *Can. Mineral.*
- O'Neill, H.S.C., Berry, A.J., Eggins, S.M., 2008. The solubility and oxidation state of tungsten in silicate melts: Implications for the comparative chemistry of W and Mo in planetary differentiation processes. *Chem. Geol.* 255, 346–359. <https://doi.org/10.1016/j.chemgeo.2008.07.005>
- Palme, H., O'Neill, H., 2013. Cosmochemical Estimates of Mantle Composition, in: *Treatise on Geochemistry: Second Edition*. <https://doi.org/10.1016/B978-0-08-095975-7.00201-1>
- Palme, H., O'Neill, H., 2003. Cosmochemical estimates of mantle composition, in: Carlson, R.W. (Ed.), *Treatise on Geochemistry, Vol. 2, The Mantle and Core*. Oxford: Elsevier-Pergamon, pp. 1–38.
- Palme, H., O'Neill, H.S.C., 2014. Cosmochemical Estimates of Mantle Composition A2 - Holland, Heinrich D, in: *Treatise on Geochemistry (Second Edition)*. pp. 1–39. <https://doi.org/http://dx.doi.org/10.1016/B978-0-08-095975-7.00205-9>
- Palme, H., Rammensee, W., 1981. The significance of W in planetary differentiation processes: Evidence from new data on eucrites. *Proc. Lunar Planet. Sci.* 12B, 949–964.
- Paulick, H., Bach, W., Godard, M., De Hoog, J.C.M., Suhr, G., Harvey, J., 2006. Geochemistry of abyssal peridotites (Mid-Atlantic Ridge, 15°20'N, ODP Leg 209): Implications for fluid/rock interaction in slow spreading environments. *Chem. Geol.* 234, 179–210. <https://doi.org/10.1016/j.chemgeo.2006.04.011>
- Pearce, J.A., Peate, D.W., 1995. Tectonic Implications of the Composition of Volcanic ARC Magmas. *Annu. Rev. Earth Planet. Sci.* 23, 251–285. <https://doi.org/10.1146/annurev.ea.23.050195.001343>
- Peters, D., Bretscher, A., John, T., Scambelluri, M., Pettke, T., 2017. Fluid-mobile elements in serpentinites: Constraints on serpentinisation environments and element cycling in subduction zones. *Chem. Geol.* 466, 654–666. <https://doi.org/10.1016/j.chemgeo.2017.07.017>
- Plank, T., Langmuir, C.H., 1993. Tracing trace elements from sediment input to volcanic output at subduction zones. *Nature* 362, 739–743. <https://doi.org/10.1038/362739a0>
- Polat, A., Longstaffe, F., Weisener, C., Fryer, B., Frei, R., Kerrich, R., 2012. Extreme element mobility during transformation of Neoproterozoic (ca. 2.7Ga) pillow basalts to a Paleoproterozoic (ca. 1.9Ga) paleosol, Schreiber Beach, Ontario, Canada. *Chem. Geol.* 326–327, 145–173. <https://doi.org/10.1016/j.chemgeo.2012.07.018>

- Prytulak, J., Nielsen, S.G., Ionov, D.A., Halliday, A.N., Harvey, J., Kelley, K.A., Niu, Y.L., Peate, D.W., Shimizu, K., Sims, K.W.W., 2013. The stable vanadium isotope composition of the mantle and mafic lavas. *Earth Planet. Sci. Lett.* <https://doi.org/10.1016/j.epsl.2013.01.010>
- Rudnick, R.L., Gao, S., 2013. Composition of the Continental Crust, in: *Treatise on Geochemistry: Second Edition*. pp. 1–51. <https://doi.org/10.1016/B978-0-08-095975-7.00301-6>
- Rudnick, R.L., Gao, S., 2003. Composition of the Continental Crust, in: Holland, H.D., Turekian, K.K. (Eds.), *Treatise on Geochemistry*. Elsevier Ltd, pp. 1–64.
- Ryan, J.G., Langmuir, C.H., 1993. The systematics of boron abundances in young volcanic rocks. *Geochim. Cosmochim. Acta.* [https://doi.org/10.1016/0016-7037\(93\)90008-K](https://doi.org/10.1016/0016-7037(93)90008-K)
- Ryan, J.G., Langmuir, C.H., 1987. The systematics of lithium abundances in young volcanic rocks. *Geochim. Cosmochim. Acta.* [https://doi.org/10.1016/0016-7037\(87\)90351-6](https://doi.org/10.1016/0016-7037(87)90351-6)
- Scambelluri, M., Philippot, P., 2001. Deep fluids in subduction zones. *Lithos.* [https://doi.org/10.1016/S0024-4937\(00\)00046-3](https://doi.org/10.1016/S0024-4937(00)00046-3)
- Schauble, E.A., 2004. Applying stable isotope fractionation theory to new systems. *Rev. Mineral. Geochemistry* 55, 65–111. <https://doi.org/10.2138/gsrmsg.55.1.65>
- Schmidt, M.W., Poli, S., 1998. Experimentally based water budgets for dehydrating slabs and consequences for arc magma generation. *Earth Planet. Sci. Lett.* 163, 361–379. [https://doi.org/10.1016/S0012-821X\(98\)00142-3](https://doi.org/10.1016/S0012-821X(98)00142-3)
- Schroeder, T., Cheadle, M.J., Dick, H.J.B., Faul, U., Casey, J.F., Kelemen, P.B., 2007. Nonvolcanic seafloor spreading and corner-flow rotation accommodated by extensional faulting at 15°N on the Mid-Atlantic Ridge: A structural synthesis of ODP Leg 209. *Geochemistry, Geophys. Geosystems* 8. <https://doi.org/10.1029/2006GC001567>
- Seifert, K., Gibson, I., Weis, D., Brunotte, D., 1996. Geochemistry of metamorphosed cumulate gabbros from Hole 900A, Iberia Abyssal Plain, in: *Proceedings of the Ocean Drilling Program, 149 Scientific Results*. <https://doi.org/10.2973/odp.proc.sr.149.221.1996>
- Seyfried, W.E., Janecky, D.R., Mottl, M.J., 1984. Alteration of the oceanic crust: Implications for geochemical cycles of lithium and boron. *Geochim. Cosmochim. Acta.* [https://doi.org/10.1016/0016-7037\(84\)90284-9](https://doi.org/10.1016/0016-7037(84)90284-9)
- Smith, D.K., Cann, J.R., 1993. Building the crust at the Mid-Atlantic Ridge. *Nature* 365, 707–715. <https://doi.org/10.1038/365707a0>



- Sohrin, Y., Isshiki, K., Kuwamoto, T., Nakayama, E., 1987. Tungsten in North Pacific Water. *Mar. Chem.* 22, 95–103.
- Sohrin, Y., Matsui, M., Nakayama, E., 1999. Contrasting behavior of tungsten and molybdenum in the Okinawa Trough, the East China Sea and the Yellow Sea. *Geochim. Cosmochim. Acta* 63, 3457–3466. [https://doi.org/10.1016/S0016-7037\(99\)00273-2](https://doi.org/10.1016/S0016-7037(99)00273-2)
- Staudigel, H., 2013. Chemical Fluxes from Hydrothermal Alteration of the Oceanic Crust, in: *Treatise on Geochemistry: Second Edition*. Elsevier Ltd., pp. 583–606. <https://doi.org/10.1016/B978-0-08-095975-7.00318-1>
- Staudigel, H., Plank, T., White, B., Schmincke, U., 1996. Geochemical fluxes during seafloor alteration of the basaltic crust: DSDP Sites 417 and 418. *Geophys. Monogr.* 96 19–38. <https://doi.org/doi:10.1029/GM096p0019>
- Sun, W., Ding, X., Hu, Y., Zartman, R.E., Arculus, R.J., Kamenetsky, V.S., Chen, M., 2011. The fate of subducted oceanic crust: A mineral segregation model. *Int. Geol. Rev.* 53, 879–893. <https://doi.org/10.1080/00206810903211930>
- Teagle, D.A.H., Alt, J.C., Bach, W., Halliday, A.N., Erzinger, J., 1996. Alteration of Upper Ocean Crust in a Ridge-Flank Hydrothermal Upflow Zone: Mineral, Chemical, and Isotopic Constraints from Hole 896A, in: *Proceedings of the Ocean Drilling Program, 148 Scientific Results*. <https://doi.org/10.2973/odp.proc.sr.148.113.1996>
- Teagle, D.A.H., Ildefonse, B., Blum, P., Abe, N., Abily, B., Adashi, Y., Alt, J.C., Anma, R., Baines, G., Deans, J., Dick, H.J.B., Endo, D., Ferré, E.C., France, L., Godard, M., Guérin, G., Harris, M., Kim, Y.M., Koepke, J.H., Kurz, M.D., Lissenberg, C.J., Miyashita, S., Morris, A., Oizumi, R., Payot, B.D., Python, M., Roy, P., Till, J.L., Tominaga, M., Wilson, D.S., Zakharova, N., 2012. IODP expedition 335: Deep sampling in ODP hole 1256D. *Sci. Drill.* 28–34. <https://doi.org/10.2204/iodp.sd.13.04.2011>
- Thiemens, M.M., Sprung, P., Fonseca, R.O.C., Leitzke, F.P., Münker, C., 2019. Early Moon formation inferred from hafnium–tungsten systematics. *Nat. Geosci.* <https://doi.org/10.1038/s41561-019-0398-3>
- Thomas, J.B., Bodnar, R.J., Shimizu, N., Sinha, A.K., 2002. Determination of zircon/melt trace element partition coefficients from SIMS analysis of melt inclusions in zircon. *Geochim. Cosmochim. Acta* 66, 2887–2901. [https://doi.org/10.1016/S0016-7037\(02\)00881-5](https://doi.org/10.1016/S0016-7037(02)00881-5)
- Thompson, J.F.H., Sillitoe, R.H., Baker, T., Lang, J.R., Mortensen, J.K., 1999. Intrusion-related gold deposits associated with tungsten-tin provinces. *Miner. Depos.* 34, 323–334. <https://doi.org/10.1007/s001260050207>

- Tominaga, M., Teagle, D.A.H., Alt, J.C., Umino, S., 2009. Determination of the volcanostratigraphy of oceanic crust formed at superfast spreading ridge: Electrofacies analyses of ODP/IODP Hole 1256D. *Geochemistry, Geophys. Geosystems* 10. <https://doi.org/10.1029/2008GC002143>
- tungsten, n., 2019. . Oxford English Dict.
- Turner, S., Beier, C., Niu, Y., Cook, C., 2011. U-Th-Ra disequilibria and the extent of off-axis volcanism across the East Pacific Rise at 9°30'N, 10°30'N, and 11°20'N. *Geochemistry, Geophys. Geosystems* 12. <https://doi.org/10.1029/2010GC003403>
- Turner, S., Foden, J., 2001. U, Th and Ra disequilibria, Sr, Nd and Pb isotope and trace element variations in Sunda arc lavas: Predominance of a subducted sediment component. *Contrib. to Mineral. Petrol.* 142, 43–57. <https://doi.org/10.1007/s004100100271>
- Urey, H.C., 1947. The thermodynamic properties of isotopic substances. *J. Chem. Soc.* 562. <https://doi.org/10.1039/jr9470000562>
- Vils, F., Tonarini, S., Kalt, A., Seitz, H.M., 2009. Boron, lithium and strontium isotopes as tracers of seawater-serpentinite interaction at Mid-Atlantic ridge, ODP Leg 209. *Earth Planet. Sci. Lett.* 286, 414–425. <https://doi.org/10.1016/j.epsl.2009.07.005>
- Von Damm, K.L., Edmond, J.M., Measures, C.I., Grant, B., 1985. Chemistry of submarine hydrothermal solutions at Guaymas Basin, Gulf of California. *Geochim. Cosmochim. Acta.* [https://doi.org/10.1016/0016-7037\(85\)90223-6](https://doi.org/10.1016/0016-7037(85)90223-6)
- Wang, Z., Park, J.W., Wang, X., Zou, Z., Kim, J., Zhang, P., Li, M., 2019. Evolution of copper isotopes in arc systems: Insights from lavas and molten sulfur in Niuatahi volcano, Tonga rear arc. *Geochim. Cosmochim. Acta* 250, 18–33. <https://doi.org/10.1016/j.gca.2019.01.040>
- Weidenschilling, S.J., Spaute, D., Davis, D.R., Marzari, F., Ohtsuki, K., 1997. Accretional evolution of a planetesimal swarm. *Icarus* 128, 429–455. <https://doi.org/10.1006/icar.1997.5747>
- Wendt, J.I., Regelous, M., Collerson, K.D., Ewart, A., 1997. Evidence for a contribution from two mantle plumes to island-arc lavas from northern Tonga. *Geology* 25, 611–614. [https://doi.org/10.1130/0091-7613\(1997\)025<0611:EFACFT>2.3.CO;2](https://doi.org/10.1130/0091-7613(1997)025<0611:EFACFT>2.3.CO;2)
- Weyer, S., Anbar, A.D., Gerdes, A., Gordon, G.W., Algeo, T.J., Boyle, E.A., 2008. Natural fractionation of <sup>238</sup>U/<sup>235</sup>U. *Geochim. Cosmochim. Acta* 72, 345–359. <https://doi.org/10.1016/j.gca.2007.11.012>

- Weyer, S., Münker, C., Mezger, K., 2003. Nb/Ta, Zr/Hf and REE in the depleted mantle: Implications for the differentiation history of the crust - mantle system. *Earth Planet. Sci. Lett.* 205, 309–324. [https://doi.org/10.1016/S0012-821X\(02\)01059-2](https://doi.org/10.1016/S0012-821X(02)01059-2)
- Weyer, S., Münker, C., Rehkämper, M., Mezger, K., 2002. Determination of ultra-low Nb, Ta, Zr and Hf concentrations and the chondritic Zr/Hf and Nb/Ta ratios by isotope dilution analyses with multiple collector ICP-MS. *Chem. Geol.* 187, 295–313. [https://doi.org/10.1016/S0009-2541\(02\)00129-8](https://doi.org/10.1016/S0009-2541(02)00129-8)
- Wilson, D.S., Teagle, D.A.H., Acton, G.D., Alt, J.C., Banerjee, N.R., Barr, S.R., Coggon, R.M., Cooper, K.M., Crispini, L., Einaudi, F., Jiang, S., Kalberkamp, U., Kerneklian, M., Laverne, C., Nichols, H.J., Sandwell, R., Tartarotti, P., Umino, S., Ziegler, C., 2003. Leg 206 Summary, in: *Proceedings of the Ocean Drilling Program Vol. 206*.
- Wilson, D.S., Teagle, D.A.H., Alt, J.C., Banerjee, N.R., Umino, S., Miyashita, S., Acton, G.D., Anma, R., Barr, S.R., Belghoul, A., Carlut, J., Christie, D.M., Coggon, R.M., Cooper, K.M., Cordier, C., Crispini, L., Rodriguez Durand, S., Einaudi, F., Galli, L., Gao, Y., Geldmacher, J., Gilbert, L.A., Hayman, N.W., Herrero-Bervera, E., Hirano, N., Holter, S., Ingle, S., Jiang, S., Kalberkamp, U., Kerneklian, M., Koepke, J., Laverne, C., Lledo Vasquez, H.L., Maclennan, J., Morgan, S., Neo, N., Nichols, H.J., Park, S.H., Reichow, M.K., Sakuyama, T., Sano, T., Sandwell, R., Scheibner, B., Smith-Duque, C.E., Swift, S.A., Tartarotti, P., Tikku, A.A., Tominaga, M., Veloso, E.A., Yamasaki, T., Yamazaki, S., Ziegler, C., 2006. Drilling to gabbro in intact ocean crust. *Science* (80-. ). 312, 1016–1020. <https://doi.org/10.1126/science.1126090>
- Yamazaki, S., Neo, N., Miyashita, S., 2009. Data report: whole-rock major and trace elements and mineral compositions of the sheeted dike&#150;gabbro transition in ODP Hole 1256D. *Proc. IODP*, 309/312 309. <https://doi.org/10.2204/iodp.proc.309312.203.2009>
- Yongbao, G., Wenyuan, L., Wang, J., Hattori, K., Zhaowei, Z., 2014. Geology, Geochemistry and Genesis of Tungsten-Tin Deposits in the Baiganhu District in the Eastern Kunlun Domain, Northwestern China. *Acta Geol. Sin.* 88, 900–902. <https://doi.org/10.2113/econgeo.109.6.1787>
- Yongliang, X., Yusheng, Z., 1991. The mobility of rare-earth elements during hydrothermal activity: A review. *Chinese J. Geochemistry* 10, 295–306. <https://doi.org/10.1007/BF02841090>
- Zack, T., 2002. Equilibrium and Disequilibrium Trace Element Partitioning in Hydrous Eclogites (Trescolmen, Central Alps). *J. Petrol.* 43, 1947–1974. <https://doi.org/10.1093/petrology/43.10.1947>

# Acknowledgements

Zunächst möchte ich mich von ganzem Herzen bei meinen Eltern Peter und Martina Reifenröther, meiner Freundin Isabelle Renerken, meinen Großeltern Hubert und Luise Schmidt, Paul und Maria Reifenröther, sowie bei Paul und Marianne Schäfer und Hans-Josef und Lydia Schmidt bedanken. Sie alle haben mich von klein auf unterstützt und standen mir immer zur Seite. Ohne die ausdauernde Unterstützung meiner Familie wäre ich niemals so weit gekommen! Ihr habt es mir immer ermöglicht an meinen Träumen zu arbeiten, ihr habt mich in schwierigen Zeiten motiviert und mir immer den Rücken freigehalten.

Mein besonderer Dank gilt auch meinem Doktorvater Carsten Munker, vielen Dank für die Unterstützung und die Möglichkeit so viel zu erreichen. Es war mir eine große Freude Teil der Arbeitsgruppe zu sein. Ebenfalls bedanken möchte ich mich bei Birgit Scheibner, für die interessanten wissenschaftlichen Diskussionen. Vielen Dank auch an Reiner Kleinschrodt für die Begutachtung meiner Arbeit. Darüber hinaus möchte ich mich bei meinen Bürokollegen Florian Kurzweil und Jonas Tusch für die wissenschaftlichen Diskussionen und großartigen Momente im Büro bedanken. Ein weiterer Dank gilt Mike Jansen für die spannende Zeit im Labor, die wissenschaftlichen Diskussionen und die Kaffees dazwischen. Darüber hinaus gilt mein Dank Franz Michael Meyer und Annika Dziggel für die Studienzeit in Aachen

Ein großer Dank gilt auch Marcel Renerken, Christiane Schnabel, Christina Obert und noch einmal Florian Kurzweil die mir durch Korrekturlesen sehr geholfen haben, die Arbeit zu verbessern und wissenschaftlich voranzubringen.

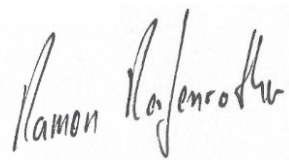
Des Weiteren gilt mein Dank Frank Wombacher und Peter Sprung, die mir insbesondere in der ersten Zeit viel im Labor und am Massenspektrometer gezeigt und geholfen haben.

Well there's a dark cloud rising from the desert floor  
I packed my bags and I'm heading straight into the storm  
Gonna be a twister to blow everything down  
That ain't got the faith to stand its ground

Springsteen, Bruce „The Promised Land“. *Darkness on the Edge of Town*. Columbia Records  
1978

# Erklärung

Ich versichere, dass ich die von mir vorgelegte Dissertation selbständig angefertigt, die benutzten Quellen und Hilfsmittel vollständig angegeben und die Stellen der Arbeit – einschließlich Tabellen, Karten und Abbildungen –, die anderen Werken im Wortlaut oder dem Sinn nach entnommen sind, in jedem Einzelfall als Entlehnung kenntlich gemacht habe; dass diese Dissertation noch keiner anderen Fakultät oder Universität zur Prüfung vorgelegen hat; dass sie – abgesehen von unten angegebenen Teilpublikationen – noch nicht veröffentlicht worden ist, sowie, dass ich eine solche Veröffentlichung vor Abschluss des Promotionsverfahrens nicht vornehmen werde. Die Bestimmungen der Promotionsordnung sind mir bekannt. Die von mir vorgelegte Dissertation ist von Prof. Dr. Carsten Münker betreut worden.

A handwritten signature in black ink, reading "Ramon Rosenroth". The signature is written in a cursive style with a large initial 'R'.

Aachen, 02.04.2020